A Szilikátipari Tudományos Egyesület lapja

építőanyag

Journal of Silicate Based and Composite Materials

A TARTALOMBÓL:

- Sintering of silica-alumina granular materials and its catalytic properties
- In-situ carbonization of natural zeolite-alumina composite materials incorporated sawdust
- Study of transverse deformation of porous alumina during uniaxial mechanical tests
- Mechanical properties of mullite reinforced ceramics composite produced from kaolin and corn starch
- Stress-strain behavior of high porous zirconia ceramic
- Examination of the influence of cobalt substitution on the properties of barium titanate ceramics

2021/4

2022: the UN International Year Of Glass

The International Commission on Glass (ICG), along with the Community of Glass Associations (CGA) and ICOM-Glass recently applied for a
United Nations International Year of Glass of 2022
and the UN General Council meeting on 18th May 2021 gave its formal approval!

The Year will celebrate the essential role glass has and will continue to have in Society. A 2 day opening event at the Palace of Nations in Geneva will feature 30 world class speakers. The event will be streamed worldwide on Zoom – places in the Hall will be at a premium! Talks will highlight the latest thinking on how GLASS can aid the development of more just and sustainable societies alongside the most recent scientific and technical breakthroughs. It will also be an important medium for art and its history. It is the one IYOG event on the calander that requires financial support and a Global sponsorship campaign has begun.

What follows is based on the formal application made to the UN and is split into the following sections:
- What glass offers society
- Planning the IYOG
- Support us with your donations
- Support received from different institutions
- Support received by country
- Concluding statement

www.iyog2022.org

ICG International Commission on Glass
COMMUNITY of GLASS ASSOCIATIONS
GLASS ICOM international committee for museums and collections of glass

építőanyag

Journal of Silicate Based and Composite Materials

2021/4

TARTALOM

132 Szemcsés szilícium-dioxid – alumínium-oxid anyagok szinterelése és katalitikus tulajdonságai
Afanasy S. APKARIAN ▪ GÖMZE László A. ▪ Jamal-Eldin F. M. IBRAHIM ▪ Sergei N. KULKOV

137 Természetes zeolit - alumínium-oxid kompozit anyagok fűrészporral való in situ karbonizálása
Jamal-Eldin F. M. IBRAHIM ▪ Afanasy S. APKARIAN ▪ Mohammed TIHTIH ▪ Sergei N. KULKOV ▪ GÖMZE László A.

145 A porózus alumínium-oxid keresztirányú deformációjának vizsgálata egytengelyű mechanikai vizsgálatok során
A. D. KASHIN ▪ A. S. KULKOV ▪ S. N. KULKOV ▪ KUROVICS E. ▪ GÖMZE L. A.

149 Kaolinból és kukoricakeményítőből előállított erősített mullit kerámiák mechanikai tulajdonságai
KUROVICS Emese ▪ Aleksey S. KULKOV ▪ Jamal-Eldin F. M. IBRAHIM ▪ A.D. KASHIN ▪ PALA Péter ▪ NAGY Veronika ▪ Sergei N. KULKOV ▪ GÖMZE László A.

154 Nagy porozitású cirkónium-oxid kerámiák alakváltozása feszültség hatására
Irina N. SEVOSTIANOVA ▪ Tatiana Yu. SABLINA ▪ Sergei N. KULKOV ▪ Mohammed TIHTIH ▪ GÖMZE László A.

160 A kobalt-szubsztitúció bárium-titanát-kerámiák tulajdonságaira gyakorolt hatásának vizsgálata
Mohammed TIHTIH ▪ Irina N. SEVOSTIANOVA ▪ Emese KUROVICS ▪ Tatiana Yu. SABLINA ▪ Sergei N. KULKOV ▪ GÖMZE László A.

CONTENT

132 Sintering of silica-alumina granular materials and its catalytic properties
Afanasy S. APKARIAN ▪ László A. GÖMZE ▪ Jamal-Eldin F. M. IBRAHIM ▪ Sergei N. KULKOV

137 In-situ carbonization of natural zeolite-alumina composite materials incorporated sawdust
Jamal-Eldin F. M. IBRAHIM ▪ Afanasy S. APKARIAN ▪ Mohammed TIHTIH ▪ Sergei N. KULKOV ▪ László A. GÖMZE

145 Study of transverse deformation of porous alumina during uniaxial mechanical tests
A. D. KASHIN ▪ A. S. KULKOV ▪ S. N. KULKOV ▪ E. KUROVICS ▪ L. A. GÖMZE

149 Mechanical properties of mullite reinforced ceramics composite produced from kaolin and corn starch
Emese KUROVICS ▪ Aleksey S. KULKOV ▪ Jamal-Eldin F. M. IBRAHIM ▪ A.D. KASHIN ▪ Péter PALA ▪ Veronika NAGY ▪ Sergei N. KULKOV ▪ László A. GÖMZE

154 Stress-strain behavior of high porous zirconia ceramic
Irina N. SEVOSTIANOVA ▪ Tatiana Yu. SABLINA ▪ Sergei N. KULKOV ▪ Mohammed TIHTIH ▪ László A. GÖMZE

160 Examination of the influence of cobalt substitution on the properties of barium titanate ceramics
Mohammed TIHTIH ▪ Irina N. SEVOSTIANOVA ▪ Emese KUROVICS ▪ Tatiana Yu. SABLINA ▪ Sergei N. KULKOV ▪ László A. GÖMZE

A finomkerámia-, üveg-, cement-, mész-, beton-, tégla- és cserép-, kő- és kavics-, tűzállóanyag-, szigetelőanyag-iparágak szakmai lapja
Scientific journal of ceramics, glass, cement, concrete, clay products, stone and gravel, insulating and fireproof materials and composites

A folyóiratot referálja · The journal is referred by:
ProQuest · Google Scholar · INDEX COPERNICUS INTERNATIONAL · THOMSON REUTERS

A folyóiratban lektorált cikkek jelennek meg.
All published papers are peer-reviewed.
Kiadó · Publisher: Szilikátipari Tudományos Egyesület (SZTE)
Elnök · President: ASZTALOS István
1034 Budapest, Bécsi út 120.
Tel.: +36-1/201-9360 ▪ E-mail: epitoanyag@szte.org.hu
Tördelő szerkesztő · Layout editor: NÉMETH Hajnalka
Címlapfotó · Cover photo: GYURKÓ Zoltán

WWW.EPITOANYAG.ORG.HU
EN.EPITOANYAG.ORG.HU

Online ISSN: 2064-4477
Print ISSN: 0013-970x
INDEX: 2 52 50 ▪ 73 (2021) 131–166

Sintering of silica-alumina granular materials and its catalytic properties

Afanasy S. APKARIAN ▪ Institute of Strength Physics and Materials Science SB RAS, National Research Tomsk State University ▪ asaktc@ispms.tsc.ru

László A. GÖMZE ▪ Institute of Ceramics and Polymer Engineering, University of Miskolc, Hungary, IGREX Engineering Service Ltd ▪ femgomze@uni-miskolc.hu

Jamal-Eldin F. M. IBRAHIM ▪ Institute of Ceramics and Polymer Engineering, University of Miskolc, Hungary ▪ jamalfadoul@gmail.com

Sergei N. KULKOV ▪ Institute of Strength Physics and Materials Science SB RAS, National Research Tomsk State University ▪ kulkov@ms.tsc.ru

Érkezett: 2021. 06. 03. ▪ Received: 03. 06. 2021. ▪ https://doi.org/10.14382/epitoanyag-jsbcm.2021.19

Abstract

In this work was developed a filtering material, where a granular glass-ceramic with a catalytically active layer applied as a carrier. The main component of the pellet batch is alkaline glass which made it possible to intensify the processes of melting and foaming of the molten glass. It has been defined physical and technical characteristic of granules and obtained that its density smaller 300 kg/m^3 and strength under compression layers between 0.8-2.6 MPa. Taking into account the physical and technical characteristics of GCM granules, studies were carried out to determine the possibility of using them as filtering media with a catalytically active layer. This makes it possible not only to dispose of cullet, but also to create a highly efficient material from it, allowing water to be purified up to standards.

Keywords: foamed glass, granular ceramics, pores, catalytic properties, iron and manganese absorption

Kulcsszavak: habosított üveg, szemcsés kerámiák, pórusok, katalitikus tulajdonságok, vas és mangán abszorpció

Afanasy S. APKARYAN
has PhD in Technical Sciences. He is head of Department and responsible for Nanotechnology in the Institute of Strength Physics and Materials Science of the Russian Academy of Science since 2005. Candidate of Technical Sciences. Specialists in the field of thermal physics and ceramic production. Associate Professor in Tomsk State University of Control Systems and Radioelectronics.

László A. GÖMZE
is establisher and professor of the Department of Ceramics and Silicate Engineering in the University of Miskolc, Hungary. He is author or coauthor of 2 patents, 6 books and more than 300 scientific papers. Recently, he is the chair of the International Organization Board of ic-cmtp6 the 6th International Conference on Competitive Materials and Technological Processes and ec-siliconf2 the 2nd European Conference on Silicon and Silica Based Materials.

Jamal Eldin F. M. IBRAHIM
is a lecturer in the University of Bahri, Khartoum, Sudan, he graduated from University of Marmara, Istanbul, Turkey, Institute of Pure and Applied Sciences, Department of Metallurgical and Materials Engineering, for the time being, he is a PhD student in the University of Miskolc, Institute of Polymer and Ceramics Engineering, under supervision of Prof. L. A. Gömze.

Sergei N. KULKOV
is professor at the Tomsk State University and head of Department of Ceramics in the Institute of Strength Physics and Materials Science of the Russian Academy of Science since 1989. His research works are represented in 5 books, more than 150 articles, 18 patents and many International Symposiums and Conferences. At present he is head of department „Theory of Strength and Mechanic of Solids", member of „The American Ceramic Society" of „The APMI - International" and the DYM AT Society (France).

1. Introduction

It is well known, the creation of new materials that provide high-quality water purification is important for human life. The water strategy developed in different countries defined the main directions of activities for the development of the country's water sector, ensuring sustainable water use, protection from the negative impact of contaminated water on humans.

For the purification of drinking water, physicochemical methods are widely used: sorption, coagulation, flotation, filtration and reagent methods. However, in areas where oil and gas production is intensively conducted, the content of iron, manganese and hydrogen sulfide in water exceeds the maximum permissible norms by 10-20 times. The filtering materials used in the different regions do not cope with water purification to standards and do not fully correspond to the solutions of the assigned tasks.

Now, the filtering media called "Manganese Greensand" is widespread - glutonite green sand, which is a natural material, covered with manganese compounds. It acts as a catalyst in the removal of soluble manganese and iron [1-3]. Manufacturing technology of "Manganese Greensand" includes pretreatment of sodium glauconite (NaZ) with a manganese chloride solution:

$$Na_2Z + MnCl_2 <=> MnZ + 2NaCl$$

The use of potassium permanganate in conjunction with these loads also allows you to remove hydrogen sulfide, oxidizing it to elemental sulfur, and partially, organic matter and biological pollution, ensuring water disinfection.

The main disadvantage of using *Manganese Greensand* is pretreatment with potassium permanganate solution, i.e. before the start of operation to obtain a layer of higher manganese oxides on the surface of the filtering material *Manganese Greensand*, the loading is pre-treated with a solution of potassium permanganate, or it is constantly dosed into water using a proportional dosing system (dosing pump) [3, 4].

As an effective material, this granular filter material is used to remove iron and manganese from water and the filter material is a catalyst that accelerates the interaction of Fe with oxygen dissolved in water, resulting in the formation of water-insoluble iron III hydroxide. After that, iron in an insoluble form is retained in the layer of filter material, therefore the efficiency of water purification with filter is strongly influenced by the pH value (PH). For effective removal of iron, it should be in the range of 6.8-8.5, for removal of manganese - more than 8. If there is insufficient dissolved oxygen in the treated water, then aerators must be used in front of the filter and does not recommended to use for the purification of chlorinated water. Free chlorine significantly reduces both the service life of the filter material and its efficiency.

To purify water from manganese and iron, a filter material called MFO-47 has been developed and is also used, containing as a basis granular material of natural origin, burnt rock, on the surface of which a catalytically active layer is formed,

consisting of a mixture of oxides MnO, Mn_2O_3 and MnO_2 [3, 5]. This method, based on the treatment of granular material with a solution of a modifying reagent containing manganese salts, does not allow efficient removal of hydrogen sulfide from water.

The aim of this work was to develop a filtering material, based on a granular glass-ceramic material (GCM) with a catalytically active layer applied as a carrier. This makes it possible not only to dispose of cullet, but also to create a highly efficient material from it, allowing water to be purified up to standards.

2. Materials preparation and its properties

The proposed composition of the charge for granules differs from those previously developed [6-8] in that the required chemical composition and structure of GCM granules are provided by using compositions including glass, a plasticizer - low-melting clay, gasifier- coke and organic additives (sawdust).

The main component of the pellet batch is alkaline glass. When choosing the glass, it was assumed that the content of alkali metal oxides in them would make it possible to intensify the processes of melting and foaming of the molten glass.

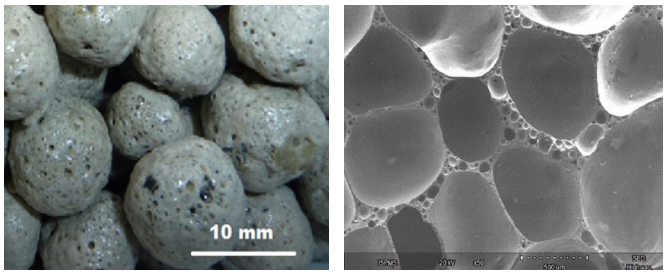

Fig. 1 GCM granules with a density of 260 kg/m³ and its cross-section
1. ábra 260 kg/m³ sűrűségű GCM granulátum és annak keresztmetszete

The introduction of a plasticizer, low-melting clay, into the batch, contributes to a directed external effect on the glass during the firing period. The main tasks of adding a plasticizer are to increase strength and reduce water absorption. An important factor for the pore formation process is the swelling interval - the difference between the maximum possible firing temperature and the temperature of the beginning of clay swelling. The firing temperature must ensure sufficient softening and viscosity of the material; otherwise the gases formed during firing will freely escape, without material swelling.

A distinctive feature of the proposed composition of the charge for the production of GCM, in contrast to traditional compositions of foam glass, is the introduction of an organic component - sawdust (dispersed cellulose). The purpose of introducing organic additives into the charge is to increase the temperature of the raw granules and to heat the coke particles with the products of thermal decomposition of cellulose, contributing to the early process of gas formation from the combustion of coke, increasing the amount and pressure of gas in the pores of the foamed melt.

When using a plasticizer in the composition of the charge, the choice of the gasifier plays a decisive role. Since the plasticizer increases the viscosity of the molten glass, it is necessary to use such blowing agents, the decomposition products of which would have a pressure capable of foaming the molten glass during firing. When justifying the choice of the gas generator, the coincidence of the temperature intervals of the appearance of the melt of the required viscosity and the formation of the highest pressure of gaseous products were taken into account for this purpose coke was used in the experiments. The maximum firing temperature for raw granules is 830-850 °C.

During the study, granules with a diameter of 0.8-10 mm were used. As a result of research, it was found that to obtain porous GCM, it is necessary to use a plasticizer of the chemical composition: SiO_2 - 70-71%; Al_2O_3 - 17-18%; Fe_2O_3 - 5-6%; SO_3 - 0.2-0.3, in which illite, chlorite, hydromuscovite, montmorillonite and organic additives predominate, providing a large amount of CO at the initial stage of the formation of a porous amorphous-crystalline glass-ceramic system. When CO interacts with iron compounds, which are part of the plasticizer, and glass, iron carbide is formed with the release of CO_2, which contributes to the intensive process of gas formation and the formation of a porous structure of granules. By changing the amount of plasticizer in the charge, the density of the granules can be varied from 200 to 300 kg/m³, the thickness of the interpore partitions is from 0.07 μm to 50 μm, and the pore area in the granules is 0.10 - 0.72 mm². The pore sizes and their location, the thickness of the glass-ceramic partitions and the glaze layer of the granules were examined under an optical microscope, *Fig. 2*.

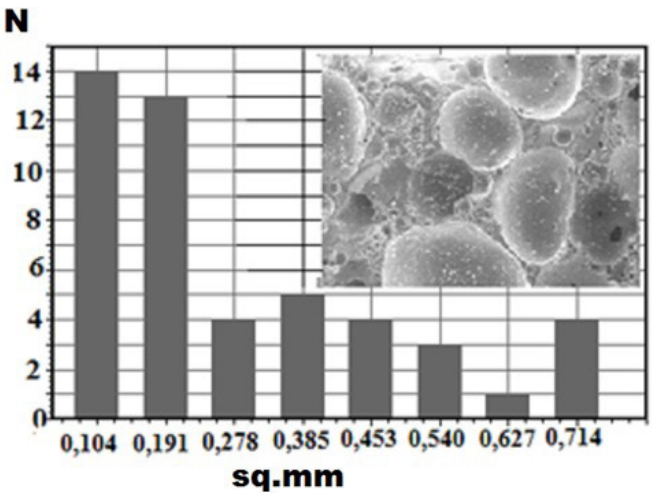

Fig. 2 Micrograph and size distribution of pores with a plasticizer content 10%
2. ábra 10% lágyító tartalmú pórusok mikroszerkezete és méreteloszlása

Density, kg/m³	Thermal conductivity, W/(m °C)	Strength under compression, MPa	Temperature operation, °C	Water absorption, %
200-290	0,067-0,087	0,82-2,61	up 820	1,7-4,8

Table 1 Physical and technical characteristics of GCM granules
1. táblázat GCM granulátumok fizikai és műszaki jellemzői

As a result of research, granules with physical and technical characteristics are presented in *Table 1* and *Fig. 3*.

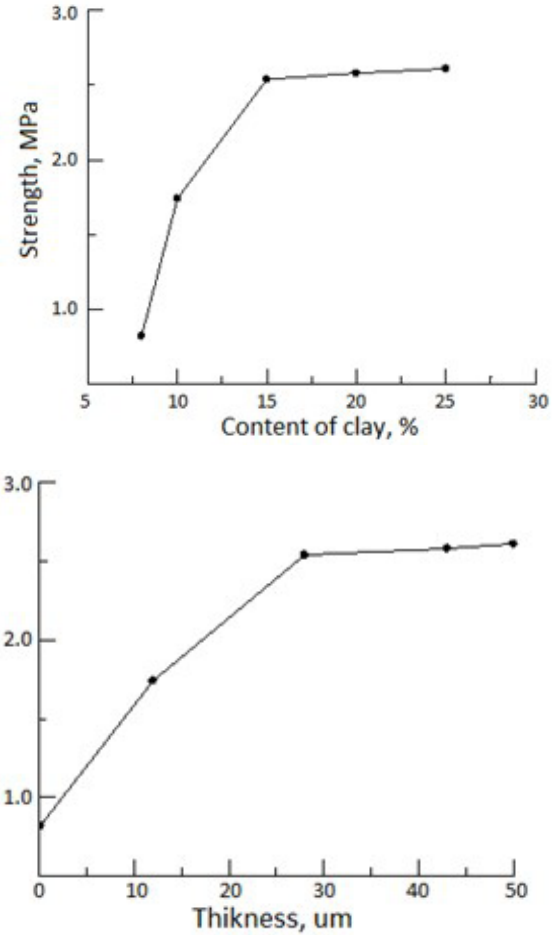

Fig. 3 Properties of GCM granules with a density of 260 kg/m³
3. ábra A 260 kg/m³ sűrűségű GCM granulátumok tulajdonságai

3. Catalytic properties of material and discussions

Taking into account the physical and technical characteristics of GCM granules, studies were carried out to determine the possibility of using them as filtering media with a catalytically active layer.

The solution to this problem is achieved by sequential processing of granular material, natural origin, solutions containing manganese salts. First, the granules are treated in a solution containing divalent manganese salts, with a solution of potassium permanganate, and then with a solution of a reagent that promotes the reduction of manganese (VII) and the formation of a mixture of manganese oxide compounds on the surface of the granular material. This method of processing a filtering granular load (natural dispersed material) with modifying reagents containing manganese compounds of different valences makes it possible to obtain on its surface a complex of not only manganese oxide compounds, but also hydroxide ones. When implementing the proposed method on the surface of the filtering media received a mixture consisting of manganese hydroxide $Mn(OH)_2$, and manganese oxides Mn_2O_3, MnO_2 [9].

It should be noted that the granular material is pre-treated with an alkali solution. NaOH or KOH at a concentration of 10 g/l is used as an alkali solution. The recovery of potassium permanganate is carried out by processing the material in a solution of 0.1-2.0% of a reducing agent. In this case, pH 8–12 was maintained throughout the entire process of formation of the catalytic layer. During processing, air was blown and the solution was stirred.

Iron is in water in the form of a compound $Fe(HCO_3)_2$. When $Fe(HCO_3)_2$ interacts with the catalytically active layer of the granule, iron is precipitated in the form of iron hydroxide $Fe(OH)_3$ according to the formula:

$$4Fe(HCO_3)_2 + 3MnO_2 + 2H_2O \rightarrow$$
$$4Fe(OH)_3\downarrow + MnO + Mn_2O_3 + 8CO_2\uparrow.$$

The results of studies of the filtering material based on GCM granules showed that with an increase in the filtration time, at a water speed of 1 dm³/min. and the volume of the passed water 100 dm³, the iron content falls from 0.76 to 0.06 mg/dm³ (*Fig. 4*).

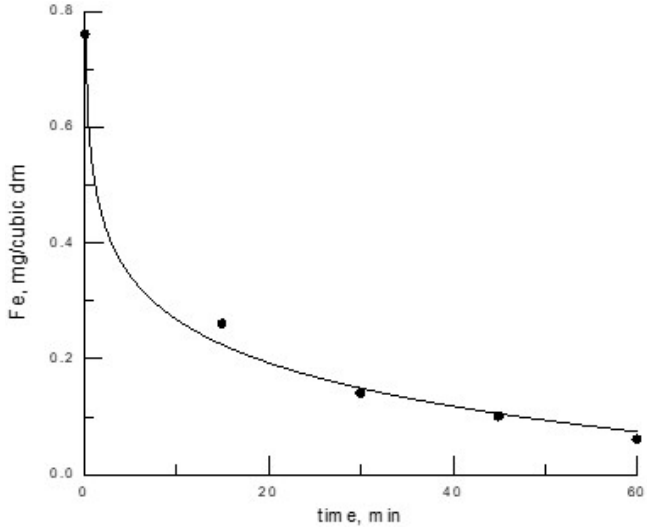

Fig. 4 Change in iron content vs. filtration time
4. ábra A vastartalom változása a szűrési idő függvényében

It has been established [2, 10] that manganese oxides pre-precipitated on the surface of GCM granules have a catalytic effect on the oxidation of manganese (II) ion by oxygen dissolved in water.

When filtering aerated water, oxygen dissolved in water is adsorbed on the surface of the granule and interacts with manganese ions to form a layer consisting of a negatively charged precipitate of manganese hydroxide $Mn(OH)_4$, which adsorbs positively charged manganese (II) ions, forming an oxide manganese Mn_2O_3 [11]:

$$Mn(OH)_4 + Mn(OH)_2 \rightarrow Mn_2O_3 + 3H_2O,$$
$$2Mn_2O_3 + O_2 + 8H_2O \rightarrow Mn(OH)_4\downarrow.$$

As a result, manganese (IV) hydroxide is again formed, which is involved in the oxidation process as a catalyst.

In water, a solution of hydrogen sulfide H_2S is a two-basic weak acid hydrogen sulfide. Acids are known to react with bases, basic oxides and salts, in this case, with $Mn(OH)_2$. An increase in the efficiency of water purification from hydrogen sulfide occurs by the reaction:

$$Mn(OH)_2 + H_2S = MnS + 2H_2O.$$

Thus, granular glass-ceramic material as a carrier with a saturated catalytically active layer consisting of manganese oxides and hydroxides is capable of effectively removing iron, manganese, and hydrogen sulfide from water [1].

The advantage of the method is the production of hydroxide and manganese oxide compounds firmly adhered to the base on the surface of the filter medium at room temperature. The catalytically active layer, due to the adhesion caused by intermolecular interaction, is firmly fixed on the surface and is not washed off. *Table 2* reflects a decrease in the efficiency of water purification from hydrogen sulfide with a decrease in manganese hydroxide in the mixture.

№	$Mn(OH)_2$ content on the surface of granules, g/kg	H_2S content in source water, mg/dm³	H_2S content in purified water, mg/dm³
1	10	0,1	0,03
2	9	0,1	0,033
3	8	0,1	0,035
4	7	0,1	0,040
5	6	0,1	0,045

Table 2 The degree of efficiency of water purification from hydrogen sulfide with a decrease in the content of manganese hydroxide in the mixture
2. táblázat A hidrogén-szulfidból történő víztisztítás hatékonyságának mértéke a keverék mangán-hidroxid-tartalmának csökkenésével

A comparative study of the processes of sorption of sulfide ions on GCM granules was carried out under static conditions. Model solutions were prepared by diluting the S2 stock solution with a concentration of 100 mg/l. The sorbent weighing 0.2 g was placed in a dry conical flask with a thin section with a volume of 250.0 ml, 100.0 ml of a model solution was added there (sorbent: solution ratio=1:500), stirred on a THYS2 universal vibration machine (Germany) for 60 min, Then the solution was separated by decantation and the mass concentration of S^{2-} was determined according to RD 52.24.450-95 by the extraction-photometric method on a PE-5400v spectrophotometer. The equilibrium concentration of sulfide ions was determined according to the results of a "blank" experiment - a model solution of the same concentration, but without a sorbent to take into account the loss of S^{2-} due to the volatilization of hydrogen sulfide. The static exchange capacity (SEC) was calculated using the equation:

$$SEC = V_{solute}\,(C_{equilibr} - C_{concentr.})/m_{corbent}$$

Table 3 shows that the concentration of hydrogen sulfide after sorption of GCM is less than that on the material - the prototype MFO-47, by 10-20 times. The static exchange capacity of the GCM is 2 - 2.7 times higher than the corresponding indicator for the MFO-47 material.

On *Fig. 5* is shown the dependence of the static exchange capacity (SEC), mg/g, on the mass concentration of S^{2-} (isotherm of sorption of sulfide ions) for the MFO-47 sorbents and GCM granules at t = 23 °C. Experimental and industrial tests have established that the complex of compounds deposited on the surface of the GCM granules determines the high catalytic activity of the load in relation to various salts of iron, manganese and hydrogen sulfide dissolved in water.

N	$C_{S^{2-}\ initial}$ mg/dm³	$C_{S^{2-}\ equilibr}$ mg/dm³	MFO-47		GCM	
			$C_{S^{2-}\ concentr}$ mg/dm³	COE mg/g	$C_{S^{2-}\ concentr}$ mg/dm³	SEC mg/g
1	0,10	0,015±0,002	0,01±0,002	0,0020	0,007±0,001	0,0040
2	0,30	0,20±0,020	0,13±0,02	0,0350	0,010±0,002	0,0945
3	0,40	0,37±0,020	0,22±0,02	0,0775	0,012±0,002	0,1780
4	0,80	0,69±0,040	0,38±0,02	0,1540	0,024±0,003	0,3330
5	1,00	0,90±0,050	0,5±0,03	0,1604	0,036±0,003	0,4310
6	1,20	1,17±0,060	0,78±0,04	0,1950	0,097±0,010	0,5360

Table 3 Static exchange capacity, SEC, of MFO-47 and developed GCM
3. táblázat Az MFO-47 és a kifejlesztett GCM statikus cserekapacitása, SEC

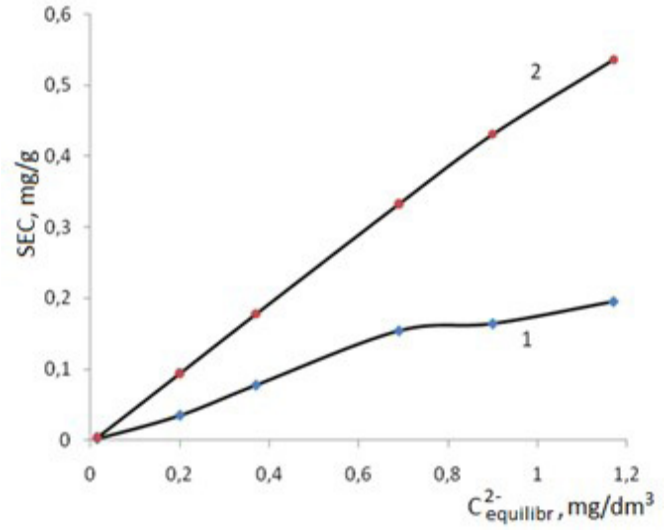

Fig. 5 Isotherms of sorption of sulfide ions on sorbents: curve 1 - MFO-47 and 2 - GCM at 23 °C
5. ábra Szulfidionok szorpció izotermái a szorbenseken 23 °C-on: 1. görbe - MFO-47 és 2. görbe - GCM

It was experimentally established that a complex of compounds on the surface of granules causes high catalytic activity towards various salts of iron, manganese and hydrogen sulfide dissolved in water.

4. Conclusions

It has been found that on the surface of the base, glass-ceramic granules, after treatment with modifying reagents, a catalytically active layer was formed containing a mixture of manganese hydroxide $Mn(OH)_2$ and manganese oxides Mn_2O_3 and MnO_2 .

It has been shown that oxides Mn_2O_3, MnO_2 and hydroxide $Mn(OH)_2$, obtained on the surface of glass-ceramic granules, make it possible to remove iron and manganese from water, reducing their content up to 15 times.

Acknowledgments

The work was performed according to the Government research assignment for ISPMS SB RAS, project FWRW-2021-0005. The described article was carried out as part of the EFOP-3.6.1-16-00011 "Younger and Renewing University – Innovative Knowledge City – institutional development of the University of Miskolc aiming at intelligent specialisation".

References

[1] Jean-Paul Duroudier (2017): Adsorption-Dryers for Divided Solids. *Elsevier Ltd.* p.296. https://doi.org/10.1016/C2016-0-00504-1

[2] Angelo Basile, Alfredo Cassano, Navin K. Rastogi (2015): Advances in Membrane Technologies for Water Treatment. *Woodhead Publishing.* p. 666 https://doi.org/10.1016/C2013-0-16469-0

[3] Berlin A. A., Wolfson S. A, Oshmyan V. G., Yenikolopyan N. S. (1990): Principles of creating composite materials. M.: Chemistry

[4] Ketov, A.A. (2001): An experience of reuse of glass cullet for production of foam structure material, *Proc. Int. Symp. "Recycling and Reuse of Glass Cullet," March 19–20, 2001*, Dundee, pp. 85–91.

[5] Apkaryan, A. and Khristyukov, V., Russian Patent #2540741, 2014.

[6] Guloyan, Yu.A. (2003): Chemical reactions between components in the production of glass-forming melt, *Glass Ceram.*, Vol. 60, Nos. 7–8, pp. 233–235. https://doi.org/10.1023/A:1027395310680

[7] Apkaryan, A.S., Kulkov, S.N., and Gömze, L.A. (2014): Foam glass ceramics as composite heat-insulating material, *Építőanyag - Journal of Silicate Based and Composite Materials*, Vol. 66. No. 2, pp. 38–42. http://dx.doi.org/10.14382/epitoanyag-jsbcm.2014.8

[8] Apkaryan, A. and Khristyukov, V. (2014): Composite granular thermal insulation material–foam glass ceramic, *Perspekt. Mater.*, No. 6, pp. 42–47.

[9] Apkaryan A.S. (2014) Investigation of the Density of Granular Foam-Glass Ceramic by Mathematical Modeling. Glass and Ceramics, *Springer. Science + Business Media. New York.* T. 71. № 5-6. C. 194-197.

[10] Kulkov S.N., Apkaryan A.S. (2018): Formation of Structure and Closed Porosity under High-Temperature Firing of Granules of Porous Glass-Ceramic Material. *Inorganic Materials: Applied Research* Vol. 9, No. 2, p.286.

[11] Apkaryan A.S., Gubaidulina T.A., Kaminskaya O.V. (2015): Foam-Glass Ceramic Based Filtering Material for Removing Iron and Manganese from Drinking Water. Glass and Ceramics, *Springer. Science + Business Media. New York.* T. 71. № 11-12. C. 413 - 416.

Ref.:

Apkarian, Afanasy S. – **Gömze**, László A. – **Ibrahim**, Jamal-Eldin F. M. – **Kulkov**, Sergei N.: *Sintering of Silica-Alumina Granular Materials and its Catalytic Properties*

Építőanyag – Journal of Silicate Based and Composite Materials, Vol. 73, No. 4 (2021), 132–136. p.

https://doi.org/10.14382/epitoanyag-jsbcm.2021.19

In-situ carbonization of natural zeolite-alumina composite materials incorporated sawdust

Jamal-Eldin F. M. IBRAHIM ▪ Institute of Ceramics and Polymer Engineering, University of Miskolc, Hungary ▪ jamalfadoul@gmail.com
Afanasy S. APKARIAN ▪ Institute of Strength Physics and Materials Science SB RAS, National Research Tomsk State University
Mohammed TIHTIH ▪ Institute of Ceramics and Polymer Engineering, University of Miskolc, Hungary ▪ medtihtih@gmail.com
Sergei N. KULKOV ▪ Institute of Strength Physics and Materials Science SB RAS, National Research Tomsk State University ▪ kulkov@ms.tsc.ru
László A. GÖMZE ▪ Institute of Ceramics and Polymer Engineering, University of Miskolc, Hungary, IGREX Engineering Service Ltd, ▪ femgomze@uni-miskolc.hu

Érkezett: 2021. 06. 03. ▪ Received: 03. 06. 2021. ▪ https://doi.org/10.14382/epitoanyag-jsbcm.2021.20

Abstract
This research study investigates the potential use of traditional raw materials to synthesize new ceramic composite materials that can be used in different industrial applications. The composite materials were developed through mechanical activation, carbonization, and reactive sintering techniques. Natural zeolite from Tokaj region, alumina from Motim, and sawdust were used as starting raw materials. Stoichiometric amounts of the raw materials were mixed and milled in planetary ball milling followed by uniaxially pressing to produce cylindrical ceramic discs. The produced green ceramics were then sintered in an electric laboratory kiln under an oxygen-free environment at 1200 °C. In-situ carbonization of the sawdust was confirmed via X-ray diffraction. The thermal properties were also investigated by derivatography. The produced ceramic specimens were tested on microstructural characteristics, porosity, density, and water absorption.
Keywords: alumina, derivatography, sawdust, SEM, XRD, zeolite
Kulcsszavak: alumínium-oxid, derivatográf, fűrészpor, SEM, XRD, zeolit

Jamal Eldin F. M. IBRAHIM
is a lecturer in the University of Bahri, Khartoum, Sudan, he graduated from University of Marmara, Istanbul, Turkey, Institute of Pure and Applied Sciences, Department of Metallurgical and Materials Engineering, for the time being, he is a PhD student in the University of Miskolc, Institute of Polymer and Ceramics Engineering, under supervision of Prof. L. A. Gömze.

Afanasy S. APKARYAN
has PhD in Technical Sciences. He is head of Department and responsible for Nanotechnology in the Institute of Strength Physics and Materials Science of the Russian Academy of Science since 2005. Candidate of Technical Sciences. Specialists in the field of thermal physics and ceramic production. Associate Professor in Tomsk State University of Control Systems and Radioelectronics.

Mohammed TIHTIH
Is a lecturer in the Sidi Mohamed Ben abdellah University, Morocco, he graduated from Faculty of sciences Dhar El Mahraz, Fez, Morocco, Department of Physics, for the time being, he is a PhD student in the University of Miskolc, Institute of Ceramics and Polymer Engineering, under supervision of Prof. L. A. Gömze.

Sergei N. KULKOV
is professor of the Tomsk State University and head of Department of Ceramics in the Institute of Strength Physics and Materials Science of the Russian Academy of Science since 1989. His research works are represented in 5 books, more than 150 articles, 18 patents and many International Symposiums and Conferences. At present he is head of department „Theory of Strength and Mechanic of Solids", member of „The American Ceramic Society" of „The APMI - International" and the DYM AT Society (France).

László A. GÖMZE
is establisher and professor of the Department of Ceramics and Silicate Engineering in the University of Miskolc, Hungary. He is author or coauthor of 2 patents, 6 books and more than 300 scientific papers. Recently, he is the chair of the International Organization Board of ic-cmtp6 the 6th International Conference on Competitive Materials and Technological Processes and ec-siliconf2 the 2nd European Conference on Silicon and Silica Based Materials.

1. Introduction

Nowadays, ceramics and ceramic composites play an important role in the industries due to the high need for porous materials with superior physical, chemical, and mechanical properties [1-8]. Many research works have been carried out to synthesize ceramics and ceramic matrix composites for different applications to satisfy this increased demand [9-12]. Several research studies focus on using relatively cheap raw materials to produce cost-effective composite materials [13-15]. Mullite strengthened carbon and silicon carbide composites are drawn a huge interest recently [16-18]. Due to their superior properties, such as relatively low density, good thermal stability, and oxidation resistance. These good characteristics make mullite-based composites a material of choice for different applications, especially optical and electronic device applications and high-temperature applications, for instance, refractory materials and coatings for a turbine blade [19-20]. The main reason beyond the synthesis of the composite materials is to overcome the brittleness of the monolithic ceramics, which restricts their applications.

Mullite ($3Al_2O_3.2SiO_2$) is an important material for both traditional and advanced ceramics. Due to its outstanding characteristics such as low thermal conductivity, low thermal expansion coefficient, and superior creep resistance, high resistance to corrosive environments, and high-temperature strength [21-22]. The formation of the mullite phase is normally taking place upon the reaction of silica (SiO_2) with alumina (Al_2O_3) at a temperature above 1000 °C [23]. The morphology and purity of the mullite phase depend on the raw materials composition, preparation method, and sintering temperature. *Fig. 1* illustrates the phase diagram of the SiO_2-Al_2O_3 system. In this system, mullite is the only stable intermediate phase at atmospheric pressure. Mullite is normally found in man-made ceramics; it can rarely be found in nature [20]. Mullite structure can incorporate variable cations such as Ga^{3+}, B^{3+}, Na^{+}, Mg^{2+}, Eu^{2+} etc., in different concentrations [24]. A dense mullite ceramic with high purity is difficult to synthesize through the traditional sintering techniques; normally, a porous ceramic with a glassy phase is obtained [25].

Carbonization is a thermochemical process in which high carbon content is produced through thermal degradation of biomass normally by pyrolysis in a reduction environment [26]. The carbonization is highly affected by temperature, moisture content, and biomass composition. Wood usually consist of cellulose (48%), hemicel1ulose (19%), lignin (24%) extractive (7.5%), Ash (1.6%) and moisture (33%). The amount

of these constituents varies from one plant species to another [27]. The cellulose consists of straight-chain macromolecules; it has a crystalline nature and is normally incorporated in a matrix of hemicellulose and lignin [28]. Cellulose is the major constituent of biomass. In contrast, hemicellulose has an amorphous structure with a low degree of polymerization. Lignin is a phenolic compound consist of a randomly connected amorphous structure that has high molecular weight. Therefore, the carbonization of these constituents takes place through a series of complex reactions [29]. This process can be observed on thermogravimetry of the biomass. The complex carbonization mechanisms could be divided into five stages. Firstly, upon heating, drying of the biomass takes place with the evaporation of some volatile organic compounds. Secondly, hemicellulose's thermal decomposition will take place to yield organic acids, methanol, and some gases. The next step involves the emission of carbon monoxide, carbon dioxide, some hydrocarbons (methane, ethane, ethylene), and some acids. After that, cellulose decomposes to give water, carbon dioxide, and carbon (charcoal). Moreover, lignin also decomposes into phenolic compounds and methanol. Finally, the carbonization is complete with the full conversion of lignin into carbon and emission of the hydrogen gas [27]. The aim of this research work was to produce composite materials based on mullite and carbon through in-situ carbonization and reactive sintering of different mixtures of Al_2O_3, natural zeolite, and sawdust, to investigate the technical feasibility of the carbonization process and to evaluate the technical features and microstructural characteristics of the produced samples.

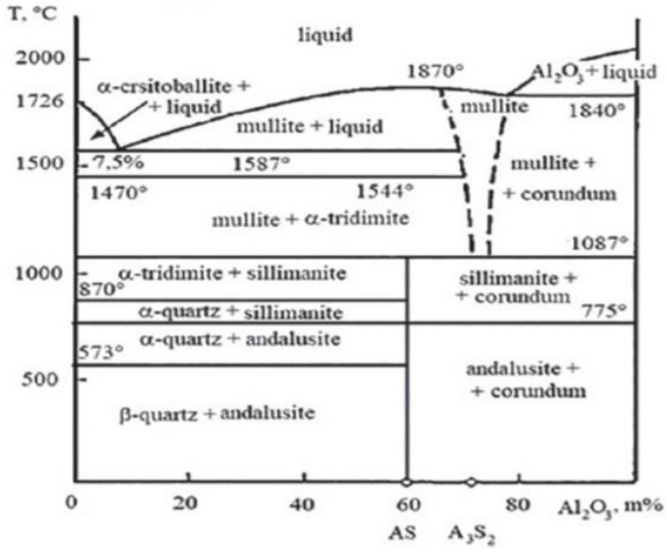

Fig. 1 SiO_2-Al_2O_3 phase diagram [30]
1. ábra SiO_2-Al_2O_3 fázisdiagram [30]

2. Materials and experiments

2.1 Materials

Natural zeolite of high availability mined from Tokaj region in Hungary was initially chosen for this study as silica (SiO_2) source because of their high silica content (83%), alumina from MOTIM company (Hungary) with a purity of 98% was used as primary raw materials. Whilst sawdust which was collected as waste material was used as a carbon source. 60 wt% of alumina and 40wt% natural zeolite were taken and mixed with various sawdust percentages (5%, 10%, 20%, and 30%).

2.2 Methods

Ceramics composites based on alumina, natural zeolite, and sawdust were produced by tuning the sawdust content, as shown in *Fig. 2*. The stoichiometric amount of the raw materials were taken according to the *Table. 1*, mixed and dry-milled for 20 minutes in planetary ball-milling at 200 rpm. The produced powders mix were then uniaxially dry-compacted at 40 MPa to form green ceramic discs with a size of 25 mm in diameter and 10 mm in thickness. The mechanical pressing process was intended to achieve closer contact between the reactants, which can enhance the physicochemical reaction rate. The prepared ceramic specimens were pressureless sintered in an electric laboratory kiln at 1200 °C in a reduction environment in a sealed container. The heating rate and residence time at the maximum temperatures were 30 °C/h and 3 h, respectively.

Alumina (wt%)	Natural zeolite (wt%)	Sawdust (wt%)
60	40	0
60	40	5
60	40	10
60	40	20
60	40	30

Table 1. The percentage of the raw materials used to prepare the mixtures
1. táblázat A keverékek elkészítéséhez felhasznált nyersanyagok százalékos aránya

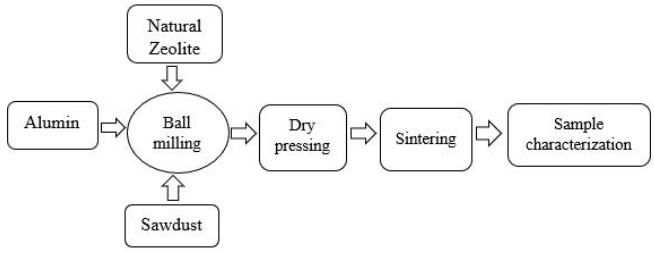

Fig. 2 Flowchart for the production of the ceramic samples
2. ábra Folyamatábra a kerámiaminták előállításához

2.3 Characterization techniques

Phase identification of the raw materials and the sintered specimens were analyzed using an X-ray diffractometer (Rigaku Miniflex II) with CuKα radiation (λ= 1.54184 Å), The scanning speed was 1°/min in 2θ intervals of 0-90 ° and a step size of 0.01015°. The oxide composition of the natural zeolite we examined via X-ray fluorescence (XRF). The thermal properties of the raw materials powders were analyzed by thermogravimetry (TG) and differential thermal (DTA) analyses using a thermal analyzer (setsys evolution 1750 SETARAM). All the thermal tests were done in air at a heating rate of 5 °C/min. The microstructural characteristics of the fracture surface of the produced composite materials were done using scanning electron microscopy (SEM, S-4800, Hitachi, Japan) at an accelerating voltage of 10 kV. Different technical characteristics, including apparent porosity, bulk density, water absorption, and volume shrinkage of the fired ceramic specimens, were obtained using Archimedes technique.

3. Results and discussions

The investigation of the prepared ceramic specimens confirms that tuning the amount of the sawdust leads to different colours and shrinkages of the samples (*Fig. 3*). This could be attributed to the physicochemical reactions, which highly alter the microstructure and the properties of the samples.

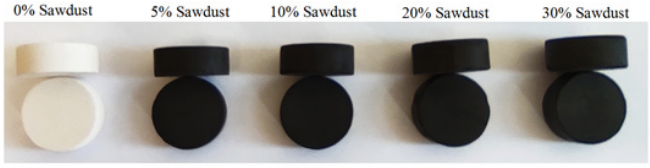

Fig. 3 Produce ceramic samples with different percentage of sawdust
3. ábra Különböző arányú fűrészporral készült kerámiaminták

3.1 XRD investigations

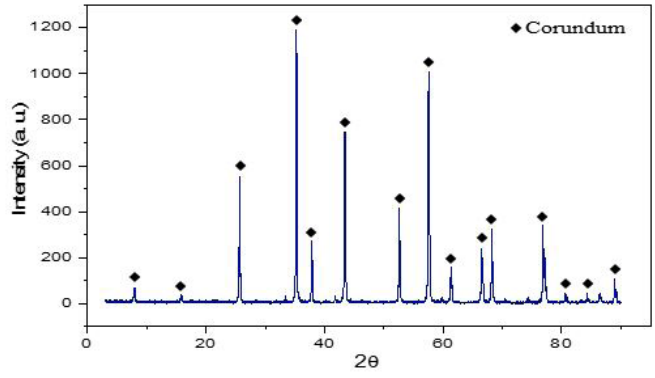

a)

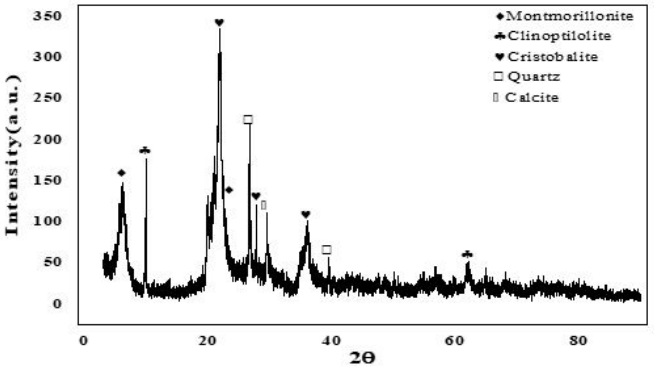

b)

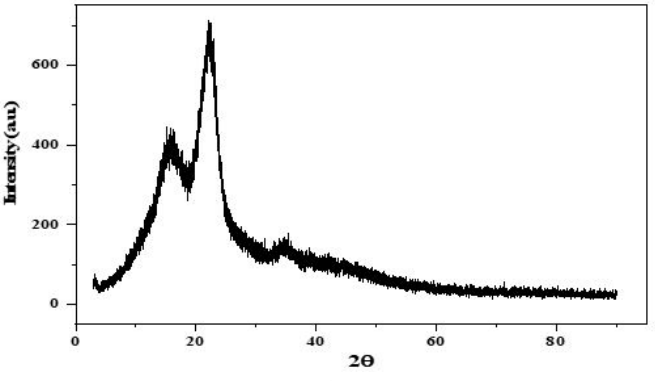

c)

Fig. 4 XRD diffraction pattern of a) alumina, b) natural zeolite, and c) sawdust
4. ábra a) alumínium-oxid, b) természetes zeolit és c) fűrészpor XRD diffrakciós mintázata

Fig. 4 a shows the XRD analysis of the alumina, which reveals the presence of single-phase corundum. The XRD patterns of natural zeolite (*Fig. 4.b*) show different mineral phases, including montmorillonite, clinoptilolite, cristobalite, quartz, and calcite. The XRD diffractogram of sawdust (*Fig. 4.c*) shows two peaks at 2θ 15.5˚ and 22.5˚, which indicate the cellulose I, moreover at 2θ= 34.6˚, a small peak is observed which assigned to cellulose I. lignin and hemicellulose, which have an amorphous structure, are expected to exist in sawdust beside the crystalline cellulose.

Table 2 shows the amount of oxide composition and loss on ignition (LOI) of the natural zeolite obtained from XRF analysis. The major phases were found to be silica with almost 83% and alumina with almost 6%, while the minor phases were MgO, Na_2O, and CaO.

Raw material	Oxides content, %							
	CaO	SiO_2	Al_2O_3	MgO	Na_2O	CO_2	H_2O	Loss on ignition
Natural zeolite	1.12	82.92	5.95	3.21	1.31	0. 88	2.87	5.50

Table 2 Chemical composition of the natural zeolite
2. táblázat A természetes zeolit kémiai összetétele

3.2 SEM investigation of the raw materials

The microstructural properties and morphological characteristics of the raw materials are shown in *Fig. 5*; alumina has a smaller grain size than natural zeolite, which has a relatively larger particle size with irregular shape, while the sawdust has an irregular shape with a porous structure.

3.3 Thermal properties of raw materials

TG/DTA curves of the natural zeolite are shown in *Fig. 6.a*. An overall weight loss of about 10.4% was recorded at 1200 °C. Firstly, 5.5% weight loss was obtained between 40 and 201.3 °C. This weight loss is attributed to the removal of free water. Secondly, 2.06% weight loss was observed between 201.3 to 524.6 °C, which assigned to the evaporation of combined water and burned out of organic content. Finally, a weight loss of 2.84% is achieved between 524.6 and 739 °C, which could be attributed to the firing of the organic content. In DTA curve, several peaks are observed, at 111 °C, an endothermic peak is remarked, this peaks could be designated to the removal of free water, two outstretched peaks are noticed between 201.3 °C and 704.6 °C, which possibly indicates the removal of crystalline water and burning of the organic matter.

Fig. 6 b shows the TG/DTA graphs of the sawdust. The TG graph shows a total weight loss of about 86.4% split into three steps of thermal disintegration. In the first step, a weight loss of 4.6% is recorded at a temperature between 40-238 ˚C; this weight loss might be due to the removal of free water (drying). In the second step, a weight loss of 43.7% was achieved in the temperature range of 238 to 333.8 °C, which could be assigned to the evaporation of the volatile organic content. Finally, 38.07% weight loss is observed in a temperature range of 333.8-647.4 °C, which ascribed to continuous burning of the organic materials achieved from the decomposition of hemicellulose, cellulose, and lignin. In the DTA graph,

broad exothermic peaks are observed in the temperature between 233-659.5 °C, which could be assigned to the thermal disintegration of hemicellulose, cellulose, and lignin respectively. The decomposition of hemicellulose normally takes place at a lower temperature since it has a smaller chain with a linear structure, while the decomposition of cellulose and lignin takes place at a relatively high temperature due to their complex structure.

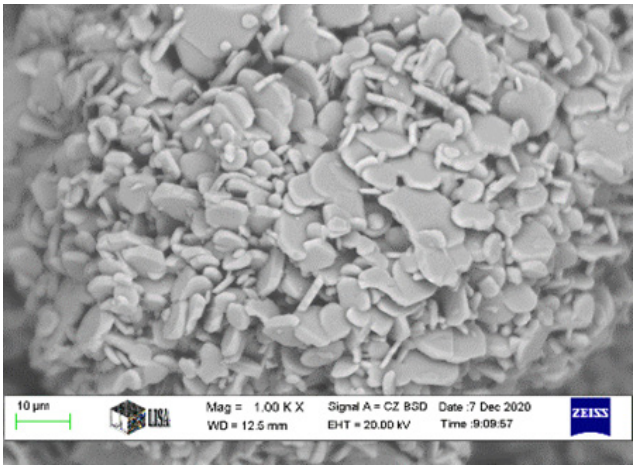

a)

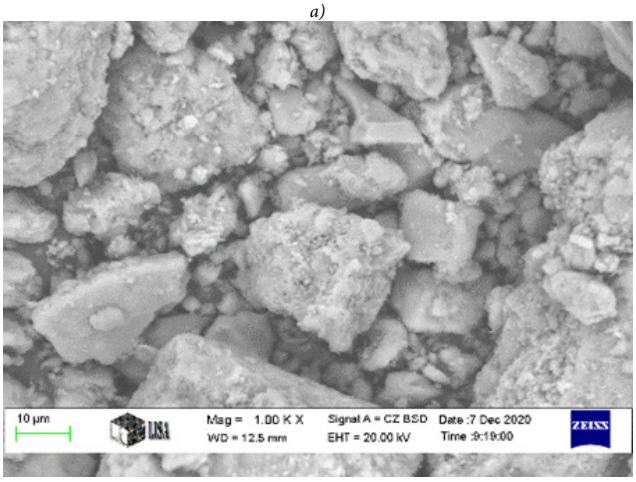

b)

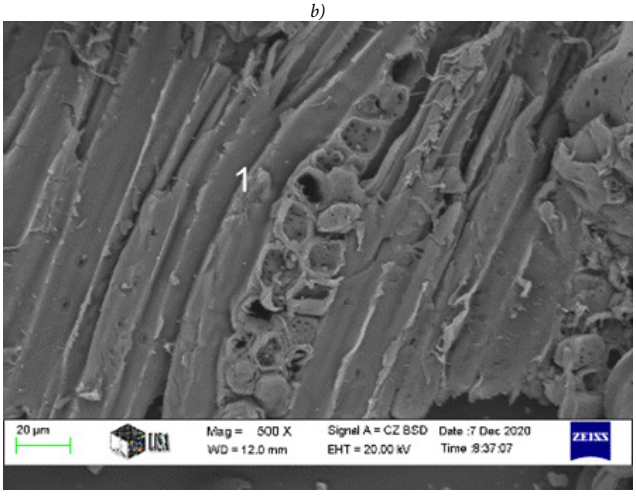

c)

Fig. 5 Scanning electron microscope images of a) alumina, b) natural zeolite, c) sawdust
5. ábra a) alumínium-oxid, b) természetes zeolit, c) fűrészpor pásztázó elektronmikroszkópos felvételei

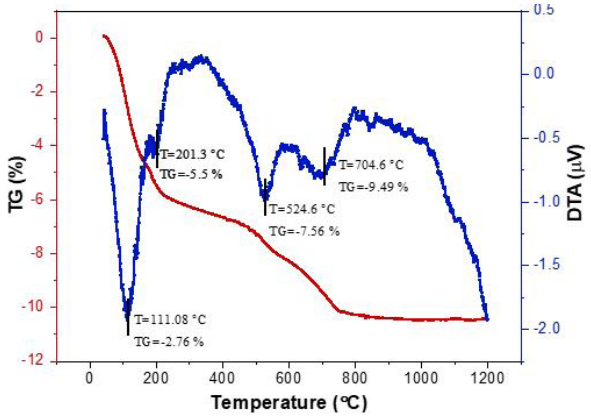

a)

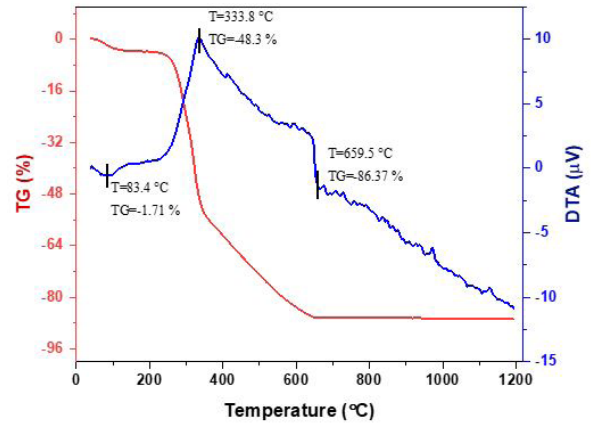

b)

Fig. 6 DTA and TG curves of a) natural zeolite, b) sawdust
6. ábra a) természetes zeolit, b) fűrészpor DTA és TG görbéi

3.4 XRD investigations of the produced ceramic samples

Fig. 7 show the XRD analysis of the sintered ceramic samples, which reveal the decomposition of clinoptilolite, montmorillonite, and calcite and the occurrence of some phsicochemical reaction that yields a mullite phase. It is worth mentioning that the XRD investigation could not detect the carbon indicating that amorphous carbon is formed.

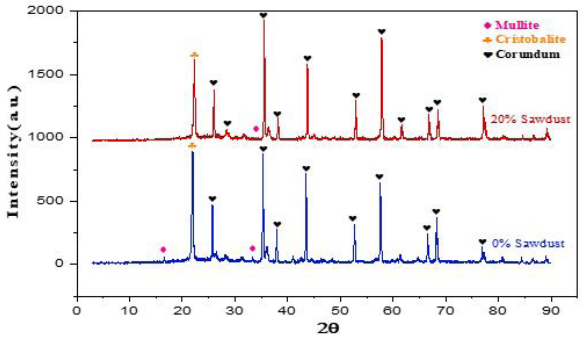

Fig. 7 XRD diffraction pattern of the produced ceramic samples
7. ábra Az előállított kerámiaminták XRD diffrakciós mintázata

3.5 Scanning electron microscopy (SEM) of the produced samples

The morphological features and the microstructural characteristics of the fractured surface of the different ceramic

samples sintered at a temperature of 1200 °C are shown in the scanning electron micrographs (*Fig. 8*). It can be seen that increasing the sawdust content increases the porosity. This occurs due to the effect of carbonization, which converts the biomass into carbon. This process is associated with the evaporation of some organic content leading to pores formation in the samples.

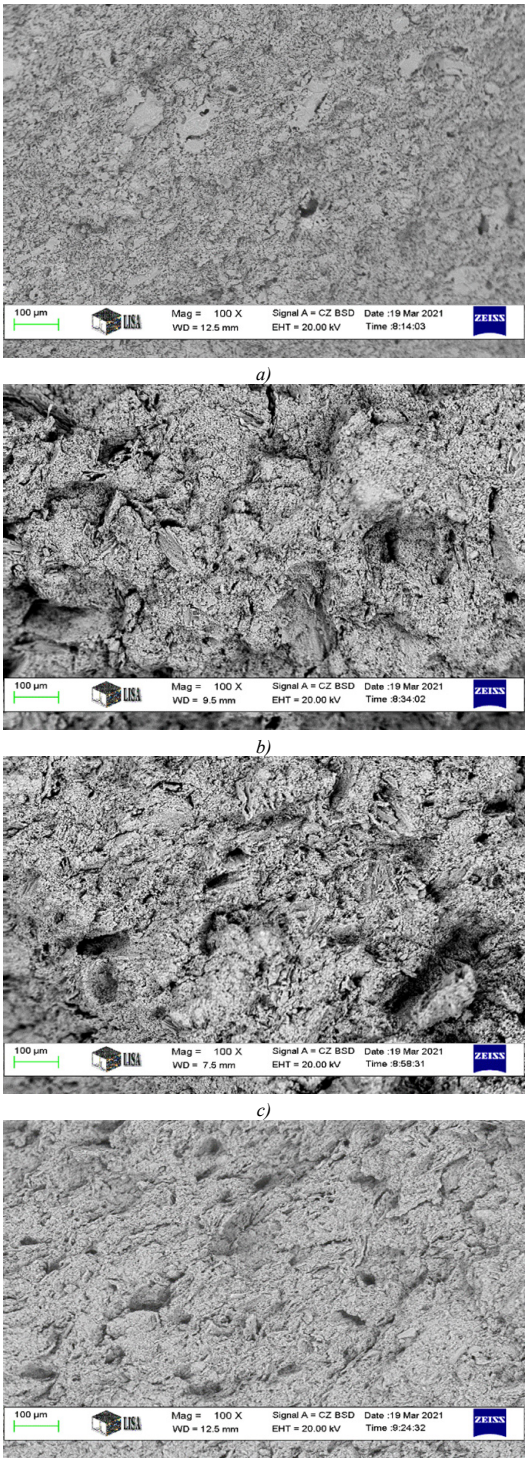

Fig. 8 SEM images of the fracture surface of the sintered samples at ×100 contain a) 0% sawdust b) 10% sawdust c) 20% sawdust, and d) 30% sawdust

8. ábra a) 0% fűrészport b) 10% fűrészport c) 20% fűrészport és d) 30% fűrészport tartalmazó szinterelt minták töretfelületének 100x-szoros nagyítású SEM felvételei

Fig. 9 exhibit a larger magnification of the fracture surfaces of the samples. A noticeable change can be observed due to the difference in the material compositions. A sheet-like structure with a smooth surface can be seen, which indicate the formation of carbon.

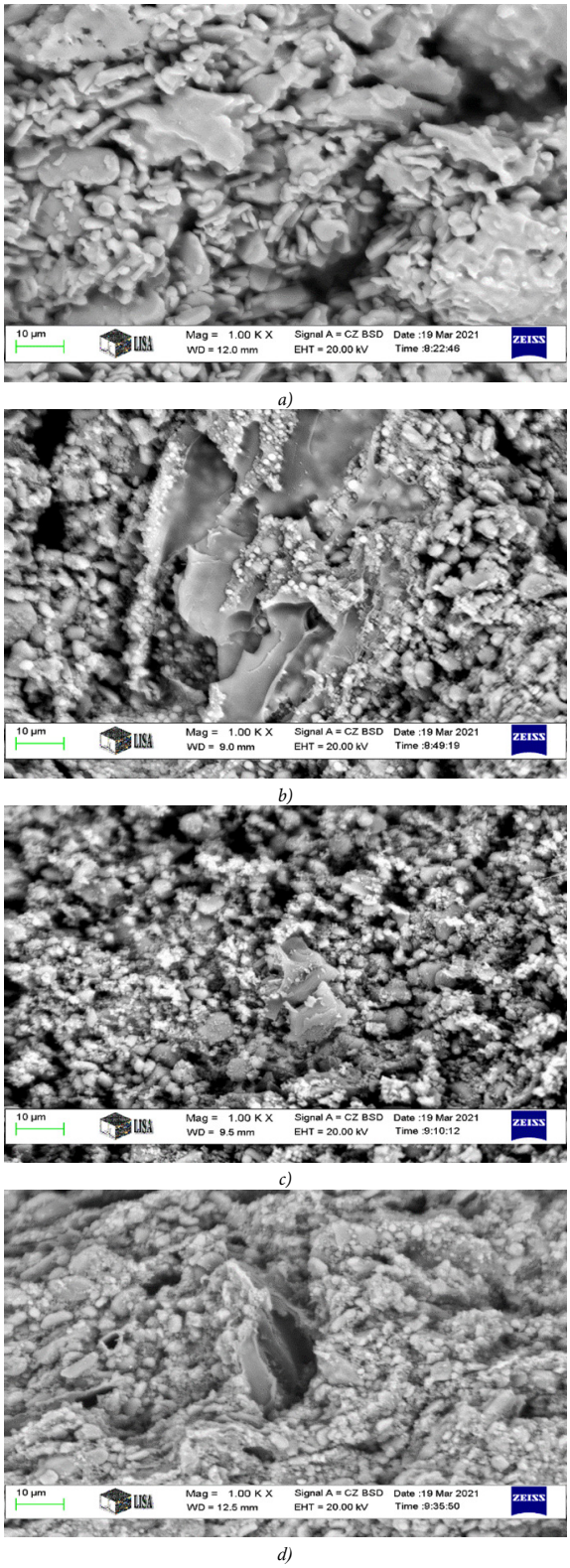

Fig. 9 SEM images of the fracture surface of the sintered samples at ×1000 contain a) 0% sawdust b) 10% sawdust c) 20% sawdust, and d) 30% sawdust

9. ábra a) 0% fűrészport b) 10% fűrészport c) 20% fűrészport és d) 30% fűrészport tartalmazó szinterelt minták töretfelületének 1000x-szeres nagyítású SEM felvételei

3.6 EDS investigation of the produced samples

EDS analysis of the samples are shown in *Fig. 10*. It confirms the formation of the carbon in the samples, which is highly influenced by the amount of sawdust used as raw material. Using 10%, 20% and 30% sawdust lead to the formation of 8%, 10.3% and 14.54% of carbon, respectively, in the samples.

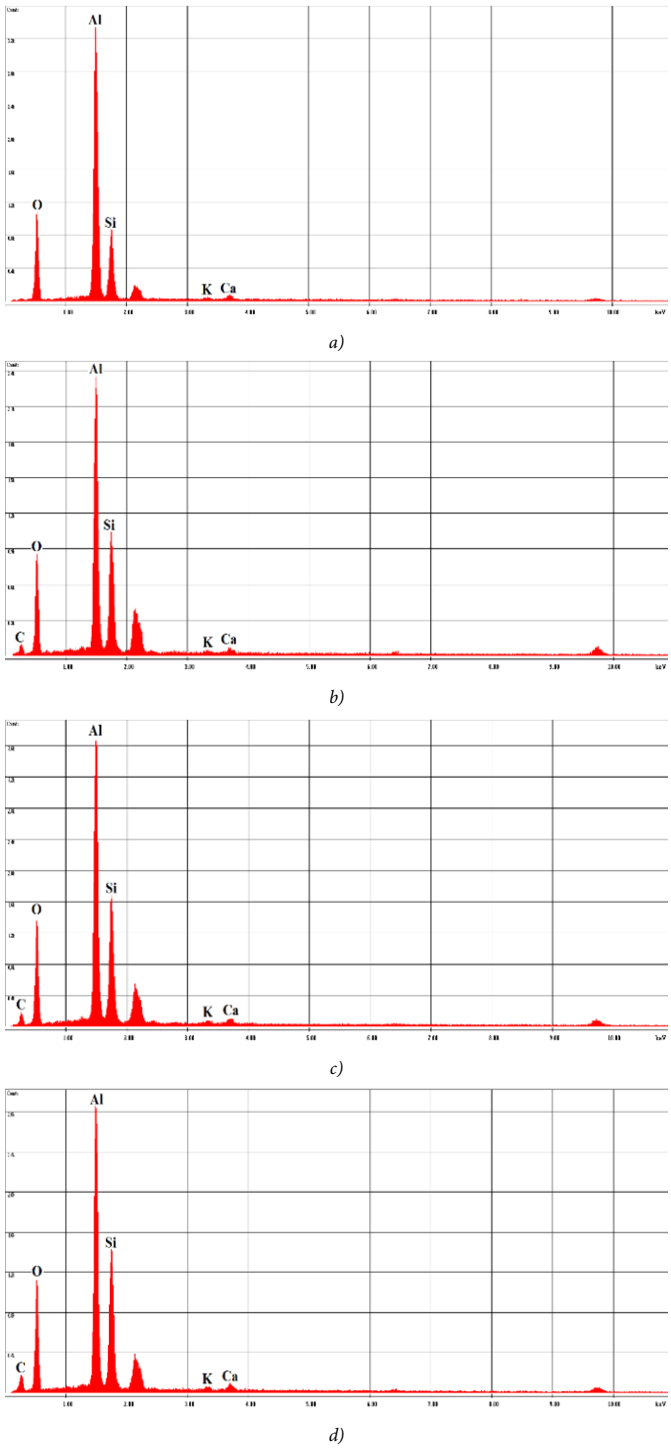

Fig. 10 EDS analysis of the sintered samples contain a) 0% sawdust b) 10% sawdust c) 20% sawdust and d) 30% sawdust

10. ábra a) 0% fűrészport b) 10% fűrészport c) 20% fűrészport és d) 30% fűrészport tartalmazó szinterelt minták EDS-elemzése

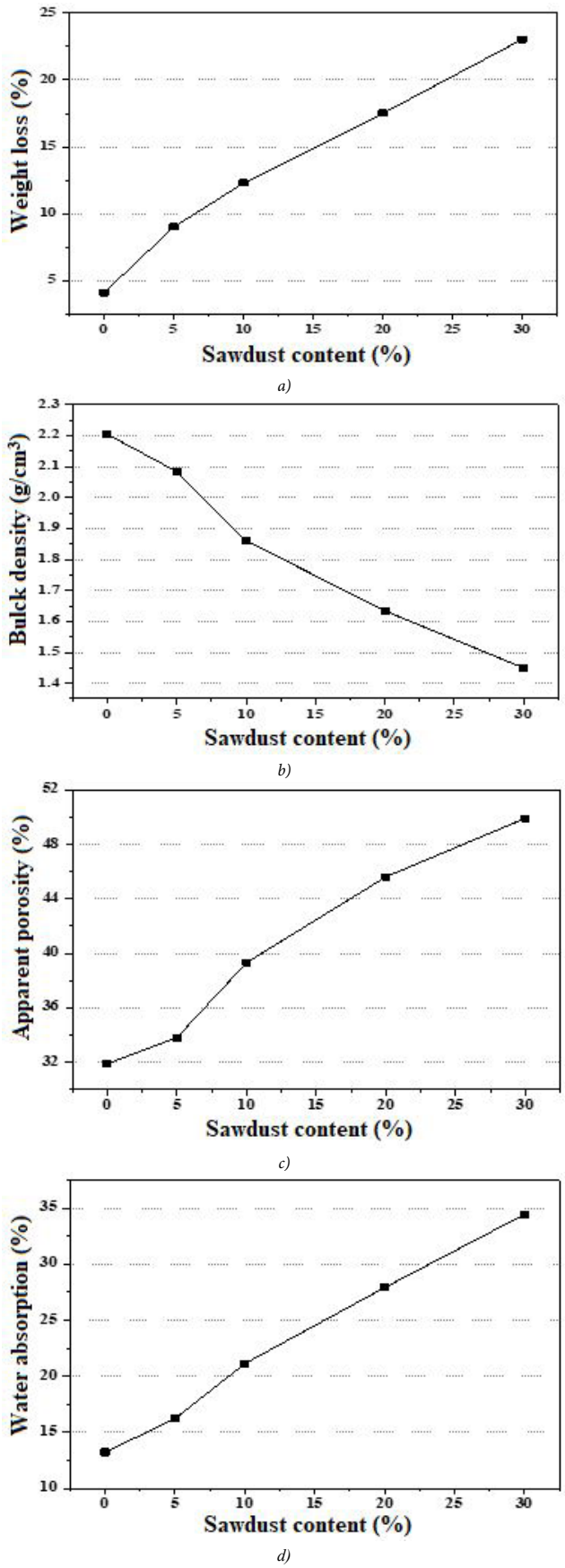

Fig. 11 The correlation between a) weight loss, b) density, c) apparent porosity, and d) water absorption of produced ceramic samples and sawdust content

11. ábra a) a tömegcsökkenés, b) a sűrűség, c) a látszólagos porozitás és d) az előállított kerámiaminták vízfelvétele fűrészportartalom függvényében

3.7 Technical properties of the produced ceramic samples

Fig. 11. a shows the weight loss measurements of the different samples. As the sawdust percentage increased in the sample. The weight loss is proportionally increased and reached a maximum value (23%) when 30% of the sawdust is used; the highest value of the weight loss is coming from the decomposition of sawdust in the reduction atmosphere, which leads to carbonization associated gasification process, moreover small amount of weight loss could be assigned to the decomposition of natural zeolite which leads to the evaporation of free water, crystalline water, and CO_2.

The density measurement of the prepared samples is illustrated in *Fig. 11.b.* With increasing the amount of sawdust, the density is noticeably decreased. This could be explained by the carbonization of sawdust which leads to the evaporation of some gases and the formation of less densified samples. This result is in good agreement with the findings obtained from the TG measurement. Moreover, above 1100 °C, decomposition of natural zeolite followed by some physicochemical reaction will take place, which might close the pores and hence increase the density.

The apparent porosity and water absorption are shown in *Fig. 11. c* and *11. d*, respectively. The two graphs show quite similar curves since the two properties are connected. Both properties exhibit increase in their value as the amount of sawdust increases. This could be explained by the fact that the carbonization process leads to the evaporation of some gases that produce pores and capillaries inside the samples, therefore increase the porosity and water absorption.

4. Conclusions

In-situ carbonization of the sawdust in the composite materials has been successfully carried out in the reduction environment. The sample without sawdust fired into white colour. In contrast, the samples which contain different amount of sawdust fired into black colour indicating the formation of carbon. The XRD analysis confirms the formation of mullite through the reactive sintering process, but it couldn't reveal the occurrence of carbon. This means an XRD amorphous carbon has been formed. The In-situ carbonization, which is associated with gasification, leads to the creation of some pores and capillaries, which affect the technical properties such as porosity, density, and water absorption. This effect can be clearly seen in the SEM images of the produced samples. Thes EDS investigation confirms the formation of carbon. The inclusion of 30 m% sawdust in the samples leads to the formation of more than 14 m% carbon in the sintered specimens.

Acknowledgments

The described article was carried out as part of the EFOP-3.6.1-16-00011 "Younger and Renewing University –Innovative Knowledge City – institutional development of the University of Miskolc aiming at intelligent specialisation" project implemented in the framework of the Széchenyi 2020 program. The work was performed according to the Government research assignment for ISPMS SB RAS, project FWRW-2021-0005.

References

[1] Shushkov, D. A., Kotova, O. B., Ibrahim, J. F. M., Harja, M., Gömze, L. A., Shchemelinina, T. N., Ignatiev, G. V., (2020) Építőanyag–JSBCM Vol. 72. No. 5. p.156. https://doi.org/10.14382/epitoanyag-jsbcm.2020.26

[2] Huang, H., He, M., Kotova, O. B., Dong, F., Gömze, L. A., Kurovics, E., LV, R., Sun, S., (2020) Építőanyag–JSBCM Vol. 72. No. 4. p.124. https://doi.org/10.14382/epitoanyag-jsbcm.2020.20

[3] Ibrahim, J. F. M., Shushkov, D. A., Kurovics, E., Tihtih, M., Kotova, O. B., Pala, P., Gömze, L. A., (2020) Építőanyag–JSBCM Vol. 72. No. 4. p.130. https://doi.org/10.14382/epitoanyag-jsbcm.2020.21

[4] Kotova, O. B., Shushkov, D. A., Gömze, L. A., Kurovics, E., Ignatiev, G. V., Sitnikov, P. A., Ryabkov, Y. I., Vaseneva, I. N., (2019) Építőanyag–JSBCM Vol. 71. No. 4. p.125. https://doi.org/10.14382/epitoanyag-jsbcm.2019.22

[5] Shchemelinina, T. N., Gömze, L. A., Kotova, O. B., Ibrahim, J. F. M., Shushkov, D. A., Harja, M., Ignatiev, G. V., Anchugova, E. M., (2019) Építőanyag–JSBCM Vol. 71. No. 4. p.131. https://doi.org/10.14382/epitoanyag-jsbcm.2019.23

[6] Ibrahim, J. F. M., Gömze, L. A., Kotova, O. B., Shchemelinina, T. N., (2019) Építőanyag–JSBCM Vol. 71. No. 4. p.120. https://doi.org/10.14382/epitoanyag-jsbcm.2019.21

[7] Abdelfattah, M., Kocserha, I., Géber, R., Tihtih, M., Móricz, F. (2020) Evaluating the properties and mineral phases of the expanded clay aggregates with the bentonite additive material, J. Phys. Conf. Ser., vol. 1527, p. 012030, https://doi.org/10.1088/1742-6596/1527/1/012030

[8] Ibrahim, J. F. M., et al (2020) J. Phys.: Conf. Ser. Vol. 1527. 012029. https://doi.org/10.1088/1742-6596/1527/1/012029

[9] Tihtih. M., et al 2020 J. Phys.: Conf. Ser. Vol. 1527. 012043. https://doi.org/10.1088/1742-6596/1527/1/012043

[10] Tihtih, M., Ponaryadov, A. V., Ibrahin, J. F. M., Kurovics, E., Kotova, E. L., Gömze, L. A., (2020) Építőanyag–JSBCM Vol. 72. No. 5. p.165. https://doi.org/10.14382/epitoanyag-jsbcm.2020.27

[11] Ibrahim, J. F. M., Mergen, A., Parlak, U., Kurovics, E., Tihtih, M., Gömze, L. A., (2021) Építőanyag–JSBCM Vol. 73. No. 1. p.24. https://doi.org/10.14382/epitoanyag-jsbcm.2021.5

[12] Tihtih, M., Limame, K., Ababou, Y., Sayouri, S., Ibrahim, J. F. M., (2019) Építőanyag–JSBCM Vol. 71. No. 6. p.190. https://doi.org/10.14382/epitoanyag-jsbcm.2019.33

[13] Ponaryadov, A. V., Kotova, O. B., Tihtih, M., Sun, S., (2019) Építőanyag–JSBCM Vol. 72. No. 5. p.152. https://doi.org/10.14382/epitoanyag-jsbcm.2020.25

[14] Kurovics, E., Kotova, O. B., Ibrahim, J. F. M., Tihtih, M., Sun, S., Pala, P., Gömze, L. A., (2020) Építőanyag–JSBCM Vol. 72. No. 4. p.144. https://doi.org/10.14382/epitoanyag-jsbcm.2020.24

[15] Gömze L. A., Kurovics, E., (2018) J. Phys.: Conf. Ser. Vol. 1045. 012011. https://doi.org/10.1088/1742-6596/1045/1/012011

[16] Kurovics, E., et al (2020) J. Phys.: Conf. Ser. Vol. 1527. 012034. https://doi.org/10.1088/1742-6596/1527/1/012034

[17] Zeng, K. H., Li, Z. Q., Liang, S. L., Lv, X., Ma, Q. S., (2017) Key Engineering Materials Vol. 727, 461. https://doi.org/10.4028/www.scientific.net/KEM.727.461

[18] Sakka, Yoshio, Donald D. Bidinger, and Ilhan A. Aksay (1995) Journal of the American Ceramic Society Vol. 78 No. 2 p.479. https://doi.org/10.1111/j.1151-2916.1995.tb08827.x

[19] Cui, K., Zhang, Y., Fu, T., Wang, J., Zhang, X., (2020) Coatings, Vol. 10. No. 7. p.672. https://doi.org/10.3390/coatings10070672

[20] Schneider, H., Fischer, R. X., Schreuer, J., (2015) Mullite: crystal structure and related properties, Journal of the American Ceramic Society Vol. 98 No. 10 p.2948. https://doi.org/10.1111/jace.13817

[21] Schneider, H., Eberhard, E., (1990) Journal of the American Ceramic Society Vol. 73. No. 7. p.2073. https://doi.org/10.1111/j.1151-2916.1990.tb05270.x

[22] Serra, M. F., Conconi, M. S., Gauna, M. R., Suárez, G., Aglietti, E. F., Rendtorff, N. M., (2016) Journal of Asian Ceramic Societies Vol. 4. No.1. p.61. https://doi.org/10.1016/j.jascer.2015.11.003

[23] Matveev, V. A., Maiorov, D. V., Kondratenko, T. V., (2020) Glass and Ceramics 1-6. https://doi.org/10.1007/s10717-020-00223-6

[24] Kurovics, E., Kotova, O. B., Gömze, L. A., Shushkov, D. A., Ignatiev, G. V., Sitnikov, P. A., Ryabkov, Y. I., Vaseneva, I. N., Gömze, L. N., (2019)

Építőanyag–JSBCM Vol. 71. No. 4. p.114. https://doi.org/10.14382/epitoanyag-jsbcm.2019.20
[25] Komarneni, S., Schneider, H., Okada, K., (2005) Mullite Synthesis and Processing, https://doi.org/10.1002/3527607358.ch4
[26] Lewandowski, W. M., Ryms, M., Kosakowski, W., (2020) Processes Vol. 8 No. 5. p.516. https://doi.org/10.3390/pr8050516
[27] Rotich, P. K., (1998) Carbonization and briquetting of sawdust for use in domestic cookers. Diss. University of Nairobi
[28] Srndovic, J. S., (2011) Interactions between wood polymers in wood cell walls and cellulose/hemicellulose biocomposites. Chalmers University of Technology
[29] Yang, J., Ching, Y. C., Chuah, C. H., (2019) Polymers Vol. 11. No. 5. p.751. https://doi.org/10.3390/polym11050751
[30] Bobkova, N. M. (2007) Fizicheskaya Himiya Tugoplavkih Nemetallicheskih i Silicatnyh Materialov, Yvyshej Shaya, Minszk, pp.88-90 [E-book] ISBN 978-985-06-1389-9

Ref.:
Ibrahim, Jamal-Eldin F. M. – **Apkarian**, Afanasy S. – **Tihtih**, Mohammed – **Kulkov**, Sergei N. – **Gömze**, László A.: *In-situ carbonization of natural zeolite-alumina composite materials incorporated sawdust* Építőanyag – Journal of Silicate Based and Composite Materials, Vol. 73, No. 4 (2021), 137–144. p. https://doi.org/10.14382/epitoanyag-jsbcm.2021.20

Study of transverse deformation of porous alumina during uniaxial mechanical tests

A. D. KASHIN ▪ Institute of Strength Physics and Materials Science SB RAS, Tomsk, 634055 Russia ▪ kash@ispms.ru
A. S. KULKOV ▪ Institute of Strength Physics and Materials Science SB RAS, Tomsk, 634055 Russia
S. N. KULKOV ▪ Institute of Strength Physics and Materials Science SB RAS, Tomsk, 634055 Russia ▪ kulkov@ms.tsc.ru
E. KUROVICS ▪ Institute of Ceramics and Polymer Engineering, University of Miskolc, Hungary ▪ fememese@uni-miskolc.hu
L. A. GÖMZE ▪ Institute of Ceramics and Polymer Engineering, University of Miskolc, Hungary, IGREX Engineering Service Ltd ▪ femgomze@uni-miskolc.hu
Érkezett: 2021. 06. 03. ▪ Received: 03. 06. 2021. ▪ https://doi.org/10.14382/epitoanyag-jsbcm.2021.21

Abstract
In this article presents the results of laboratory tests and analysis of the mechanical behavior of Al_2O_3-based samples during mechanical uniaxial compression testing. The samples with different porosities are obtained via different sintering temperatures. It has been shown that an increase of strength and, accordingly, decrease in porosity are significantly determined the changes of the Poisson's ratio under loading, and this change begins long before the appearance of the first internal microcracks in the internal parts of the material, i.e., the appearance of excess volume. These results clearly show the phenomenon of dilatancy, with a sharp increase of effective Poisson's ratio.
Keywords: Al_2O_3, porosity, dilatancy, compression testing, transverse strain, X-ray diffraction
Kulcsszavak: Al_2O_3, porozitás, dilatáció, nyomószilárdság teszt, keresztirányú alakváltozás, röntgendiffrakció

A. D. KASHIN
is working as research assistant under supervision of Prof. Kulkov at Institute of Strength Physics and Materials Science of the Russian Academy of Sciences in Tomsk.

Aleksey S KULKOV
is physicist and has got PhD scientific degree at Tomsk State University in Russian Federation. At present he is working as research fellow at Institute of Strength Physics and Materials Science of the Russian Academy of Sciences in Tomsk.

Sergei N. KULKOV
is professor at the Tomsk State University and head of Department of Ceramics in the Institute of Strength Physics and Materials Science of the Russian Academy of Science since 1989. His research works are represented in 5 books, more than 150 articles, 18 patents and many International Symposiums and Conferences. At present he is head of department „Theory of Strength and Mechanic of Solids", member of „The American Ceramic Society" of „The APMI - International" and the DYM AT Society (France).

Emese KUROVICS
is graduated in the University of Miskolc, Institute of Ceramics and Polymer Engineering as a material engineer, where she actually continues her study as PhD student under supervision of Prof. L. A. Gömze.

László A. GÖMZE
is establisher and professor of the Department of Ceramics and Silicate Engineering in the University of Miskolc, Hungary. He is author or coauthor of 2 patents, 6 books and more than 300 scientific papers. Recently, he is the chair of the International Organization Board of ic-cmtp6 the 6th International Conference on Competitive Materials and Technological Processes and ec-siliconf2 the 2nd European Conference on Silicon and Silica Based Materials.

1. Introduction

The analysis of the current state of ceramic materials researching shows that the main interest is represented by the studies of correlation between porosity and strength of ceramics. The main researches of Al_2O_3-based ceramic materials are carried out in the field of compression testing, structure analysis, X-ray diffraction etc. [1-7]. There is much less attention given to the research of the dilatancy phenomenon, based on the Poisson's ratio change of Al_2O_3 samples with different porosities obtained at different sintering temperatures.

Identification of unstable crack growth threshold (threshold of absolute dilatancy) can be done with a good level of precision, but identification of the onset crack initiation (threshold of relative dilatancy) is not easy, especially in porous materials [8-9]. In last years various authors have proposed different methods for crack initiation threshold identification [10-11], for example, the change in Poisson's ratio as an indicator for establishing crack initiation threshold.

The increase in the specific volume of the material during the dilatancy process corresponds to an increase in the effective Poisson's ratio. Formally, during measurements, it is possible to obtain an increase in this value to 1 or more, although, as is known, for continuous media, the maximum possible value of the Poisson's ratio (the ratio of the values of longitudinal and transverse relative deformations) can be not more than 0.5. Ceramic materials and rocks very often have residual porosity, so under the influence of stresses, compaction of the material can occur, and at the same time, due to the anisotropy of loading, the initial value of the Poisson's ratio can be very small. At high stresses, compaction is replaced by dilatancy with an increase in the effective Poisson's ratio and subsequent fracture.

Apparently, the appearance of microcracks in such materials occurs at stresses below the elastic limit, but in general, the loading diagram corresponds to an elastic-plastic body.

Literature data shows that when loading, for example, soil, there is a non-linearity not only in the volume deformability (compression), but also in shear deformation, which are caused not only by tangential, but also by normal stresses, with the appearance of the dilatancy effect, which in the case of crushing, i.e., micro-destruction, leads to the need to take into account other effects – hardening, deformation rate, etc.

However, cumulative studies of Al_2O_3 samples obtained at different sintering temperatures and comprehensively investigated by these methods with the data capturing of transverse deformation in situ, have not been properly carried out yet. The correlation between Poisson's ratio change and transverse strain has also not been thoroughly researched in this class of materials. It is known that Al_2O_3 exhibits a phenomenon of dilatancy under load, but the effect of this phenomenon has not been properly explored yet.

Thus, the **aim** of this paper is to study the internal structure of alumina samples with different porosities and their mechanical behavior under uniaxial loading tests.

2. Materials and methods

Ceramic samples in the form of rectangular parallelepipeds with the initial dimensions 36 x 7 x 6 mm were obtained by pressing commercially pure Al_2O_3 powder. It was mechanically processed in a ball mill in the span of 70 hours, which resulted in producing fine particles with a homogeneous size distribution.

The samples were sintered in the Nabertherm LHT 02/17 high-temperature muffle furnace. The various batches of samples were first slowly heated (within 6 hours) to the set temperatures of 1350°C, 1450°C, 1550°C and 1650°C. Then they were held for 1 hour and then slowly cooled down to 40°C. This was done with the purpose of obtaining Al_2O_3 samples with different porosities ranging in between 15 to 50%. Sintered Al_2O_3 samples were mechanically treated using the Struers Secotom-10 precision cutting machine to achieve their plane-parallel flatness. After the three-point bending tests, the samples were cut to 15 mm in height with the 7 x 6 mm cross section for compression testing and simultaneous measuring of transverse strain.

Both bending and compression tests were carried out using the Instron-1185 universal testing machine for determining flexural and compressive strength, technical elastic moduli and longitudinal strain values of the Al_2O_3 samples. Transverse strain was measured mechanically using a strain gauge device - multiturn measuring head - with an accuracy of 1 μm.

The structure parameters and detailed microstructural study of the samples were investigated using the X-ray diffractometer with filtered CuK_α radiation. For the analysis of the polished sample surface the Vega 3 SBH scanning electron microscope was used.

3. Results and discussion

The porosity of the sintered samples varies from 48% at 1350 °C down to 16% at 1650 °C, which correlates well with the already existing data [12]. *Fig. 1a* shows the typical polished surface of the Al_2O_3 sample with 16% porosity. The grain size in the samples obtained at all sintering temperatures varies from 2 to 6 microns. At the same time, as the sintering temperature increases, the percentage of grains with a size of 4 to 6 microns increases. The pore sizes in the samples vary from 1 to 7 microns; for samples with a sintering temperature of 1350 °C and 1450 °C, the main pore size is from 1 to 4 microns, and for the highest temperatures the percentage of pores with a size of 4 to 7 microns increases, which coincides with the literature data [12-13]. The dependence of the porosity on the sintering temperature of the Al_2O_3 samples is shown in the *Fig. 1b*. As can be seen, the porosity of the samples decreases almost linearly with the increase of the sintering temperature, which corresponds with the literature data [13]. Extrapolation of this curve using ***log*** function to determine the temperature at which the porosity of the sample will smaller when 1% one obtained this temperature approximately equal 1850 °C.

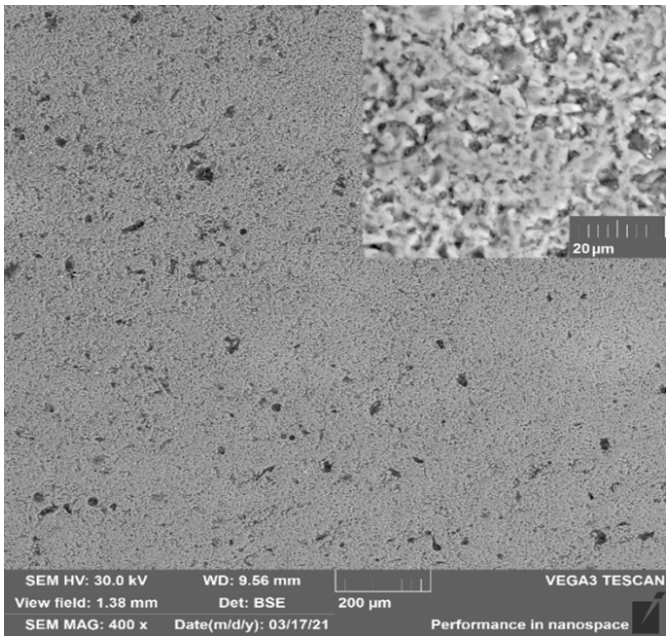

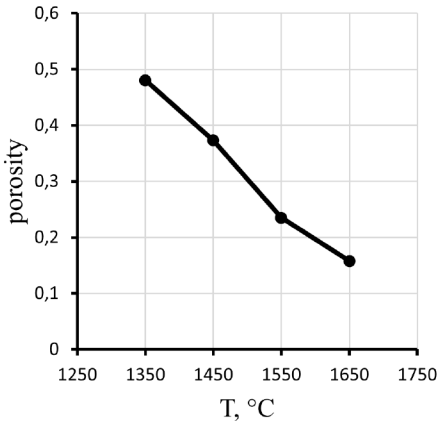

Fig. 1 Polished surface of the Al_2O_3 samples with 16% porosity (a); Dependence of the porosity of the Al_2O_3 samples vs. sintering temperature (b).
1. ábra A 16%-os porozitású Al_2O_3 minták csiszolt felülete (a); Az Al_2O_3 minták porozitása a szinterelési hőmérséklettől függően (b).

The X-ray diffraction studies of the sample surfaces has shown, *Fig. 2a*, that the angles positions of diffraction peaks correspond to the rhombohedral structure of alumina and almost does not change with increasing temperature, which coincides with the literature data [14]. Only the width of X-ray lines had changed with increase of sintering temperature, therefore we have calculated the coherent diffraction domains sizes (CDD) for (012)-line with smallest angle diffraction, *Fig. 2b*, from which one can see that dependency of the coherent diffraction domains sizes for different sintering temperatures of the Al_2O_3 samples are increase with the increase of the sintering temperature and CDD changes from 450 angstroms at the lowest sintering temperature up to 610 angstroms at the highest temperature of 1650 °C. On this figure a dash line is showing the initial powder's CDD, which equals approximately to 400 Å, therefore extrapolation of this dependence on lower temperature had obtained that CDD changes after heating of the samples only after 1250 °C.

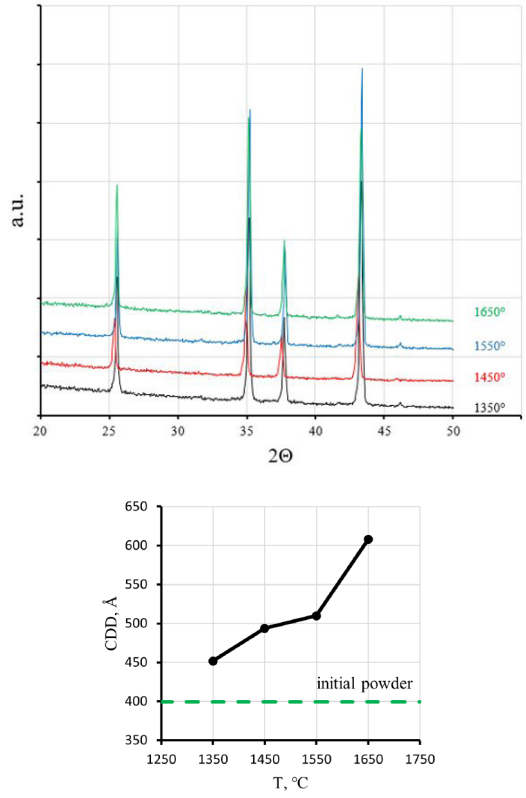

Fig. 2 *X-ray diffraction patterns of the Al_2O_3 samples sintered at different temperatures (a); Dependence of the coherent diffraction domain (CDD) on the sintering temperature (b)*

2. ábra *Különböző hőmérsékleteken szinterelt Al_2O_3 minták röntgendiffrakciós mintázata (a); A koherens diffrakciós domén (CDD) mérete a szinterelési hőmérséklettől függően (b)*

Fig. 3 shows the bending (a) and compressive (b) strengths of samples. The values of flexural strength vary between 8 MPa at 1350 °C and 87 MPa at 1650 °C with an almost linear increase and correlate with porosity of the samples (*Fig. 1b*). The correlation between the compressive strength and the sintering temperature of the alumina samples is shown in the *Fig. 3b*, the values are varied between 28 and 229 MPa. As one can see from these data the well-known correlation between the compressive and bending stresses occurs: compressive stresses exceed the bending stresses by 3 times.

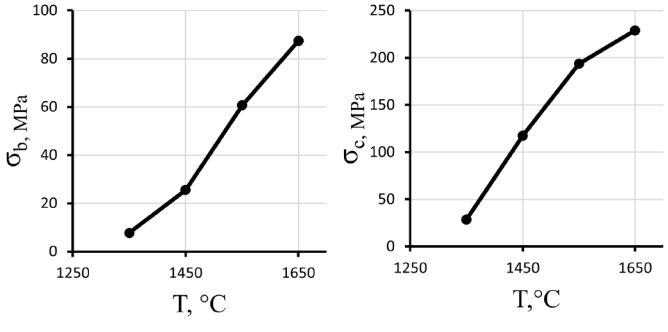

Fig. 3 *Dependency of the bending (a) and compression strengths (b) vs. the sintering temperature*

3. ábra *A hajlító (a) és a nyomószilárdságok (b) szinterelési hőmérséklettől függően*

A typical stress-strain curve during the uniaxial compression test is shown on the *Fig. 4*. The slope of curve in its linear part stipulates the technical Young's moduli of sintered samples, which is equal approximately 10.5 GPa. This modulus is rather small, probably due to a high porosity of sintered ceramics, but the samples sintered at the highest temperature and having the lowest porosity have the highest modulus of elasticity.

In this figure one can see some special region on stress-strain curve: small interruption of increasing stresses, marked with an arrow, which, as a rule, stipulate an internal micro-fault. This fact may be interpreted as due to the dilatancy effect when compressing the ceramic.

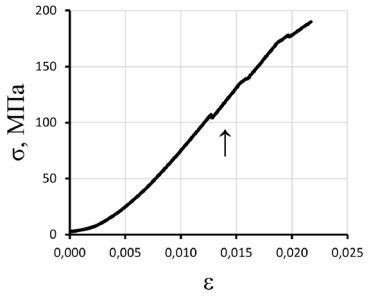

Fig. 4 *Typical stress – strain curve for the uniaxially compressed Al_2O_3 samples; sintering temperature 1450 °C.*

4. ábra *Az 1450 °C-on szinterelt, egytengelyesen összenyomott Al_2O_3 minták tipikus feszültség - alakváltozás görbéje*

In *Fig. 5* the similar stress-strain dependence for the sample sintered at 1350 °C and the correlation between longitudinal – transverse strains measured during the compression test. The slopes of the linear approximations for the longitudinal-transverse strain curve will define the effective Poisson's ratio. At the initial stage of loading the effective Poisson's coefficient has a relatively good value 0.16 and correlate with table data, but at the strain of 0.0125 it sharply changes up to 1.6. This means that during the sample compression the appearance of an excess internal volume in the sample takes place even before the macrofracture effect, forming in internal parts of the sample [15]. These results clearly show the phenomenon of dilatancy, with a sharp increase of effective Poisson's ratio.

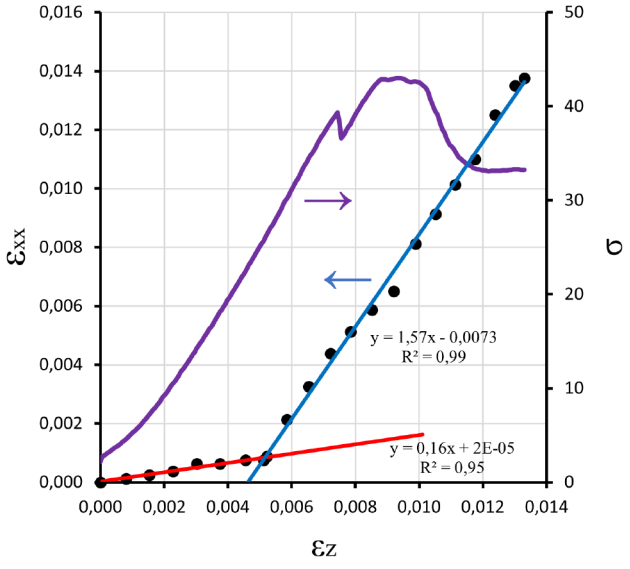

Fig. 5 *Stress-strain curve and the corresponding "longitudinal – transverse" strains for sample sintered at 1350 °C*

5. ábra *A feszültség-alakváltozás görbe és a megfelelő „hosszirányú - keresztirányú" alakváltozás az 1350 °C-on szinterelt minták esetén*

Fig. 6a shows the dependence of the change in the effective Poisson's ratio vs. density of the sintered samples. From the obtained **Δν** values one can see that an increase in strength and, accordingly, decrease in porosity significantly determines the changes of the Poisson's coefficient under loading, and this change begins long before the appearance of the first internal microcracks in the volume of the material, i.e., the appearance of excess volume. Therefore, the dilatancy can occur more easily with the increase in temperature. A similar pattern is observed in the analysis of CDD (*Fig. 6b*), i.e., with the growth of CDD, the formation of internal defects (microcracks) that cause the dilatancy effect can more easily occur in the material.

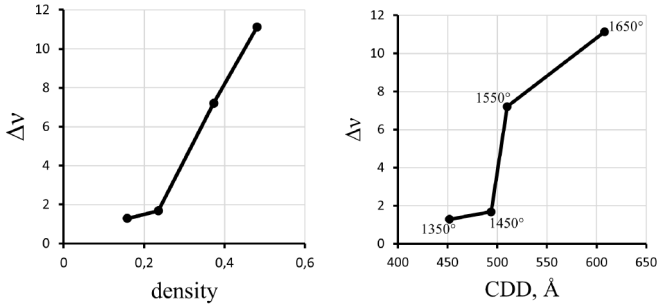

Fig. 6 Correlation between Poisson's ratio difference (Δν) and density of the samples (a); Correlation between Poisson's ratio difference (Δν) and coherent diffraction domain (CDD) (b).

6. ábra A Poisson-féle aránykülönbség (Δν) és a minták sűrűsége közötti összefüggés (a); Korreláció Poisson-aránykülönbség (Δν) és koherens diffrakciós domén (CDD) között (b).

4. Conclusions

It has been observed, that under uniaxial compression the transverse strain measuring allows a determination of Poisson's coefficient for ceramic samples under investigation.

It has been shown that an increase of strength and, accordingly, decrease in porosity are significantly determined the changes of the Poisson's ratio under loading, and this change begins long before the appearance of the first internal microcracks in the internal parts of the material, i.e., the appearance of excess volume. These results clearly show the phenomenon of dilatancy, with a sharp increase of effective Poisson's ratio.

Acknowledgments

The work was performed according to the Government research assignment for ISPMS SB RAS, project FWRW-2021-0005. The described article was carried out as part of the EFOP-3.6.1-16-00011 "Younger and Renewing University –Innovative Knowledge City – institutional development of the University of Miskolc aiming at intelligent specialisation" project implemented in the framework of the Széchenyi 2020 program. The realization of this project is supported by the European Union, co-financed by the European Social Fund.

References

[1] Gömze, L.A., Kulkov, S.N., Kurovics, E. et al, (2018) Investigation of mineralogical composition and technological properties of conventional brick clays, *Építőanyag-JSBCM* Vol. 70, No. 1. p.8 https://doi.org/10.14382/epitoanyag-jsbcm.2018.2

[2] Buzimov A.Y., Eckl W., Gömze L.A. et al, (2018) Effect of mechanical treatment on properties of Si-Al-O zeolites, *Építőanyag-JSBCM* Vol. 70, No. 1. p.23. https://doi.org/10.14382/epitoanyag-jsbcm.2018.5

[3] Gnanavelbabu A., Sunu Surendran K.T., Kumar S., (2020) Influence of ultrasonication power on grain refinement, mechanical properties and wear behaviour of AZ91D/nano-Al_2O_3 *composites*, *Mater. Res. Express* Vol.7 016544 https://doi.org/10.1088/2053-1591/ab64d7

[4] Gevorkyan E.S., Rucki M., Torosyan K.S., Kislitsa M.V. and Y Gutsalenko U.G., (2019) Composite materials based on fine-dispersed Al_2O_3 *with enhanced physical and mechanical properties*, *J. Phys: Conf. Ser.* Vol. 1347 012046 https://doi:10.1088/1742-6596/1347/1/012046

[5] Shirin Pourhosseini, Hossein Beygi and Seyyed Abdolkarim Sajjadi, (2018) Effect of metal coating of reinforcements on the microstructure and mechanical properties of Al-Al_2O_3 *nanocomposites*, *J. Mater. Sci. Technol.*, Vol. 34, No. 2, 145–152 https://doi.org/10.1080/02670836.2017.1366708

[6] Zenkour, A.M., (2020) Quasi-3D Refined Theory for Functionally Graded Porous Plates: Displacements and Stresses, *Phys. Mesomech*., Vol. 23, No. 1 p.39 https://doi.org/10.1134/S1029959920010051

[7] Zenkour A.M., Radwan A.F. (2021) A Nonlocal Strain Gradient Theory for Porous Functionally Graded Curved Nanobeams under Different Boundary Conditions, *Phys. Mesomech*., Vol. 23, No. 6 p.601. https://doi.org/10.1134/s1029959920060168

[8] Azmah Hanim Mohamed Ariff , Mohamad Aznan Mohamad Najib , Suraya Mohd Tahir , Azizan As'Arry & Norkhairunnisa Mazlan, (2020) Effect of sintering temperature on the properties of porous Al_2O_3-10 wt% RHA/10 wt% Al composite, *Advances in Materials and Processing Technologies*, https://doi.org/10.1080/2374068X.2020.1785204

[9] Cieślik J., (2014) Onset of Crack Initiation in Uniaxial and Triaxial Compression Tests of Dolomite Samples, *Studia Geotech. et Mech*. Vol. XXXVI, No. 1, p.23 https://doi.org/10.2478/sgem-2014-0003

[10] Diederichs M.S., (2007) The 2003 Canadian Geotechnical Colloquium: Mechanistic interpretation and practical application of damage and spalling prediction criteria for deep tunnelling, *Can. Geotech. J*., Vol.44, pp. 1082–1116 https://doi.org/10.1139/T07-033

[11] Nicksiar M., Martin C.D., (2012) Evaluation of Methods for Determining Crack Initiation in Compression Tests on Low-Porosity Rocks, *Rock Mech. Rock Eng*., Vol. 45, pp.607–617 https://doi.org/10.1007/s00603-012-0221-6

[12] Kulkov A.S., Smolin I.Yu., and Mikushina V.A., (2018) Investigation of mechanical response of Al_2O_3 *ceramic specimens to loading with consideration for their structural features*, *AIP Conf. Proc.* Vol. 2051, 020162 https://doi.org/10.1063/1.5083405

[13] Shengfang Shi, Sunghun Cho, Tomoyo Goto, Tohru Sekino, (2020) The effects of sintering temperature on mechanical and electrical properties of Al_2O_3/Ti composites, *Mater. Today Commun*. Vol. 25 101522 https://doi.org/10.1016/j.mtcomm.2020.101522

[14] Momohjimoh I., Saheb N..Hussein M.A, Laoui T.,Al-Aqeeli N., (2020) Electrical conductivity of spark plasma sintered Al_2O_3–SiC and Al_2O_3-carbon nanotube nanocomposites, *Ceram. Int.* Vol. 46 pp. 16008–16019 https://doi.org/10.1016/j.ceramint.2020.03.151

[15] Cao, K., Khan, N., Liu, W. et al. (2021) Prediction Model of Dilatancy Stress Based on Brittle Rock: A Case Study of Sandstone, *Arab J Sci Eng* Vol. 46, pp. 2165–2176 https://doi.org/10.1007/s13369-020-05041-0

Ref.:
Kashin, A. D. – **Kulkov**, A. S. – **Kulkov**, S. N. – **Kurovics**, E. – **Gömze**, L. A.: *Study of Transverse Deformation of Porous Alumina during Uniaxial Mechanical Tests*
Építőanyag – Journal of Silicate Based and Composite Materials, Vol. 73, No. 4 (2021), 145–148. p.
https://doi.org/10.14382/epitoanyag-jsbcm.2021.21

Mechanical properties of mullite reinforced ceramics composite produced from kaolin and corn starch

Emese KUROVICS ▪ Institute of Ceramics and Polymer Engineering, University of Miskolc, Hungary ▪ fememese@uni-miskolc.hu
Aleksey S. KULKOV ▪ Institute of Strength Physics and Materials Science SB RAS, National Research Tomsk State University
Jamal-Eldin F. M. IBRAHIM ▪ Institute of Ceramics and Polymer Engineering, University of Miskolc, Hungary ▪ jamalfadoul@gmail.com
A. D. KASHIN ▪ Institute of Strength Physics and Materials Science SB RAS, Tomsk, 634055 Russia ▪ kash@ispms.ru
Péter PALA ▪ Refratechnik Hungaria Ltd, Hungary
Veronika NAGY ▪ Institute of Ceramics and Polymer Engineering, University of Miskolc, Hungary
Sergei N. KULKOV ▪ Institute of Strength Physics and Materials Science SB RAS, National Research Tomsk State University ▪ kulkov@ms.tsc.ru
László A. GÖMZE ▪ Institute of Ceramics and Polymer Engineering, University of Miskolc, Hungary, IGREX Engineering Service Ltd ▪ femgomze@uni-miskolc.hu

Érkezett: 2021. 06. 03. ▪ Received: 03. 06. 2021. ▪ https://doi.org/10.14382/epitoanyag-jsbcm.2021.22

Abstract

In this research, the authors have prepared mullite-containing ceramics by mixing Sedlecky ml kaolin, Nabalox 315 alumina and corn starch as a bio-origin additive. Pellets were prepared from the mixtures using an uniaxial compression process. The pressed samples were pre-sintered at 1250 °C using oxidation and reduction atmospheres and then sintered at a temperature above 1400 °C in nitrogen gas. In this way, the typical carbothermal reduction and nitridation processes of clay minerals were performed, reinforced mullite ceramics were prepared and their main mechanical properties were investigated. Based on the obtained results, sintering in nitrogen gas resulted in a more wear-resistant surface layer.

Keywords: kaolinite, mullite, nitridation, reduction, wear resistance
Kulcsszavak: kaolinit, mullit, nitridálás, redukálás, kopásállóság

Emese KUROVICS
is graduated in the University of Miskolc, Institute of Ceramics and Polymer Engineering as a material engineer, where she actually continues her study as PhD student under supervision of Prof. L. A. Gömze.

Aleksey S. KULKOV
is physicist and has got PhD scientific degree at Tomsk State University in Russian Federation. At present he is working as research fellow at Institute of Strength Physics and Materials Science of the Russian Academy of Sciences in Tomsk.

Jamal Eldin F. M. IBRAHIM
is a lecturer in the University of Bahri, Khartoum, Sudan, he graduated from University of Marmara, Istanbul, Turkey, Institute of Pure and Applied Sciences, Department of Metallurgical and Materials Engineering, for the time being, he is a PhD student in the University of Miskolc, Institute of Polymer and Ceramics Engineering, under supervision of Prof. L. A. Gömze.

A. D. KASHIN
is working as research assistant under supervision of Prof. Kulkov at Institute of Strength Physics and Materials Science of the Russian Academy of Sciences in Tomsk.

Péter PALA
Is a chemical engineer who finished his study at the University of Pannonia. He has been working in the ceramics industry since 2003, at present he is the managing director of Refratechnik Hungaria Ltd.

Veronika NAGY
is a student of the Faculty of Materials Science and Engineering at University of Miskolc.

Sergei N. KULKOV
is professor of the Tomsk State University and head of Department of Ceramics in the Institute of Strength Physics and Materials Science of the Russian Academy of Science since 1989. His research works are represented in 5 books, more than 150 articles, 18 patents and many International Symposiums and Conferences. At present he is head of department „Theory of Strength and Mechanic of Solids", member of „The American Ceramic Society" of „The APMI - International" and the DYM AT Society (France).

László A. GÖMZE
is establisher and professor of the Department of Ceramics and Silicate Engineering in the University of Miskolc, Hungary. He is author or coauthor of 2 patents, 6 books and more than 300 scientific papers. Recently, he is the chair of the International Organization Board of ic-cmtp6 the 6th International Conference on Competitive Materials and Technological Processes and ec-siliconf2 the 2nd European Conference on Silicon and Silica Based Materials.

1. Introduction

The microstructure, properties and applications of the technical ceramics are greatly influenced by the production techniques [1-3]. Starting with the raw materials, relatively inexpensive natural materials can be used to achieve cost-benefit relationship, but the main drawback is the existence of some quantity of impurities in these raw materials [4-6]. Therefore, during the manufacturing of some high-tech ceramics and composite, high purity synthetic materials are usually used. The produced materials are normally made under special circumstances, for example, preparation of barium-titanate nanopowders through sol-gel method [7-9]. After the starting raw materials are selected, the next step is the formation and sintering process, then finishing the product. The main properties of the ceramics are significantly influenced by the applied temperatures and conditions of the heat treatment [10-12].

Mullite or mullite-containing ceramics can be made from different raw materials. The cost-effective way to produce the mullite phase is through thermal decomposition of kaolin or other aluminosilicates [13-15]. Mullite-based ceramics or high purity mullite ceramics can be formed by the reaction of free SiO_2 and Al_2O_3 [16-19]. By controlling the reaction conditions and heat treatment, a high-tech ceramic powder or products can be prepared from kaolin clay minerals. For example, through the carbothermal reduction reaction (CRR) or the carbothermal reduction and nitridation process (CRN). Using CRR or CRN method, silicon carbide (SiC), silicon oxynitride (Si_2ON_2), silicon nitride (Si_3N_4), SiAlONs and also aluminum nitride AlN can be prepared. In the CRN method, a mixture of various aluminosilicates, like kaolinite and active carbon or carbon black, as a carbon source is sintered at high temperature (1400-1650 °C) using flowing nitrogen gas to create the new crystalline or amorphous phases in the material [20-27]. These new phases and their microstructure can improve the mechanical properties of the mullite-based ceramics.

This research aims to produce mullite-containing ceramics with a reinforced structure during the sintering of kaolin-based ceramics using nitrogen gas above 1400 °C.

2. Materials and experiments

In this research, the authors prepared mullite-containing ceramics by mixing Sedlecky ml kaolin, Nabalox 315 alumina and corn starch as a bio-origin carbon source additive. The kaolin was the main raw material. For making the mixtures, 10 wt.% alumina and other 0, 10, 20, 30 and 40 wt.% corn starch were added to the ceramic powders. The measured powders were milled and homogenized in a planetary ball mill, then cylindrical samples with a diameter of 25 mm were prepared by the uniaxial powder compression process. The pressed samples were pre-sintered at 1250 °C using oxidation (OX) and reduction (RED) atmosphere and then sintered at a temperature above 1400 °C using nitrogen gas (OX-NIT, RED-NIT).

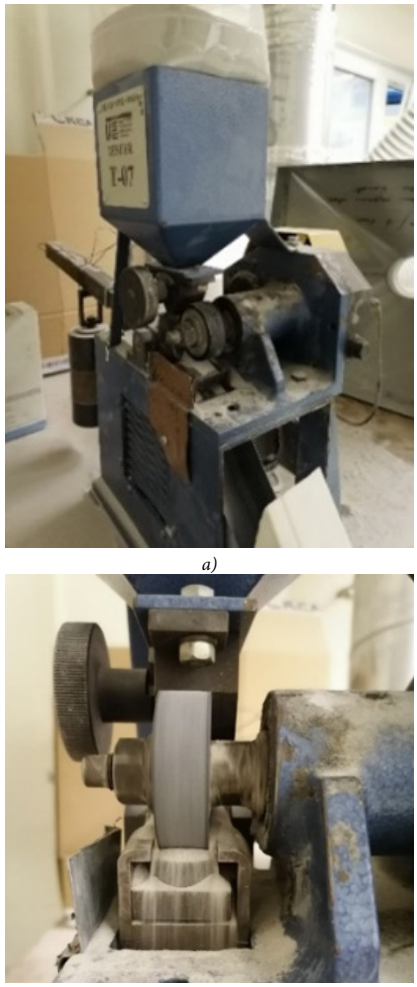

a)

b)

Fig. 1 The abrasion wear resistance tester
1. ábra A kopásállóságmérő

In this way, partly the typical carbothermal reduction and nitridation processes of clay minerals were performed and mullite-based ceramic samples were prepared with a silicon nitride and SiAlON-reinforced surface layer. To compare the properties, a part of the samples was sintered in an oxidation atmosphere at a temperature above 1400 °C (14 OX). The phase compositions of the sintered ceramics were determined by an X-ray diffractometer. Thereafter the mechanical properties of the samples such as micro-Vickers hardness (HV 0,1), abrasion resistance, compressive strength were investigated. During the abrasive wear test (*Fig. 1*), the sample was pressed to the rotating wheel by using a weight on the load arm. The role of the weight is to control the contact pressure. During the test, quartz sand was fed between the rotating wheel and the test sample through a feeder. After the specified times (5, 25 minutes), the sample was removed. The amount of material removed can be determined using the following formula:

$$V_{worn} = \frac{m_1 - m_2}{\rho_{sample}} \cdot 1000 \qquad (1)$$

where V_{worn} is the worn volume loss [mm^3], m_1 is the original weight of the sample [g], m_2 is the weight after the test [g], ρ_{sample} is the density of the sample [g/cm^3] [28].

3. Results and discussions

The distinctive properties of the samples have changed after the different heat treatments. *Fig. 2* shows how the color of samples is changed depending on the used sintering processes.

Fig. 2 The pressed samples after the pre-sintering and sintering processes
2. ábra A préselt minták az elő-szinterelési és szinterelési folyamatok után

The phase compositions of prepared samples were determined by using powder samples which were taken from the pressed samples after their heat treatment. The pre-sintered samples made without corn additive, were found to contain 43% mullite, 25% cristobalite, 1% quartz, 9% corundum and 22% X-ray amorphous based on the XRD analysis. Usually, increasing the amount of vegetable additive increase the amount of X-ray amorphous phase and decreases the amount of corundum and cristobalite phases. Using higher sintering temperature, the mullite crystal structure is changed and the amount of it increases from 43% to 70% because the Al_2O_3 from the corundum phase and the free SiO_2 which was formed during the thermal decomposition of kaolin will create more secondary mullite crystals. After the phase composition analysis of the powders, no significant difference was found between the compositions of the samples made with different production methods. But when the XRD analysis were done just on the surface of the sintered samples, some new crystalline phases (*Fig. 3*) can be found. After the reduction pre-sintering, the test samples have hercynite and SiC phases while during the nitridation sintering process, nitrogen-containing phases are formed like Si_2ON_2 and Si_3N_4. The RED and RED-NIT type samples are containing 20-44% X-ray amorphous phases, which may hide additional nitrogen-containing nanocrystals. This is due to the fact that after the second heat treatment, the quantity of the measured X-ray amorphous phase is increased.

The amount of cristobalite phases was decreased when the added amount of corn additive increased. Therefore, the ceramics made with corn additive can contain higher amounts of nitrogen-containing phases.

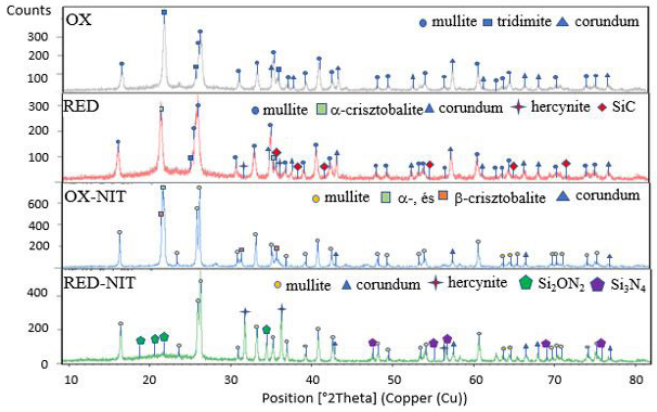

Fig. 3 The phase composition on the surface of the sintered samples made with 40 wt.% corn additive
3. ábra A 40 tömeg% kukorica-adalékkal készített szinterezett minták felszínének fázisösszetétele

During the research work, three characteristic mechanical properties of the samples were investigated after each sintering method. Based on the results, the mechanical properties of the ceramic samples have been carried out after the nitridation sintering. *Fig. 4* shows the micro-Vickers hardness of the ceramic samples as a function of their porosity which was determined through Archimedes water absorption test. Different colors indicate the type of the sintering methods in the Figure: black – oxidation, red – reduction pre-sintering, blue – oxidation pre-sintering and nitridation sintering, green – reduction pre-sintering and nitridation sintering and finally turquoise – oxidation sintering. Generally, the micro-hardness of sintered mullite ceramics is twice the hardness of the original pre-sintered sample. Samples pre-sintered in the oxidation atmosphere have the lowest hardness. During the reduction pre-sintering, carbon-containing phases like SiC particles have formed. These SiC particles increase the micro hardness of the ceramic samples. The micro hardness value of the samples sintered at 1450°C (14 OX) is lower than that obtained after the nitridation sintering.

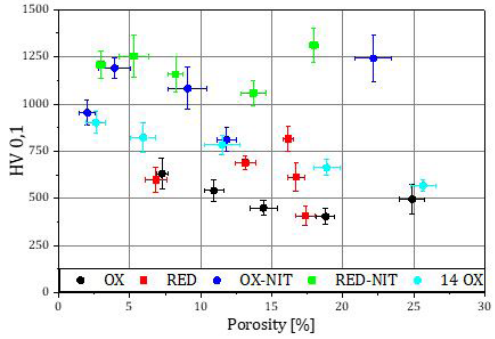

Fig. 4 The micro-Vickers hardness as function of porosity of the ceramic samples
4. ábra A mikro-Vickers keménység a kerámiaminták porozitásának függvényében

Fig. 5 shows the worn material volume after different abrasion time (5 and 25 minutes) as function of the porosity of the sintered samples. As the value of porosity increases, the volume of material worn per unit time increases. Especially in the case of reduction pre-sintering, the wear of ceramic samples increases dramatically. However, there is a significant improvement, thanks to the nitridation sintering. With a longer wear time, the same amount of wear can be measured for example, in the case of oxidation pre-sintering, the volume of material worn during 5 minutes of wear is the same as in the case of nitridation sintering after 25 minutes. In the case of reduction pre-sintering and nitridation sintering, the difference is even greater due to the high wear of the pre-sintered samples. As a result of nitridation sintering, the authors were able to produce mullite-based ceramic samples with higher wear resistance characteristics.

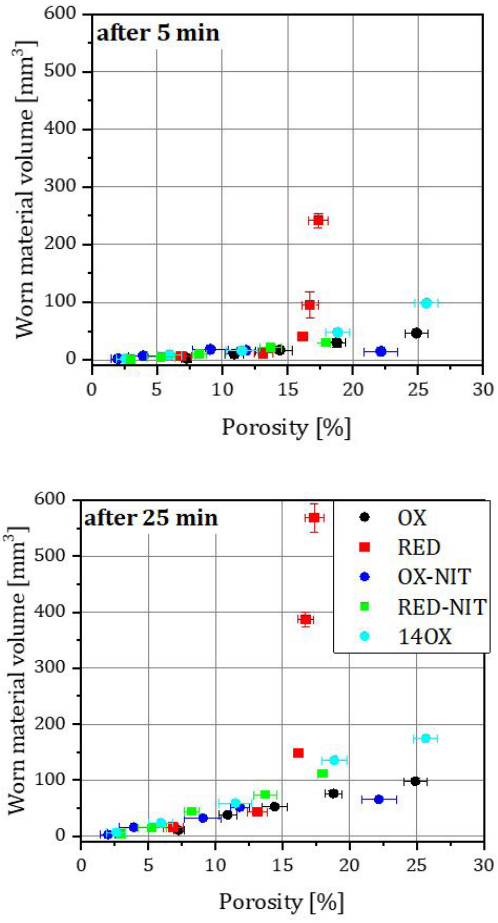

Fig. 5 The worn material volume of the ceramic samples after 5- and 25-minutes abrasion time
5. ábra A kerámiaminták kopott anyagmennyisége 5 és 25 perces koptatási idő után

Fig. 6 shows the change in compressive strength according to the change in porosity. An increase in porosity (less dense ceramic sample) has a negative effect on the mechanical strength. The compressive strength values of the samples prepared by the oxidation pre-sintering method are almost independent of the amount of corn additive. In comparison, the reduction pre-sintering significantly increases the compressive strength of the prepared ceramic samples, but with increasing the porosity of samples, their strength will decrease. For the specimens made without corn, the average strength of the

ceramics increased from 63 MPa (OX) to 215 MPa (RED). This improvement in strength is due to a new microstructure created by sintering in the reduction atmosphere. As a result of nitridation sintering, there is a further improvement in compressive strength.

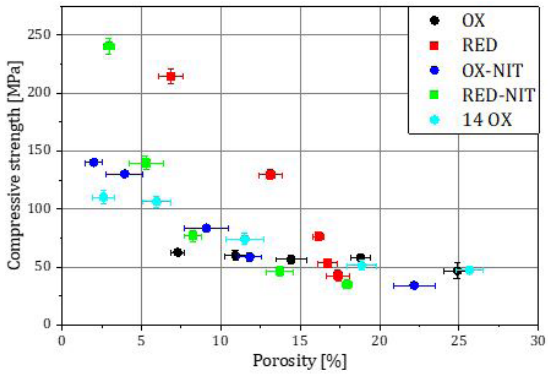

Fig. 6 The compressive strength of the ceramic samples
6. ábra A kerámiaminták nyomószilárdsága

4. Conclusions

Pre-sintering in the reduction atmosphere has formed carbides (SiC) in the structure of the mullite ceramics; because of this, the ceramics have higher micro hardness (HV 0,1) and strength. During the high-temperature nitridation sintering the mullite crystal structure has changed and different nitrogen-containing phases are formed on the surface of the mullite-based ceramic samples depending on the quantity of the corn additive. The properties of the pre-sintered ceramic specimens have significantly improved after the sintering in nitrogen gas. Based on the results, the authors have successfully produced mullite ceramics with a mechanically wear resistant surface layer which are containing silicon nitride, by using high temperature (> 1400 °C) sintering in nitrogen gas.

Acknowledgements

The described article was carried out as part of the EFOP-3.6.1-16-00011 "Younger and Renewing University – Innovative Knowledge City – institutional development of the University of Miskolc aiming at intelligent specialisation" project implemented in the framework of the Széchenyi 2020 program. The realization of this project is supported by the European Union, co-financed by the European Social Fund. Vickers hardness test was performed at the Institutes of Faculty of Mechanical Engineering and Informatics, University of Miskolc.

The work was performed according to the Government research assignment for ISPMS SB RAS, project FWRW-2021-0005.

References

[1] Otitoju, T.A., Okoye, P.U., Chen, G., Li, Y., Okoye, M.O., Li, S. (2020) Advanced ceramic components: materials, fabrication, and applications, Journal of Industrial and Engineering Chemistry Vol. 85, pp. 34–65. https://doi.org/10.1016/j.jiec.2020.02.002

[2] Kulkov, S., Buyakova, S., Gömze, L.A. (2014) Structure and mechanical properties of ZrO_2-based systems, Építőanyag – JSBCM, Vol. 66. No. 1. pp. 1–6. https://doi.org/10.14382/epitoanyag-jsbcm.2014.1

[3] Gömze, L.A., Liszátzné Helvei, Á., Simonné Odler, A., Szabó, M. (2001) Ceramic Yearbook I. 2001, ÉTK and MÉASZ, Budapest, ISBN 963 512 774 X pp.30-85 https://www.researchgate.net/publication/Keramiaipari_evkonyv_I_2001

[4] Jia, Shuhai (2005) Synthesis of SiC Ceramics from Coal Gangue, Materials Science Forum Vols. 486-487. pp. 378-381. https://doi.org/10.4028/www.scientific.net/MSF.486-487.378

[5] Abdelfattah, M., Kocserha, I., Géber, R., Tihtih, M., Móricz, F. (2020) Evaluating the properties and mineral phases of the expanded clay aggregates with the bentonite additive material, J. Phys.: Conf. Ser. Vol. 1527 012030 https://doi.org/10.1088/1742-6596/1527/1/012030

[6] Svidró, J., Svidró, J. T., Diószegi, A. (2020): The role of purity level in foundry silica sand on its thermal properties J. Phys.: Conf. Ser. Vol. 1527 012039 https://doi.org/10.1088/1742-6596/1527/1/012039

[7] Tihtih, M., Limame, K., Ababou, Y., Sayouri, S., Ibrahim, J.F.M. (2019) Sol-gel synthesis and structural characterization of Fe doped barium titanate nanoceramics Építőanyag – JSBCM, Vol. 71, No. 6, 190–193. p. https://doi.org/10.14382/epitoanyag-jsbcm.2019.33

[8] Tihtih, M., Ponaryadov, A.V., Ibrahim, J.F.M., Kurovics, E., Kotova, E.L., Gömze, L.A. (2020) Effect of temperature on the structural properties of barium titanate nanopowders synthesis via sol-gel process Építőanyag – JSBCM, Vol. 72, No. 5, 165–168. p. https://doi.org/10.14382/epitoanyag-jsbcm.2020.27

[9] Tihtih, M., Ibrahim, J. F. M., Kurovics, E., Abdelfattah, M. (2020) Study on the effect of Bi dopant on the structural and optical properties of $BaTiO_3$ nanoceramics synthesized via sol-gel method, J. Phys.: Conf. Ser. Vol. 1527 012043 https://doi.org/10.1088/1742-6596/1527/1/012043

[10] Ma, B., Li, Y., Yan, C., Ding, Y. (2012) Effects of synthesis temperature and raw materials composition on preparation of β-Sialon based composites from fly ash, Trans. Nonferrous Met. Soc. China Vol. 22. Issue 1. pp. 129-133. https://doi.org/10.1016/S1003-6326(11)61151-5

[11] Kurovics, E., Gömze, L.A., Ibrahim, J.F.M., Gömze, L.N. (2019) Effect of composition and heat treatment on porosity and microstructures of technical ceramics made from kaolin and IG-017 additive, IOP Conf. Ser.: Mater. Sci. Eng. Vol. 613 012025 https://doi.org/10.1088/1757-899X/613/1/012025

[12] Sassi, M., Ibrahim J. F. M., Simon, A. (2020) Characterization of foam glass produced from waste CRT glass and aluminium dross, J. Phys.: Conf. Ser. Vol. 1527 012037 https://doi.org/10.1088/1742-6596/1527/1/012037

[13] Naimuddin Ahmen (1964) Studies on the dissociation of mullite, Thesis, University of London, https://spiral.imperial.ac.uk/bitstream/10044/1/16253/2/Ahmed-N-1964-PhD-Thesis.pdf

[14] Kurovics, E., Kotova, O.B., Ibrahim, J.F.M., Tihtih, M., Sun, S., Pala, P., Gömze, L.A. (2020) Characterization of phase transformation and thermal behavior of Sedlecky Kaolin Építőanyag – JSBCM, Vol. 72, No. 4, pp. 144–147. https://doi.org/10.14382/epitoanyag-jsbcm.2020.24

[15] Ondruška, J., Húlan, T., Sunitrová, I., Csáki, Š., Łagód, G., Struhárová, A., Trník, A. (2021) Thermophysical Properties of Kaolin–Zeolite Blends up to 1100 °C, Crystals, Vol. 11, No. 2. p. 165. https://doi.org/10.3390/cryst11020165

[16] Schneider, H., Schreuer, J., Hildmann, B. (2008) Structure and properties of mullite — A review. Journal of the European Ceramic Society, 28, pp. 329–344, http://dx.doi.org/10.1016/j.jeurceramsoc.2007.03.017

[17] Moreno, E.A.X., Scian, A.N. (2015) High Purity Mullite by Slip Casting Method from Calcined Alumina and Kaolinitic Clay, Procedia Materials Science Vol. 8, pp. 245-250 https://doi.org/10.1016/j.mspro.2015.04.070

[18] Mahnicka-Goremikina, L., Svinka, R., Svinka, V. (2018) Influence of ZrO_2 and WO_3 doping additives on the thermal properties of porous mullite ceramics, Ceramics International, https://doi.org/10.1016/j.ceramint.2018.06.125

[19] Mahnicka-Goremikina, L., Svinka, R., Svinka, V., Grase, L., Goremikins, V. (2020) The formation of phases with low or negative linear thermal expansion coefficient in porous mullite ceramics Építőanyag – JSBCM, Vol. 72, No. 3, 91–98. p. https://doi.org/10.14382/epitoanyag-jsbcm.2020.15

[20] Yuan, W., Li, J., Pan, C., Deng, C., Zhu, H. (2012) Synthesis of Al_4SiC_4 powders from kaolin grog, aluminum and activated carbon as raw

materials, Advanced Materials Research Vols. 399-401. pp. 788-791., https://doi.org/10.4028/www.scientific.net/AMR.399-401.788
[21] Lee, J.G., Cutler, I.B. (1979) Sinterable sialon powder by reaction of clay with carbon and nitrogen, American Ceramic Society Bulletin, Vol. 58. pp. 869-871.
[22] Xu, L.-H., Lian, F., Zhang, H., Bi, Y.-B., Cheng, K., Qian, Y.-B. (2004) Optimal design and preparation of beta-SiAlON multiphase materials from natural clay, Materials and Design Vol. 27 (2006) 595–600 https://doi.org/10.1016/j.matdes.2004.12.017
[23] Panda, P. K., Mariappan, L., Kannan, T. S. (2000) Carbothermal reduction of kaolinite under nitrogen atmosphere, Ceramics International, Vol. 26. Issue 5. pp. 455-461. https://doi.org/10.1016/S0272-8842(99)00068-1
[24] Çalışkan, F., Demir, A., Tatlı, Z. (2013) Fabrication of Si_3N_4 preforms from Si_3N_4 produced via CRN technique, Journal of Porous Materials, Vol. 20, p. 1501, https://doi.org/10.1007/s10934-013-9736-9
[25] Tatlı, Z., Demir, A., Yılmaz, R., Caliskan, F., Kurt, A. O. (2007) Effects of processing parameters on the production of β-SiAlON powder from kaolinite, Journal of the European Ceramic Society Vol. 27. pp. 743–747. https://doi.org/10.1016/j.jeurceramsoc.2006.04.062
[26] Kurovics, E., Udvardi, B., Román, K., Ibrahim, J. F. M., Gömze, L. A. (2019) Examination of the carbonization process using kaolin and sawdust. WIT Transactions on Engineering Sciences Vol. 124 p. 17 https://doi.org/10.2495/MC190021
[27] Kurovics, E., Kotova, O. B., Gömze, L. A., Shushkov, D. A., Ignatiev, G. V., Sitnikov, P. A., Ryabkov, Y. I., Vaseneva, I. N., Gömze, L. N. (2019) Preparation of particle-reinforced mullite composite ceramic materials using kaolin and IG-017 bio-origin additives. Építőanyag – JSBCM Vol. 71 No. 4 p. 114 https://doi.org/10.14382/epitoanyag-jsbcm.2019.20
[28] ASTM G 65-00 Standard Test Method for Measuring Abrasion Using the Dry Sand/Rubber Wheel Apparatus, (2000) United States

Ref.:
Kurovics, Emese – **Kulkov**, Aleksey S. – **Ibrahim**, Jamal-Eldin F. M. – **Kashin**, A. D. – **Pala**, Péter – **Nagy**, Veronika – **Kulkov**, Sergei N. – **Gömze**, László A.: *Mechanical properties of mullite reinforced ceramics composite produced from kaolin and corn starch*
Építőanyag – Journal of Silicate Based and Composite Materials, Vol. 73, No. 4 (2021), 149–153. p.
https://doi.org/10.14382/epitoanyag-jsbcm.2021.22

Stress-strain behavior of high porous zirconia ceramic

Irina N. SEVOSTIANOVA ▪ Institute of Strength Physics and Materials Science, SB RAS, Tomsk, Russia ▪ sevir@ispms.ru

Tatiana Yu. SABLINA ▪ Institute of Strength Physics and Materials Science, SB RAS, Tomsk, Russia ▪ sabtat@ispms.ru

Sergei N. KULKOV ▪ Institute of Strength Physics and Materials Science, SB RAS, Tomsk, Russia ▪ kulkov@ms.tsc.ru

Mohammed TIHTIH ▪ Institute of Ceramics and Polymer Engineering, University of Miskolc, Hungary ▪ medtihtih@gmail.com

László A. GÖMZE ▪ Institute of Ceramics and Polymer Engineering, University of Miskolc, Hungary, IGREX Engineering Service Ltd ▪ femgomze@uni-miskolc.hu

Érkezett: 2021. 06. 03. ▪ Received: 03. 06. 2021. ▪ https://doi.org/10.14382/epitoanyag-jsbcm.2021.23

Annotation

In this work, we studied the deformation behavior of ZrO_2 ceramics stabilized with 5.5 wt.% Y_2O_3 with a porosity of 4 - 42% during diametral compression tests ("Brazilian" test). It has been shown that with an increase in porosity from 4 to 42%, the ultimate tensile strength in diametral compression decreases from 115 to 9 MPa. The ultimate strain before fracture decreases from 1 to 0.8%. The effective modulus also decreases with increasing of porosity. The analysis of the "stress-strain" curves showed that the deformation behavior of ceramics is influenced by both the volume and the morphology of the pore space. It been shown that two strain exponent were observed, which indicate a change of deformation mechanism of the ceramic during loading. X-ray diffraction analysis carried out from the front surface of fracture fragments of samples with porosities of 4, 17, and 42% showed that in these materials microstructural parameters such us the size of the coherently diffracting domains of the tetragonal phase and lattice microdistortion changes in comparison with the initial state after sintering. These materials microstructural parameters are changes non-uniformly, which indicate the inhomogeneity of the deformation of this brittle material during compression.

Keywords: ceramics, lattice microdistortion, porous, stress, zirconia
Kulcsszavak: kerámia, rácsos mikrotorzítás, porózus, feszültség, cirkónia

Irina N. SEVOSTYANOVA
PhD Education: 1987: Tomsk Polytechnic Universityengineer.1993-1996: Institute of Strength Physics and Materials Science of the Russian Academy of Sciences in Tomsk - PhD student. 2001: PhD degree from the Institute of Strength Physics and Materials Science of the Russian Academy of Sciences in Tomsk. Field of research: Structure and mechanical property of porous ceramics based zirconia and alumina.

Tatiana Yu. SABLINA
has PhD Education since 1989 at present she is working at the Tomsk State University and Institute of Strength Physics and Materials Science of the Russian Academy of Sciences in Tomsk.

Sergei N. KULKOV
is professor at the Tomsk State University and head of Department of Ceramics in the Institute of Strength Physics and Materials Science of the Russian Academy of Science since 1989. His research works are represented in 5 books, more than 150 articles, 18 patents and many International Symposiums and Conferences. At present he is head of department „Theory of Strength and Mechanic of Solids", member of „The American Ceramic Society" of „The APMI - International" and the DYM AT Society (France).

Mohammed TIHTIH
Is a lecturer in the Sidi Mohamed Ben abdellah University, Morocco, he graduated from Faculty of sciences Dhar El Mahraz, Fez, Morocco, Department of Physics, for the time being, he is a PhD student in the University of Miskolc, Institute of Ceramics and Polymer Engineering, under supervision of Prof. L. A. Gömze.

László A. GÖMZE
is establisher and professor of the Department of Ceramics and Silicate Engineering in the University of Miskolc, Hungary. He is author or coauthor of 2 patents, 6 books and more than 300 scientific papers. Recently, he is the chair of the International Organization Board of ic-cmtp6 the 6th International Conference on Competitive Materials and Technological Processes and ec-siliconf2 the 2nd European Conference on Silicon and Silica Based Materials.

1. Introduction

The study of the deformation and fracture behavior in a brittle porous material under its mechanical loading has recently attracted considerable attention of researchers [1-5]. These studies are important for estimation of the fundamental base for the synthesis of new composite materials which can be used for extremely loaded conditions, as biomaterials, filters, and soundproof materials for various anti-noise devices. Mechanical strength is a key parameter for many ceramic applications where porous ceramic parts are subjected to compression, bending, tension and shear [6]. Also, these data can be very useful for the model study of mechanical properties and processes of fracture of rocks [7]. Today, most mechanical tests have been carried out on dense materials with a uniform structure. The processes of deformation and fracture of porous ceramic materials are being actively investigated, and in literature there are some results of measuring of elastic constants with different porosity [8]. The effects of nonlinear elasticity under mechanical loading of porous ceramics based on zirconia are described in [9]. It has been determined that deformation of materials with a complex internal structure, local strains due to relative displacements and deformations of its structural components play a significant role, which noticeably changes the elastic characteristics of materials. In the literature, this behavior is discussed in terms of the transition from brittle fracture to quasi-plastic [10-13]. This was previously observed in the case of concrete [14], ferroelectric ceramics [15], and a glass or ceramic matrix composites [16]. Recently, a similar deformation behavior was observed for uniaxial compression tests of porous ceramics [17-18], as well as in bending tests of refractory materials [19]. At the same time, works in which other schemes of loading brittle materials are used are not enough. So the performance of direct tests for uniaxial tension of brittle materials is associated with the technical problem of applying tensile axial forces to the sample [20]. To determine the tensile strength of brittle materials, an indirect method for determining the tensile strength of the material, the so-called "Brazilian test", is successfully used, when tensile stresses are formed in the center of the sample [21-23]. The particular qualities of the stress-strain state of the samples during the Brazilian test continue to attract the interest of many researchers from the moment of its proposal. Investigations are carried out by various experimental [22-24] and numerical methods [25-28]. Nevertheless, investigations of the deformation behavior of ceramic materials based on

zirconia in a wide range of changes in pore sizes and pore volume have been insufficiently conducted.

The aim of this work was to study the stress-strain behavior of porous zirconia ceramics with a wide range of porosity during diametral compression tests.

2. Materials and methods

To obtain experimental samples, we used zirconia powder (ZrO_2) stabilized with 5.5 wt% yttrium oxide (Y_2O_3). The study of the ZrO_2 -5.5 wt% Y_2O_3 powder (ZrO_2 (Y)) was carried out on a VEGA Tescan 3 SBH scanning electron microscope. The particle size distribution of the powder, including agglomerates, and a typical SEM image of the powder are shown in *Fig. 1*.

The powder is a finely dispersed mixture of agglomerated particles of irregular shape. The particle size of the powder varies from 0.1 to 2 **μm**, and the fraction of particles up to 0.5 **μm** is about 70%. The specific surface area of the powder (S_{sp}), measured on a SORBI-4.1 device, by low-temperature nitrogen adsorption by the 4-point BET method [29] is 8.05 ± 0.085 m^2/g. According to the results of X-ray phase analysis, the powder consists of tetragonal and monoclinic phases of zirconia. The content of the monoclinic phase in the powder is 44%.

Experimental samples traditional methods of powder metallurgy were prepared. The plasticized (5% carboxymethyl cellulose (CMC) aqueous solution) powder was cold isostatic compaction with a hydraulic press under a pressure of 50 MPa and followed low-temperature annealing of the compacts to remove the binder was carried out at a temperature of 1100 °C with a heating rate of 1.5 °C/min in the MgO powder fill. The final sintering of the samples was carried out in a high-temperature air muffle furnace LHT "Nabertherm" according to the modes presented in *Table 1*. To obtain samples with different porosities, the sintering temperature and isothermal holding time were varied.

The pore structure of the sintered ceramics was studied on polished surfaces using VEGA Tescan 3 SBH scanning electron microscope. The determination of the average pore size and their size distribution was carried out using the ImageJ program; in this case, at least three images of the structure and at least 1000 measurements were used. The ratio of pores size smaller than 30 μm and over 30 μm of all investigated ceramics was calculated by the methods of stereometric metallography [30]. The two-dimensional distribution of pores by size was transformed into a three-dimensional distribution using the basic stereometric equation of Saltykov [30]. Zirconia phase fractions were quantified on sintered and fractured specimens using the X-ray diffraction analysis (XRD). XRD spectra were collected over a 2θ range between 20° and 80° using a powder diffractometer equipped with a Cu X-ray source with a step size of 0.05°with statistical accuracy better 3%. XRD line profile analysis was used to determine of the size of the coherently diffracting domain (D) and crystal lattice microdistortion ($<\varepsilon^2>^{1/2}$) of tetragonal phase of zirconia. The size of the coherently diffracting domains (sCDDs) was calculated by the Scherrer equation [31] for the lines (111) and crystal lattice microdistortion was calculated according to the Stokes – Wilson equation [32] for the lines (004).

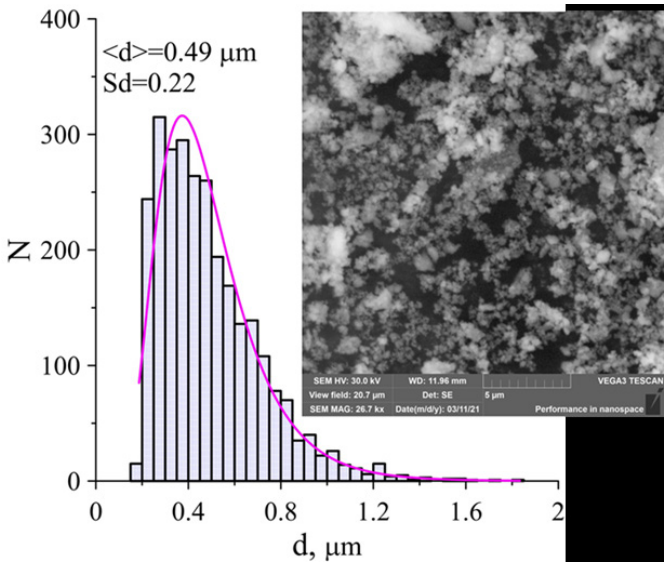

Fig. 1 Particle size distribution of zirconia powder. The insets show the SEM image of the powders
1. ábra A cirkóniumpor részecskeméret-eloszlása. A porok SEM felvétele

The porosity and phase composition of the specimens before diametral compression tests (in the initial state), depending on the sintering conditions, are given in *Table 1*.

Sample number	Sintering conditions, T, °C; τ, h	Porosity, %	Phase composition, %
1	T = 1600 °C, τ = 1 h	4	ZrO_2(*t**) – 80; ZrO_2(c**) – 20
2	T = 1500 °C, τ = 1 h	17	ZrO_2(*t*) – 80; ZrO_2(c) – 20
3	T = 1400 °C, τ = 3 h	29	ZrO_2(t) – 88; ZrO_2(c) – 9 ZrO_2(m***) – trace (less 3)
4	$T_{спек}$ = 1400 °C, τ = 2 h	33	ZrO_2(*t*) – 93; ZrO_2(c) – 6 ZrO_2(*m*) – trace (less 3)
5	$T_{спек}$ = 1350 °C, τ = 1 h	42	ZrO_2(*t*) – 95; ZrO_2(c) – 4 ZrO_2(*m*) – trace (less 3)

*t** – tetragonal phase ZrO_2;
c** – cubic phase ZrO_2;
*m**** – monoclinic phase ZrO_2

Table 1 Porosity and phase composition of ZrO_2 (Y) ceramic samples depending on sintering conditions
1. táblázat ZrO_2(Y) kerámiaminták porozitása és fázisösszetétele a szinterelési körülményektől függően

The phase composition of ceramic samples sintered at temperatures of 1500 and 1600 ° C is represented by high-temperature tetragonal and cubic phases of zirconia in a ratio of 80:20, respectively. With a decrease of the sintering temperature, the ratio of the tetragonal and cubic phases changes, with a decrease in the content of the cubic phase and the appearance of traces of the monoclinic ZrO_2 phase, *Table 1*.

Diametral compression tests (the Brazilian test) of ceramic samples with a diameter of 27.5±0.3 mm and a height of 11.3±0.2 mm were carried out on a universal testing machine "Instron" at a loading rate of 0.1 mm/min with automatic recording of the loading diagram "load - displacement" taking

into account the rigidity of the loading system. The calculation of stresses was performed according to [33].

3. Results and discussion

The pore structure of ZrO_2 (Y) ceramic samples with different porosity and pore space morphology is shown in *Fig. 2*. Interparticle isolated porosity of ceramics with a porosity of 4% (sample 1, table 1), is observed. The average pores size is ≈ 4 μm and the maximum pores size does not exceed 30 μm, *Fig. 2 (a)*. Two types of pores and a bimodal pore size distribution in the structure of ceramic samples with a porosity of 17% and higher (samples 2 - 5, table 1), are observed, *Fig. 2 (b)*. In addition to interparticle porosity (1 - 30 μm), the ceramic contains large interagglomerate pores of irregular shape with sizes of 30 - 80 μm, the number of which increases with increasing porosity.

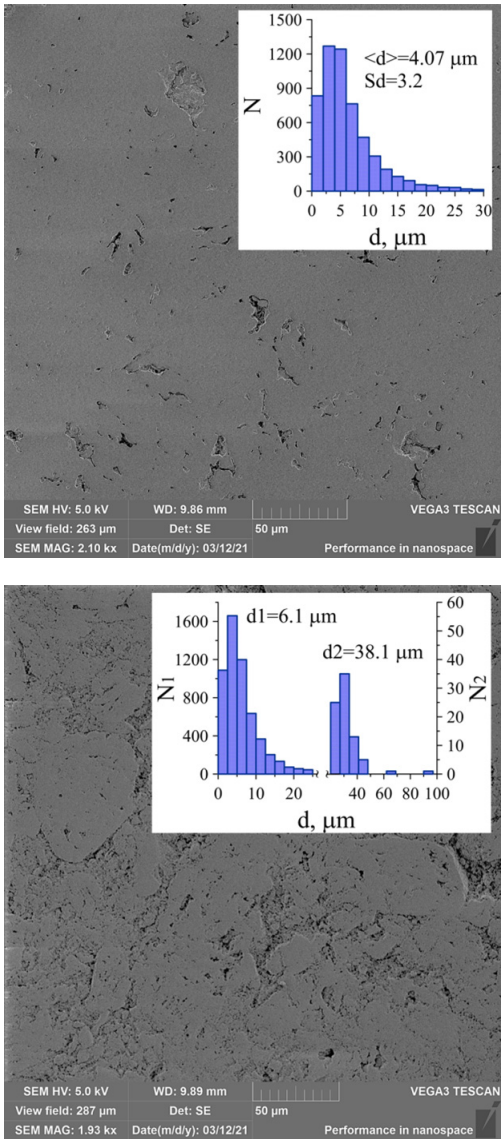

Fig. 2 *Typical image of the porous structure: (a) – ceramic with porosity 4%; (b) - ceramic with porosity 42%. The insets show the pore size distribution of ceramics with different pore space morphology*

2. ábra *A porózus szerkezet tipikus képe: (a) - 4%-os porozitású kerámia; (b) - 42%-os porozitású kerámia. A különböző pórustér morfológiájú kerámiák pórusméret-eloszlása*

The changes in the average pore size of the studied ceramics are shown in *Table 2*. It can be seen that with the porosity of the samples increasing, the average pore size (<d>) increases from 4 to 6.4 μm. In this case, with an increase in the average pore size, the size dispersion of powders also grows. Also, with an increase in porosity, an increase of the average size of both small <d1> and large pores <d2> is observed. From the histogram shown in *Fig. 2 (a)*, it can be seen that in the sample with a porosity of 4%, pores larger than 30 μm are absent. In samples with a porosity of 17% and higher, the pore volume with sizes of pores larger than 30 μm increases with increasing porosity but does not exceed 10 vol.%.

Sample number	Porosity, %	<d> ± 0.2 μm	Sd	<d1> ± 0.2 μm	<d2> ± 1 μm	V_{por} (Size of pores <30 μm), %	V_{por} (Size of pores >30 μm), %
1	4	4.07	3.2	-	-	100	-
2	17	4.95	4.5	3.8	28.3	97	3
3	29	5.3	4.7	4.74	32.4	95	5
4	33	5.33	5.6	4.9	39	90	10
5	42	6.4	5.8	6.1	38.1	93	7

Table 2 *Change in the average pore size in ceramics with different porosities*

2. táblázat *A kerámia próbatestek átlagos pórusméretének változása a porozitástól függően*

Fig. 3 (a) shows the "stress-strain" curves during diametral compression tests of ceramic specimens with different porosities. The diametral compression experiments showed that the behavior of all specimens upon loading was typical as for brittle materials. An analysis of the deformation curves showed that for samples with porosities of 4 and 17% were deformed elastically up to its fracture. The deformation curves of specimens with a higher porosity are showing a deviation from linearity before their fracture. The deviation from linearity of specimens with a porosity of 27% and higher was observed in other works [8, 12] for other loading schemes of porous ceramics and may be associated with the appearance and accumulation of defects in the form of microcracks during loading, which is representative of the quasi-brittle fracture of porous ceramic materials.

Re-plotting of the «σ – ε» dependences in double logarithmic coordinates $Ln(\sigma/\sigma_0)$ – Ln(ε), they were transformed into two parts, which can be approximated by linear functions with varying inclination to the X-axis (Ln(ε)), and therefore, with different exponent of strain hardening n of the Hollomon equation [34]. The inset in *Fig. 3 (a)* shows a representative curve with different exponents of strain hardening n1 and n2. The exponent of strain hardening n1, calculated from linear functions, increase from 1.45 to 1.7 with an increase of samples porosity from 4 to 33% and in a sample with a porosity of 42%, a decrease in n1 is observed, *Fig. 3 (b)*. The exponent of strain hardening n2 practically does not change with an increase of the porosity of the samples and is equal to ~ 1.2.

It should be noted that on all dependences «Ln(σ) – Ln(ε)» the strain exponents n are large 1, which probably corresponds to the nonlinear elastic behavior of ceramics under load with a change of porosity. In this case, the change in the angle of inclination of the linear sections on the curves «Ln(σ) – Ln(ε)»

may indicate a change in the mechanism of deformation of the ceramic during loading. The change in the slope on the curves for ceramics with porosities of 4 and 17% can be associated with microcracking caused by the tetragonal-monoclinic phase transformation during loading. On the fracture surface of samples with porosity of 4 and 17% according to the X-ray phase analysis the formation of a monoclinic phase with a volume content of 30% and 12%, respectively, are observed.

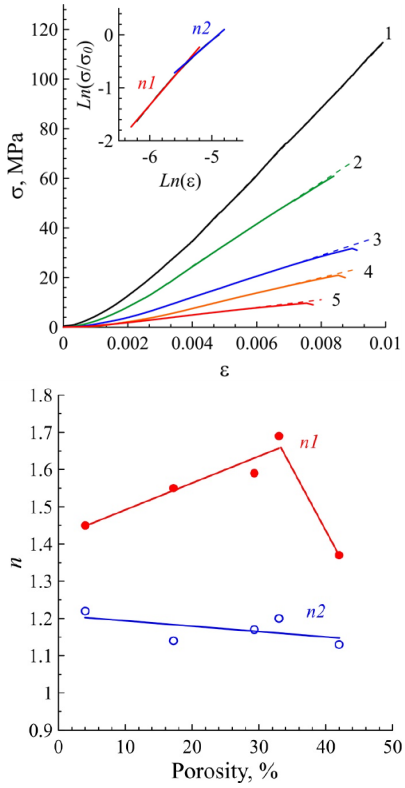

Fig. 3 Deformation curves of ZrO_2(Y) ceramic specimens with different porosity during diametral compression tests (a). At the curves, numbers indicate the sample numbers, according to Table 1. (The inset in Fig. 3 (a) shows the deformation curve with a porosity of 42% in the coordinates $Ln(\sigma/\sigma_0)$ – $Ln(\varepsilon)$); Dependence of the exponents of strain hardening n1 and n2 vs the samples porosity (b)

3. ábra Különböző porozitású ZrO_2 (Y) kerámia minták deformációs görbéi a diametrális kompressziós vizsgálatok során (a). A görbéknél a számok az 1. táblázat szerinti mintaszámokat jelölik. (A 3. ábra a) betétje a deformációs görbét 42%-os porozitással mutatja az $Ln(\sigma/\sigma_0)$ – $Ln(\varepsilon)$) koordinátákban); Az n1 és n2 a terhelési keményedés kitevőinek függése a minták porozitásától (b)

The formation of microcracks in ceramics with a porosity of 29% and higher during deformation is caused by the fracture of bridges and lintels of the interpore frame. On the fracture surfaces of ceramics samples with a porosity of 29% and higher, no increase of the monoclinic phase was observed in comparison with the initial state.

The tensile strength (σ_t) decreases with an increase of porosity, *Fig. 4 (a)*. The change of σ_t from porosity is well described by a power function with a high correlation coefficient (R = 0.99).

Analysis of the change of the ultimate strain before fracture (ε), obtained from the deformation curves «σ – ε» (*Fig. 3 (a)*), showed that the strain (ε) decreases slightly from 1 to 0.8% with an increase of the samples porosity (curve 1, *Fig. 4 (b)*).

The effective modulus of elasticity (E_{eff}), calculated from the slope of the stress-strain curves are decreases with increasing samples porosity (curve 2, *Fig. 4 (b)*).

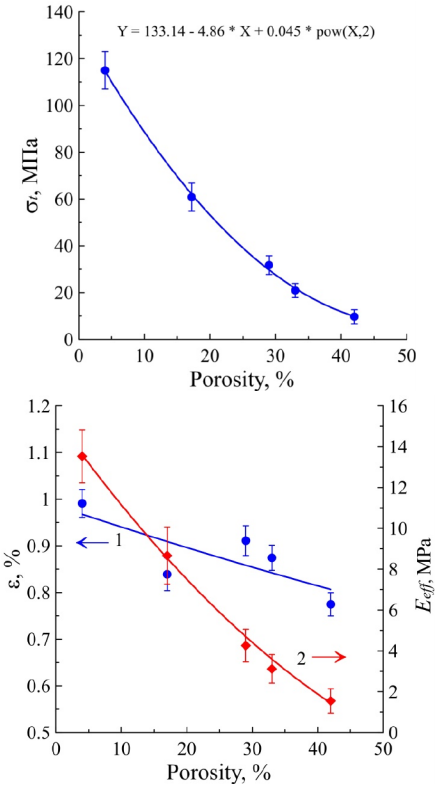

Fig. 4 Dependence of tensile strength vs samples porosity (a); Dependence of ultimate strain before fracture (ε) (curve 1) and the effective modulus of elasticity (E_{eff}) (curve 2) vs samples porosity (b)

4. ábra A szakítószilárdság függése a minták porozitásától (a); A törés előtti végső fajlagos alakváltozás (ε) (1. görbe) és az effektív rugalmassági modulus (E_{eff}) (2. görbe) függése a minták porozitásától (b)

After diametral compression tests of samples with porosity of 4, 17, and 42%, X-ray diffraction analysis was carried out from the front surface of fracture fragments of the samples.

Fig. 5 Macrophotographs of samples with different porosity (a - 4% ; b - 17%; c - 42%) after diametral compression tests with XRD schemes

5. ábra Különböző porozitású minták makrofotói (a - 4%; b - 17%; c - 42%) XRD sémákkal végzett diametrális kompressziós tesztek után

The size of the coherently diffracting domains and the crystal lattice microdistortion from different place of the fracture

fragments are determined. X-ray diffraction analysis was carried out for the local points from fractured fragments along the loading axis during diametral compression tests, in the direction starting from the point of contact of the sample with the active platform of the testing machine towards the passive platform with a step of 2-3 mm, the areas for X-ray studies for each point was approximately 4 mm^2. *Fig. 5 (a, b, c)* shows macro photographs of samples with different porosities after diametral compression tests with X-ray diffraction analysis schemes.

The dependences of the size of the coherently diffracting domains and the crystal lattice microdistortion of samples with porosities of 4, 17, and 42% are shown in *Fig. 6*. It follows from the figure that for all samples with different porosity a dispersion both sizes of the CDD and crystal lattice microdistortion are decrease with increase a distance from the active platform of the testing machine and does not exceed 10%. These data indicate the appearances of deformation inhomogeneity of porous ceramics under diametral compression along the compression axis.

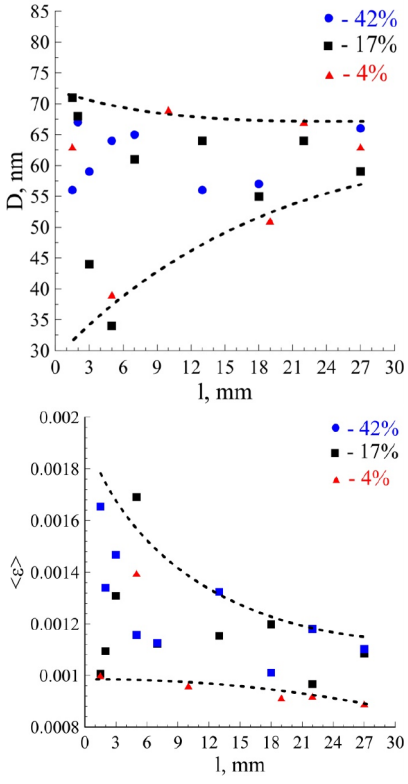

Fig. 6 *Change of the size of the CDD (a) and the crystal lattice microdistortions (b) of fracture fragments of ceramic samples with porosity of 4, 17 and 42% after diametral compression tests. The start point (zero) is corresponds to the point of contact of the sample with the active platform of the testing machine, and last point (30mm) is corresponding to the point of contact of the sample with the top (passive) platform of the testing machine*

6. ábra *A kerámiai minták 4, 17 és 42% porozitású töretdarabjainak CDD méretének (a) és kristályrácsos mikrotorzulásának (b) változása a diametrális kompressziós vizsgálatok után. A kiindulási pont (0 mm) a minta és a tesztgép aktív platformjának érintkezésénél, az utolsó pont (30 mm) pedig a minta és a tesztelő gép felső (passzív) platformjának érintkezése*

4. Conclusions

It has been shown that with an increase of the porosity of ceramic, there are a decrease in the ultimate tensile strength in diametral compression from 115 to 9 MPa and the ultimate deformation to fracture. The effective modulus of elasticity calculated from the slope of the stress-strain curves also decreases with increasing of porosity.

It been shown that two strain exponent were observed, which indicate a change of deformation mechanism of the ceramic during loading. The decrease of n2 in ceramics with porosities of 4 and 17% is due to the phase transformation from the tetragonal to the monoclinic phase under the action of applied stresses, and in ceramics with porosity above 29%, it is associated with the formation of multiple microcrack defects during deformation.

It has been shown that in these materials microstructural parameters - coherently diffracting domains of the tetragonal phase and the crystal lattice microdistortions, are changes non-uniformly, which indicate the inhomogeneity of the deformation of this brittle material during compression.

Acknowledgments

The work was performed according to the Government research assignment for ISPMS SB RAS, project FWRW-2021-0005. The described article was carried out as part of the EFOP-3.6.1-16-00011 "Younger and Renewing University –Innovative Knowledge City – institutional development of the University of Miskolc aiming at intelligent specialisation" project implemented in the framework of the Széchenyi 2020 program.

References

[1] Anderson, T.L., (2017) Fracture mechanics: fundamentals and applications, CRC Press, 680 pp.

[2] Bažant, Z.P., Planas, J., (1998) Fracture and Size Effect in Concrete and Other Quasibrittle Materials, CRC Press, New York, 136 pp.

[3] Kaczmarek, M. Goueygou, M., (2006) Dependence of elastic properties of materials on their porosity: Review of models. Journal of Porous Media, 9 (4), pp. 335-355. https://doi.org/10.1615/JPorMedia.v9.i4.50

[4] Goldstein, R.V., Osipenko, N.M., 2019. About compression fracture. Physical Mesomechanics, 22 (6), pp. 439-455. https://doi.org/10.1134/S1029959919060018

[5] Ibrahim, J.F.M.., Gömze, L.A., Kotova, O.B., Shchemelinina, T.N., Shushkov, D.A., Ignatiev, G.V., Anchugova, E.M., (2019) The influence of composition, microstructure and firing temperature on the density, porosity, and shrinkage of new zeolite-alumina composite material. Építőanyag - JSBCM 70(4), pp.120-124. https://doi.org/10.14382/epitoanyag-jsbcm.2019.21

[6] Rice, R.W., (1989) Relation of tensile strength-porosity effects in ceramics to porosity dependence of Young's modulus and fracture energy, porosity character and grain size. Mater Sci Eng, A, 112, pp. 215-224.

[7] Junhong, Yu., Xinchun, Shang., (2019) Analysis of the influence of boundary pressure and friction on determining fracture toughness of shale using cracked Brazilian disc test. Engineering Fracture Mechanics, 212, pp. 57-69. https://doi.org/10.1016/j.engfracmech.2019.03.009

[8] Grigorev, M.V., Savchenko, N.L., Sablina, T.Yu., Kurovics, E., Sevostyanova, I.N., Buyakova, S.P., Gomze, L.A., Kulkov, S.N., (2018) Deformation and fracture of alumina ceramics with hierarchical porosity. Építőanyag - JSBCM. 70(1), pp. 18-22. https://doi.org/10.14382/epitoanyag-jsbcm.2018.4

[9] Kulkov, S.N., Maslovskii, V.I., Buyakova, S.P., Nikitin, D.S., (2002) The non-hooke's behavior of porous zirconia subjected to high-rate compressive deformation. Technical Physics, 47(3), pp. 320-324. https://doi.org/10.1134/1.14631212002

[10] Meille, S., Lombardi, M., Chevalier, J., Montanaro, L., (2012) Mechanical properties of porous ceramics in compression: On the transition between

elastic, brittle, and cellular behavior. Journal of the European Ceramic Society, 32, pp. 3959–3967. https://doi.org/10.1016/j.jeurceramsoc.2012.05.006
[11] Ohji, T., Fukushima, M., (2012) Macro-porous ceramics: processing and properties. Int. Mater.Rev., 57, pp. 115–131. https://doi.org/10.1179/1743280411Y.0000000006
[12] Savchenko, N.L., Sablina, T.Yu., Sevostyanova, I.N., Buyakova, S.P., Kulkov, S.N., (2016) Deformation and fracture of porous brittle materials under different loading schemes. Russian Physics Journal, 58(11), pp. 1544-1548. https://doi.org/10.1007/s11182-016-0680-4
[13] Šavija, B., Smith, G.E., Liu, D., Schlangen, E., Flewitt, P.E.J., (2019) Modelling of deformation and fracture for a model quasi-brittle material with controlled porosity: Synthetic versus real microstructure. Engineering Fracture Mechanics, 205, pp. 399-417. https://doi.org/10.1016/j.engfracmech.2018.11.008
[14] Bocca, P., Carpinteri, A., Valente, S., (1991) Mixed mode fracture of concrete. Int J. Sol. Struct., 27, pp. 1139–1553. https://doi.org/10.1016/0020-7683(91)90115-V
[15] Lynch, C.S., Hwang, S.C., McMeeking, R.M., (1995). Micromechanical theory of the nonlinear behavior of ferroelectric ceramics. Proc SPIE; 2427:300–12 http://dx.doi.org/10.1117/12.200926
[16] Prewo, K.M., (1986). Tension and flexural strength of silicon carbide fibre-reinforced glass ceramics. J Mater Sci, 21(3), pp.590–600 https://link.springer.com/article/10.1007/BF02403007
[17] Bruno, G., Efremov, A.M., Levandovsky, A.N., Clausen, B., (2011) Connecting the macro and microscopic strain response in porous ceramics: modeling and experimental validation. J Mater Sci., 46(1), pp. 61–73. https://link.springer.com/article/10.1007/s10853-010-4899-0
[18] Pozdnyakova, I., Bruno, G., Efremov, A.M., Clausen, B., Hughes, D.J., (2009) Stress dependent elastic properties of porous cellular ceramics. Adv Eng Mater., 11, 1023–9. https://doi.org/10.1002/adem.200900192
[19] Ghassemi-Kakroudi, M., Huger, M., Gault, C., Chotard, T., (2009). Damage evaluation of two alumina refractory castables. J. Eur. Ceram. Soc., 29, 2211–8 https://doi.org/10.1016/j.jeurceramsoc.2008.12.019
[20] Turon –Vinas, M., Anglada, M., (2018) Dental Materials, 34(30), pp. 365-375. https://doi.org/10.1016/j.dental.2017.12.007
[21] Dar, U.A., Gao, G., Wang, Y., (2019) Ceram. Int. 45(6), pp. 7931–7944. https://doi.org/10.1016/j.ceramint.2019.01.106
[22] Garcia-Fernandez, C.C., Gonzalez-Nicieza, C., Alvarez-Fernandez, M.I., Gutierrez-Moizant, R.A., (2018) Analytical and experimental study of failure onset during a Brazilian test. International Journal of Rock Mechanics and Mining Sciences, 103, pp. 254-265. https://doi.org/10.1016/j.ijrmms.2018.01.045
[23] Sheikh, M. Z., Wang Z., Du, B., et al., (2019) Ceram. Int., 45, pp. 7931–7944. https://doi.org/10.1016/j.ceramint.2019.01.106
[24] Sevostyanova, I.N., Sablina, T.Yu., Gorbatenko, V.V., Kulkov, S. N., (2019) Strain Localization during Diametral Compression of $ZrO_2(Y_2O_3)$ Ceramics. Technical Physics Letters, 45(9), pp. 943–946. https://doi.org/10.1134/S1063785019090281
[25] Li, D., Wong, L.N.Y., (2003) Rock Mech. Rock Eng., 46, pp. 269–287. https://doi.org/10.1007/s00603-012-0257-7
[26] Mousavi Nezhad, M., Fisher, Q.J., Gironacci, E., et al., (2018) Rock Mech. Rock Eng., 51, pp. 1755–1775. https://doi.org/10.1007/s00603-018-1429-x
[27] Goltsev, V.Yu., Osintsev, A.V., Plotnikov A.S., (2017) Application of a disk specimen loaded according to the "Brazilian test" for evaluating the brittle strength of materials of non-geological origin. Letters on materials, 7(1), pp. 21-25. https://doi.org/10.22226/2410-3535-2017-1-21-25
[28] Kulkov, S.N., Smolin, I.Yu., Mikushina, V.A., Sablina, T.Yu., Sevostyanova, I.N., Gorbatenko, V.V., (2020) Studying Strain Localization in Brittle Materials during the Brazilian Test. Russian Physics Journal, 63, pp. 976–983. https://doi.org/10.1007/s11182-020-02126-z
[29] Gregg S.J., Sing K.S.W., (1982) Adsorption, Surface Area and Porosity, 2nd ed., ACADEMIC PRESS, 304 p.
[30] Saltykov, S.A., (1976) Stereometricheskaya metallografiya [Stereometric metallography]. Moscow, Metallurgiya, 270 p.
[31] Scherrer, P., (1918) Bestimmung der Größe und der inneren Struktur von Kolloidteilchen mittels Röntgenstrahlen. Göttinger Nachrichten Gesellschaft, 2, pp. 98– 101.
[32] Stokes, A.R., Wilson, A.J.C., (1944) The diffraction of X rays by distorted crystal aggregates Proceedings of the Physical Society, pp. 174–181.
[33] Timoshenko, S.P., Goodier, J.N., (1951) Theory of Elasticity, OCR. Second Edition. – McGraw-Hill book company, Inc., 506 pp.
[34] Hertzberg, R.W., (1977) Deformation and Fracture Mechanics of Engineering Materials. John Wiley and Sons Ltd, London, 605 pp.

Ref.:
Sevostianova, Irina N. – **Sablina**, Tatiana Yu. – **Kulkov**, Sergei N. – **Tihtih**, Mohammed – **Gömze**, László A.: *Stress-strain behavior of high porous zirconia ceramic*
Építőanyag – Journal of Silicate Based and Composite Materials, Vol. 73, No. 4 (2021), 154–159. p.
https://doi.org/10.14382/epitoanyag-jsbcm.2021.23

Examination of the influence of cobalt substitution on the properties of barium titanate ceramics

Mohammed TIHTIH ▪ Institute of Ceramics and Polymer Engineering, University of Miskolc, Hungary ▪ medtihtih@gmail.com
Irina N. SEVOSTIANOVA ▪ Institute of Strength Physics and Materials Science, SB RAS, Tomsk, Russia ▪ sevir@ispms.ru
Emese KUROVICS ▪ Institute of Ceramics and Polymer Engineering, University of Miskolc, Hungary ▪ fememese@uni-miskolc.hu
Tatiana Yu. SABLINA ▪ Institute of Strength Physics and Materials Science, SB RAS, Tomsk, Russia ▪ sabtat@ispms.ru
Sergei N. KULKOV ▪ Institute of Strength Physics and Materials Science, SB RAS, Tomsk, Russia ▪ kulkov@ms.tsc.ru
László A. GÖMZE ▪ Institute of Ceramics and Polymer Engineering, University of Miskolc, Hungary, IGREX Engineering Service Ltd ▪ femgomze@uni-miskolc.hu

Érkezett: 2021. 06. 03. ▪ Received: 03. 06. 2021. ▪ https://doi.org/10.14382/epitoanyag-jsbcm.2021.24

Abstract

Cobalt (Co) doped Barium titanate ($BaTiO_3$) powders, with Co concentration (0,5 and 10 mol%), are synthesized by the sol-gel technique and characterized by Thermogravimetric analysis (TGA), and Differential thermal analysis (DTA), X-Ray diffraction (XRD), Fourier Transform Infrared (FT-IR) and scanning electron microscopy (SEM). X-ray diffraction (XRD) patterns of the obtained powders, calcined at a relatively low temperature (1000 °C/3 h), found their crystallization in the pure perovskite structure without the appearance of secondary phases. XRD results reveal that the Co decreases the lattice parameters, the volume of the unit cell and the crystallite size of $BaTiO_3$. The investigations carried out by FT-IR spectroscopy allow the investigation of the substitution procedure behavior associated to the Co incorporation into $BaTiO_3$ lattice. The evolution of the physical parameters as functions of the dopant content have been examined based on XRD and FT-IR results. Furthermore, the morphology and the shape variation of particle size were studied through SEM.

Keywords: barium titanate, co-doping, ferroelectrics, synthesis, XRD, SEM
Kulcsszavak: bárium-titanát, co-dopping, ferroelektromos, szintézis, XRD, SEM

Mohammed TIHTIH
Is a lecturer in the Sidi Mohamed Ben abdellah University, Morocco, he graduated from Faculty of sciences Dhar El Mahraz, Fez, Morocco, Department of Physics, for the time being, he is a PhD student in the University of Miskolc, Institute of Ceramics and Polymer Engineering, under supervision of Prof. L. A. Gömze.

Irina N. SEVOSTYANOVA
PhD Education: 1987: Tomsk Polytechnic Universityengineer.1993-1996: Institute of Strength Physics and Materials Science of the Russian Academy of Sciences in Tomsk - PhD student. 2001: PhD degree from the Institute of Strength Physics and Materials Science of the Russian Academy of Sciences in Tomsk. Field of research: Structure and mechanical property of porous ceramics based zirconia and alumina.

Emese KUROVICS
is graduated in the University of Miskolc, Institute of Ceramics and Polymer Engineering as a material engineer, where she actually continues her study as PhD student under supervision of Prof. L. A. Gömze.

Tatiana Yu. SABLINA
has PhD Education since 1989 at present she is working at the Tomsk State University and Institute of Strength Physics and Materials Science of the Russian Academy of Sciences in Tomsk.

Sergei N. KULKOV
is professor of the Tomsk State University and head of Department of Ceramics in the Institute of Strength Physics and Materials Science of the Russian Academy of Science since 1989. His research works are represented in 5 books, more than 150 articles, 18 patents and many International Symposiums and Conferences. At present he is head of department „Theory of Strength and Mechanic of Solids", member of „The American Ceramic Society" of „The APMI - International" and the DYM AT Society (France).

László A. GÖMZE
is establisher and professor of the Department of Ceramics and Silicate Engineering in the University of Miskolc, Hungary. He is author or coauthor of 2 patents, 6 books and more than 300 scientific papers. Recently, he is the chair of the International Organization Board of ic-cmtp6 the 6th International Conference on Competitive Materials and Technological Processes and ec-siliconf2 the 2nd European Conference on Silicon and Silica Based Materials.

1. Introduction

Recently, the research progression in the area of technical ceramics [1]–[7] has drawn great attention [4], [8]–[17]. Perovskite ferroelectric materials (ABO_3) have had great interest due to the presence of a ferroelectric phase, their relatively simple structure which can allow theoretical interpretations and finally the feasibility of modifying their physical properties by numerous ionic substitutions. In addition, these materials exhibit high-physical performance, dielectric, electro-optical, and electronic properties [18]–[23], which make the materials widely used in various applications in different areas.

Barium titanate ($BaTiO_3$) is one of the most important perovskite materials. It is a ferroelectric material, with piezoelectric properties and photorefractive effect. As a solid, it has five phases ranging from low to high temperature: rhombohedral, orthorhombic, tetragonal, cubic and hexagonal crystal structure. Indeed, all of the crystal structures show the ferroelectric effect except cubic structure. It has the appearance of a transparent powder or white crystals. It is soluble in concentrated sulfuric acid perhaps not in water.

Interesting and exotic properties are theoretically expected in doped $BaTiO_3$ like ferromagnetism at room temperature enhanced dielectric properties etc. [24]. Moreover the synthesis technique also influences the level of doping and physical properties. Based on this fact, several studies are made adopting various synthesis methods such as solid state ceramic technique, laser ablation, sol-gel and chemical routes etc. [25]–[27]. In response to these reports, various types of doping have been attempted for $BaTiO_3$ including Fe, Mn, Co etc. [24]–[28].

In the present paper, Co-doped $BaTiO_3$ (BTCox) ceramics, with x = (0, 5 and 10%) were prepared using the sol-gel technique, the choice of this method of processing was based on its various advantages, low processing temperature, high purity, homogeneity and an excellent control of the stoichiometry of the products [29]. We have investigated the phase and structural properties of the prepared samples

using X-ray diffraction (XRD), Fourier Transform Infrared (FT-IR) spectrometer and Scanning Electronic Microscopy (SEM). Experimental results are analyzed and then discussed as function of the doping concentration and compare the obtained values to those of the literature.

2. Experimental methods

2.1 Materials and synthesis method

Crystalline powders BTCox were synthesized and obtained using sol-gel method [30] through the destabilization of colloidal solution (DCS). This process provides numerous advantages such as an excellent control of the stoichiometry and a good homogeneity of the powders in spite of crystallization at relatively low temperature [8], [10], [29].

The powders were prepared using barium acetate trihydrate ($Ba(CH_3COO)_2$, $3H_2O$) (99.9% purity), titanium isopropropoxide $Ti[OCH(CH_3)_2]_4$ (97% purity) and Cobalt acetate $Co(CH_3CO_2)_2{\cdot}4\ H_2O$(99.9% purity) as precursors, lactic acid ($CH_3CH(OH)COOH$) as peptizing agent and distilled water as solvent. The different steps relating to the preparation of BTCox powders are shown schematically in the flowchart in *Fig. 1*. A white sol with adequate proportions was obtained, which was dried in an oven at 80 °C for 72 h to obtain a dry gel. The raw powders, after grinding, were calcined in air in a programmable oven at the temperature of 1000 °C for 3 h.

The samples in pellet shapes were obtained by pressure with an uniaxial pressure equal to 10 tonnes/cm^2. Then, the pellets were sintered 1200 °C for 6 h reached with a heating rate 5 °C/min.

2.2 Characterization

Thermal study using Thermogravimetric analysis (TGA), and Differential thermal analysis (DTA) were performed on the sample BTCo15. The crystallinity and phases of the ceramic powders were examined using X-ray diffraction. The powder X-ray pattern was recorded for all samples with various cobalt concentrations by using an X-ray diffractometer equipped with [XPERT-PRO diffractometer with Cu-Kα radiation (λ = 1.5405980 Å)]. XRD spectrum was recorded in the 2θ range of 20 to 80°. The morphology of the ceramic powders was characterized by Scanning electron microscopy (SEM). Moreover, the functional groups in powders were detected by using of a Bruker-Tensor 27 spectrophotometer FT-IR spectroscopy in the wave number range 450- 4000 cm^{-1}.

3. Results and discussion

3.1 Thermal analysis

Fig. 2 shows the thermal analysis (TGA and DTA) of the sample 15% doped $BaTiO_3$, performed in air up to 1200 °C with a temperature rate 5° C / min. The TGA curve reveals three steps of decomposition (corresponding to an overall mass loss of approximately 28mg). The first step (33-320 °C), represents a weight loss which attributed to the elimination of water and excess lactic acid. This mass loss is accompanied by an endothermic peak in the DTA curve. The second stage (320–631 °C), represents a progressive mass loss, accompanied by several peaks endothermic and the other exothermic peaks in the DTA curve which can be attributed to the decomposition of the organic matter and the elimination of CO_2. In this temperature range, rearrangements of chemical bonds in the gel occur and the gel is converted to polymers [31]. The last stage of mass loss located in the range of (631–1000 °C) was detected, accompanied by an endothermic peak in the DTA curve, which is attributed to the decomposition of organic polymers and the formation of inorganic substances (the starting formation of BTCo0.15). No reaction or mass loss was noticed above 1000 ° C, showing complete crystallization of the ceramic powders. This relatively low temperature compared to other reported from other works using different synthetic techniques [32] is due to the sol gel preparation method [8], [30].

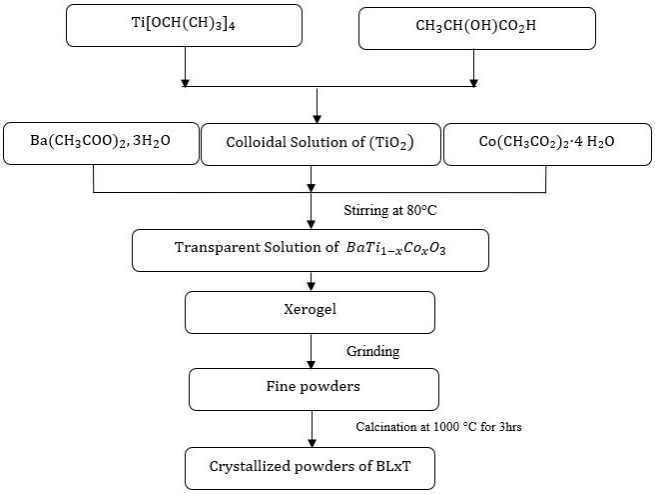

Fig. 1 Flow chart of the sol-gel processing of (x= 0, 0.05 and 0.1) powder ceramics
1. ábra A (x= 0, 0.05 és 0.1) kerámia porok szol-gél eljárásának folyamata

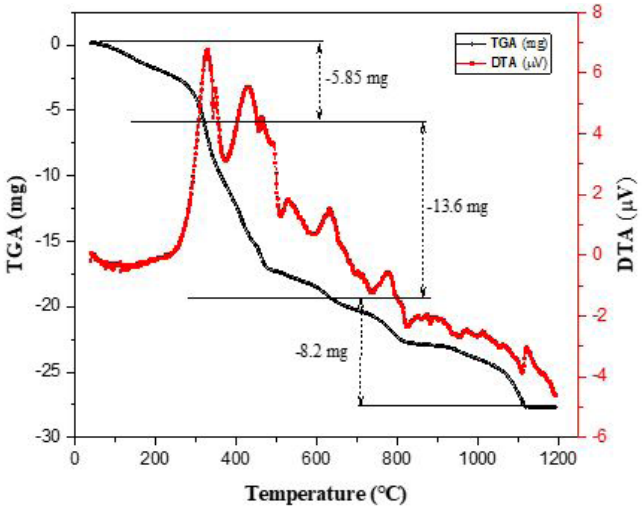

Fig. 2 TG/DTA curves of the (ceramic sample
2. ábra A (kerámiaminta TG/DTA görbéi

3.2 Structural study

XRD patterns of the as-prepared powders were investigated, and they are reported as function of the Cobalt concentrations in *Fig. 3*. It shows that the BTCo crystallize in the perovskite phase without any secondary phase. The peaks are indexed as

the respective planes on the basis of JCPDS cards. Phan et al.[33] prepared BTCo usnig classical solid state reaction method, after annealing at 1300 °C—4h, but with the presence of the secondary phases. The diffractograms reveal well-resolved peaks, which are a clear indication of the good particles's crystallinity. These peaks are assigned in pure sample, i.e., x=0% to the perovskite structure with the tetragonal phase, which exists throughout the whole concentration ranges. This is supported by the presence of well resolved (002)-(200) doublet peaks around 2θ of 44-46° on the diffractogram.

The lattice parameters (a and c) were determined from XRD data analysis considering tetragonal phase with an accuracy of ±0.002 Å using the following relations;

$$\frac{1}{d^2} = \frac{h^2+k^2}{a^2} + \frac{l^2}{c^2} \quad (1)$$

Where a is the lattice constant, d is interplanar spacing and (hkl) are Miller indices.

The fitted and calculated parameters are given in *Table 1*. The values of lattice constants (a and c) are given in *Table 1* and were found that the lattice constant *a* increase while *c* decreases with Co concentration. Lattice parameters of pure the $BaTiO_3$ sample are in good agreement with reported values a = b = 3.988 Å and c =4.026 Å (α = β = γ =90°) [33]. Moreover, the decrease in lattice parameters can be attributed to Co^{2+} ions (0.58 Å) replacing the Ti^{4+} (0.605 Å), having higher ionic radii.

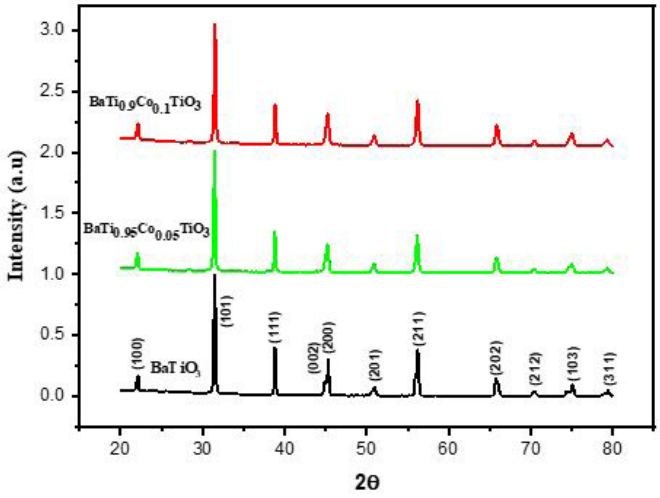

Fig. 3 XRD patterns of Co-doped $BaTiO_3$ powder samples calcined at 1000°C for 3h
3. ábra Az 1000 °C-on 3 órán át kalcinált Co-adalékolt $BaTiO_3$ porminták XRD mintája

Sample	Lattice parameters					
	a (Å)	c (Å)	V	Tetrago-nality	Crystal-lite size (nm)	Lattice strain ($\times 10^{-3}$)
$BaTiO_3$	3.9917	4.0247	64.1304	1.0082	42.2725	1.38
$BaTi_{0.95}Co_{0.05}O_3$	3.9945	4.0146	64.0594	1.0050	56.3634	2.87
$BaTi_{0.9}Co_{0.1}O_3$	3.9948	4.0113	64.0136	1.0041	59.0017	2.56

Table 1. Lattice parameters, tetragonality, unit cell volume (V), Lattice strain and Crystallite size of Co-doped $BaTiO_3$
1. táblázat A Co-adalékolt $BaTiO_3$ rácsparaméterei, tetragonitása, egységnyi térfogata (V), rácsfeszítése és és kristálymérete

The unit cell volume (V) is known to be most basic characteristic of the solid-state structure and the values of the unit cell volume are given in *Table 1*. The unit cell volume decreases as Co concentration increases. The decrease in unit cell volume can be attributed to changes in the crystal structure.

Scherrer formula takes into account only the influence of crystallite size on the XRD peak broadening, however, it doesn't provide anything about the sample's microstructures of the lattice i.e., regarding the intrinsic strain, which gets developed in the nanocrystals due to the grain boundary, point defect, stacking faults and triple junction [34]. Many approaches exist, such as Warren-Averbach and Williamsons Hall method, etc., which takes into account the effect of the strain induced XRD peak broadening and can be used to calculate the intrinsic strain along with the particle size. Among these approaches, Williamson–Hall (W–H) method is a very simple and The Williamson–Hall (W–H) approach is a simple and straightforward one. [34], [35].

The crystallite size and micro-strain was calculated using Williamson-Hall (W-H) plot which explains x-ray diffraction peak broadening [36].

$$\beta = \beta_{size} + \beta_{strain} \quad (2)$$

$$\beta = \frac{0.94\lambda}{D\cos\theta} + 4\varepsilon\tan\theta \quad (3)$$

Where, β is the full width of half maximum, ε is the strain, and D is the crystallite size. *Figures 4(a), (b)* and *(c)* show the linear plots, the intercepts and the slopes pointing out the crystallite size, as well as the strain of the prepared plotted samples as plotted by Williamson-Hall method. The crystallite size and the strain of single-phase samples are shown in *Table 1*. The nature of the strain formed was determined by the nature of the slope, that is, with a positive slope indicating a tensile strain and the negative slope indicating a compressive strain [37].

The results revealed that all the samples had a positive slope and were subjected to tensile strain. The strain values of BTCo0.05 compound was found to be higher than the value of the other samples (Pure BaTiO3 and BTCo0.1). The higher value of lattice strain induced in the BTCo0.05 sample is considered due to the creation of oxygen vacancies [38]. *Table 1* illustrates the obtained crystallite size and the deviation of strain values BTCox (x=0, 5 and 10%) samples. In addition, the crystallite size was found in the range of 42.27-59 nm (from W- H plot).

3.3 Morphological investigation

Fig. 5 shows the evolution of the morphology and grain size of the $BaTi_{1-x}Co_xO_3$ (x=0, 0.05 and 0.1) powders as a function of the cobalt concentrations. *Fig. 5a* shows that the microstructure is completely anarchic, this is due to the shape of the precursors which have not yet reacted with each other, while the SEM image of the BTCo0.05 powder (*Fig. 5b*) we notice the start of the incorporation of the precursors together, which is in good agreement with the results of the previous characterizations. Concerning *Fig. 5c*, we obtained a fine microstructure of average size less than 1 µm, homogeneous and of regular and well-defined shape, which indicates that the powder crystallizes in the perovskite phase without the presence of impurities.

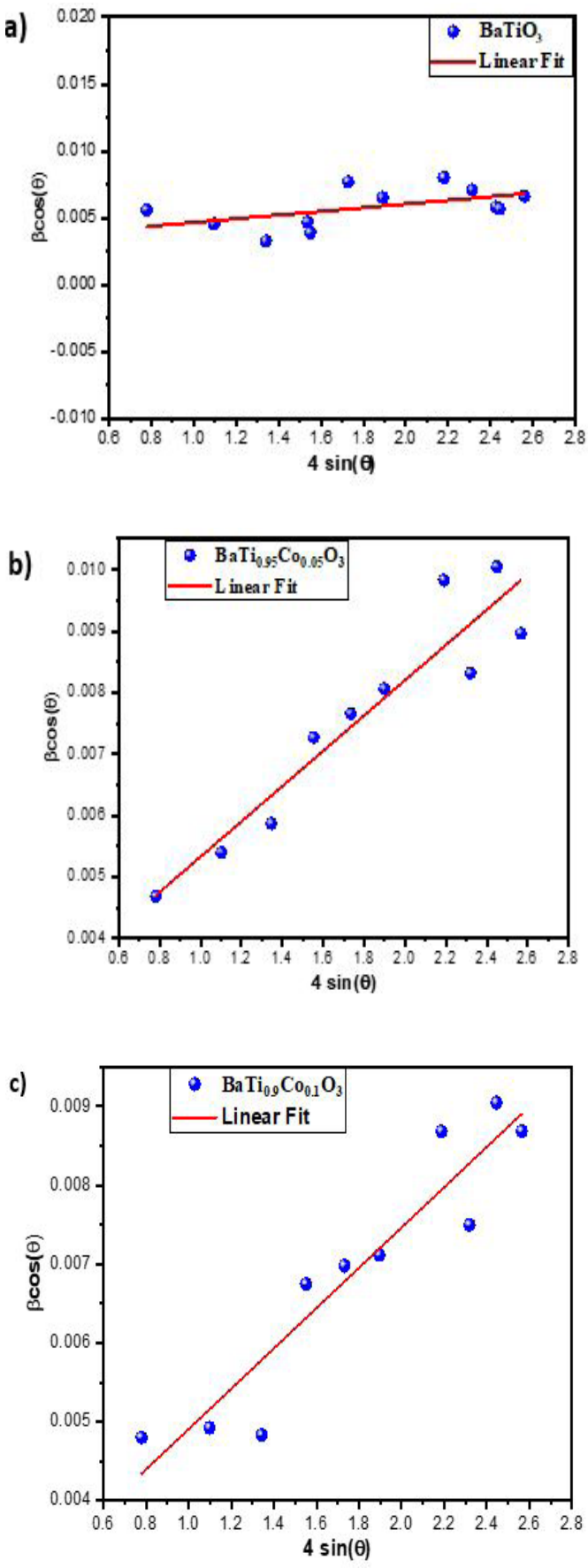

Fig. 4 Williamson–Hall plot of pure and Co doped $BaTiO_3$ samples

4. ábra A tiszta és a Co adalékolt $BaTiO_3$ minták Williamson – Hall diagramja

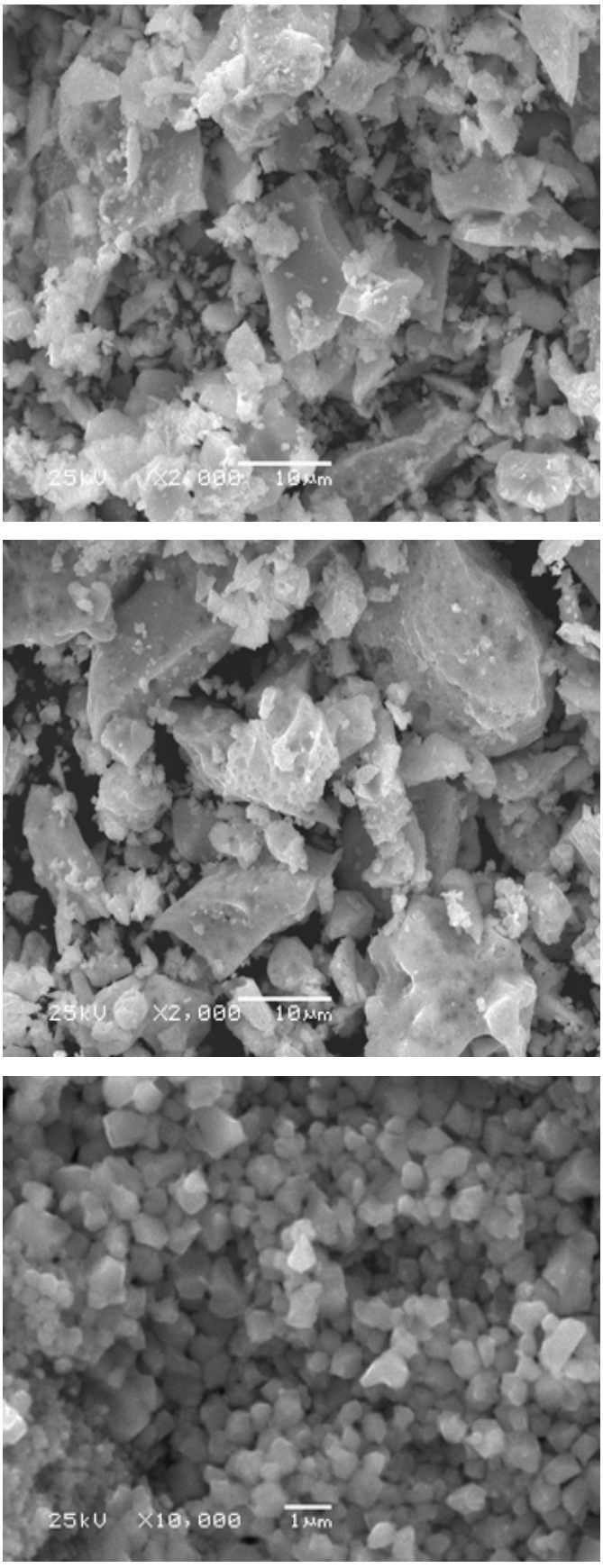

Fig. 5 Morphology images of pure and Co-doped $BaTiO_3$ samples. a) $BaTiO_3$, b) $BaTi_{0.95}Co_{0.05}O_3$, c) $BaTi_{0.9}Co_{0.1}O_3$

5. ábra A tiszta és a Co adalékolt $BaTiO_3$ minták mikroszerkezete. a) $BaTiO_3$, b) $BaTi_{0.95}Co_{0.05}O_3$, c) $BaTi_{0.9}Co_{0.1}O_3$

3.4 FT-IR study

IR spectra of the as prepared (BTCox) powders, heat treated at 1000 °C for 3 h, were recorded in a wavelength range of 400 cm^{-1} to 4000 cm^{-1}. Indeed, the above XRD results is supported by FTIR spectra, as shown in *Fig. 6*. The peak of absorption at 990 cm^{-1} attributed to the vibration of the Ti-OR bond [39] dimens slightly in intensity and is transformed into a single band indicating the disappearance of the alkoxide groups. The characteristic absorption at the range of 1455 cm^{-1} to 1457 cm^{-1} are assigned to the stretching vibrations of carboxylate as there is a small amount of $BaCO_3$ [40]. In addition, Indeed, we can always observe the appearance of a single absorption bands at around 493, 480 and 490 cm^{-1} respectively, which can be assigned to the stretching and bending vibrations of the Ti-O bond in $[TiO_6]^{2-}$ octahedron. The obtained results are therefore in good agreement with those of X-ray diffraction.

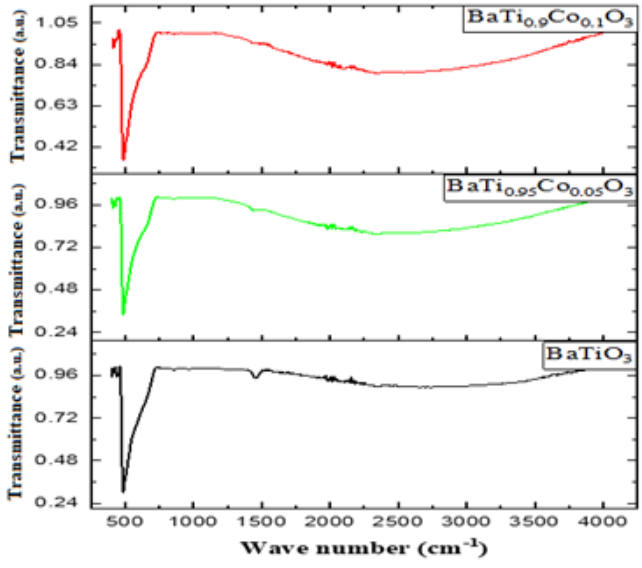

Fig. 6 FT-IR spectra of $BaTi_{1-x}Co_xTiO_3$ (x=0, 5 and 10%) ceramics calcined at 1000 °C/4h.

6. ábra Az 1000 °C-on 4 óra alatt kalcinált $BaTi_{1-x}Co_xTiO_3$ (x=0, 5 és 10%) kerámiák FT-IR spektrumai

4. Conclusions

Cobalt doped barium titanate powders (BTCo) ceramics, with Co contents (0, 5, and 10 mol%), were successfully synthesized by the sol-gel method and characterized by X-Ray diffraction (XRD), scanning electron microscopy (SEM) and FT-IR spectroscopy. XRD results show that the cobalt diminishes the lattice tetragonality of $BaTiO_3$. The XRD pattern confirms that the successful formation of the single-phase (tetragonal) perovskite structure of the all presented ceramic samples. Moreover, the corresponding XRD spectra are exempt of any extra secondary phase indicating a complete incorporation of Co^{2+} in the $BaTiO_3$ structure then confirmed by FT-IR analysis. The line broadening of $BaTiO_3$ is attributed to small lattice strain and crystallite size. This broadening was examined by W-H plot and size-strain plot. According to SEM characterizations, BTCo ceramics were well synthesized, and particle size decreases as dopant concentration increase. In addition, the presented powders samples are relatively homogeneous, consisting of regularly oriented grains in the form of anarchic for 0% and 5% of Co and spherical for 10% Co doped $BaTiO_3$. For further understanding more samples with mediate composition will be prepare and studied for structural and physical properties.

Acknowledgments

The described article was carried out as part of the EFOP-3.6.1-16-00011 "Younger and Renewing University –Innovative Knowledge City – institutional development of the University of Miskolc aiming at intelligent specialisation" project implemented in the framework of the Széchenyi 2020 program. The work was performed according to the Government research assignment for ISPMS SB RAS, project FWRW-2021-0005.

References

[1] Gömze, L. A., Kulkov, S. N., Kurovics, E., Buyakov, A. S., Buyakova, S. P., Buzimov, A. Y., Géber, R., Grigoriev, M. V., Kocserha, I., Kulkov, A. S., Sablina, T. Yu., Savchenko, N. L., Sevostyanova, I. N., Simon, A. (2018) Investigation of mineralogical composition and technological properties of conventional brick clays, Építőanyag – JSBCM, Vol. 70, No. 1, 8–12. p. https://doi.org/10.14382/epitoanyag-jsbcm.2018.2

[2] Kurovics, E., Kotova, O. B., Gömze, L. A., Shushkov, D. A., Ignatiev, G. V., Sitnikov, P. A., Ryabkov, Y. I., Vaseneva, I. N., Gömze, L. N. (2019) Preparation of particle-reinforced mullite composite ceramic materials using kaolin and IG-017 bio-origin additives, Építőanyag – JSBCM, Vol. 71, No. 4, 114–119. p. https://doi.org/10.14382/epitoanyag-jsbcm.2019.20

[3] Kurovics, E., Shmakova, A., Kanev, B. and Gömze, L. A. (2017) Development ceramic composites based on Al_2O_3, SiO_2 and IG-017 additive, IOP Conf. Ser. Mater. Sci. Eng., vol. 175, 012013 https://doi.org/10.1088/1757-899X/175/1/012013

[4] Kurovics, E., Ibrahim, J. F. M., Gömze, L. A. (2020) Influence of compaction times and pressures on rheological properties of kaolin and sawdust powder mixtures, J. Phys. Conf. Ser., vol. 1527, no. 1, 012002 https://doi.org/10.1088/1742-6596/1527/1/012002

[5] Ibrahim, J. F. M., Kurovics, E., Gömze, L. A. (2020) Investigation of the Rheological Properties of Complex Zeolite-Alumina Mixtures, J. Phys. Conf. Ser., vol. 1527, no. 1, 012009 https://doi.org/10.1088/1742-6596/1527/1/012009

[6] Gerezgiher, A. G., Tamási, K., Ibrahim, J. F. M., Kónya, C., Szabó, T. (2020) Thermoplastic corn starch reinforced with pine wood fibre and calcium carbonate precipitate filler, J. Phys. Conf. Ser., vol. 1527, no. 1, 012042 https://doi.org/10.1088/1742-6596/1527/1/012042

[7] Kotova, O. B., Razmyslov, I. N., Ibrahim, J. F. M., Shushkov, D. A. (2020) Mineral composition of bauxite residue and their surface for innovation materials, Építőanyag – JSBCM, vol. 72, no. 4, pp. 135–139, https://doi.org/10.14382/epitoanyag-jsbcm.2020.22

[8] Tihtih, M., Ibrahim, J. F. M., Kurovics, E. Abdelfattah, M. (2020) Study on the effect of Bi dopant on the structural and optical properties of BaTiO 3 nanoceramics synthesized via sol-gel method, J. Phys. Conf. Ser., vol. 1527, p. 012043, https://doi.org/10.1088/1742-6596/1527/1/012043

[9] Kurovics, E., Gömze, L. A., Ibrahim, J. F. M., Gömze, L. N. (2019) Effect of composition and heat treatment on porosity and microstructures of technical ceramics made from kaolin and IG-017 additive, IOP Conf. Ser. Mater. Sci. Eng., vol. 613, no. 1, 012025 https://doi.org/10.1088/1757-899X/613/1/012025

[10] Tihtih, M., Ponaryadov, A. A., Ibrahim, J.-E. F. M., Kurovics, E., KOTOVA, E. L., Gömze, L. A. (2020) Effect of temperature on the structural properties of barium titanate nanopowders synthesis via sol-gel process, Építőanyag – JSBCM, vol. 72, no. 5, pp. 165–168, https://doi.org/10.14382/epitoanyag-jsbcm.2020.27

[11] Kurovics, E., Ibrahim, J. F. M., Tihtih, M., Udvardi, B., Nuilek, K., Gömze, L. A., (2020) Examination of mullite ceramic specimens made by conventional casting method from kaolin and sawdust, J. Phys. Conf. Ser., vol. 1527, p. 012034, https://doi.org/10.1088/1742-6596/1527/1/012034

[12] Ibrahim, J.-E. F. M. et al., (2020) Effect of composition and sintering temperature on thermal properties of Zeolite-Alumina Composite Materials, Építőanyag – JSBCM, vol. 72, no. 4, pp. 131–134, https://doi.org/10.14382/epitoanyag-jsbcm.2020.21

[13] Abdelfattah, M., Kocserha, I., Géber, R., Tihtih, M., Móricz, F., (2020) Evaluating the properties and mineral phases of the expanded clay aggregates with the bentonite additive material, J. Phys. Conf. Ser., vol. 1527, p. 012030, https://doi.org/10.1088/1742-6596/1527/1/012030

[14] Ibrahim, J. F. M., et al., (2020) Preparation and Investigation of Alumina-Zeolite Composite Materials, J. Phys. Conf. Ser., vol. 1527, no. 1, https://doi.org/10.1088/1742-6596/1527/1/012029

[15] Kurovics, E. et al., (2020) Characterization of phase transformation and thermal behavior of Sedlecky Kaolin, Építőanyag – JSBCM, vol. 72, no. 4, pp. 144–147, https://doi.org/10.14382/epitoanyag-jsbcm.2020.24

[15] Ponaryadov, A. V., Kotova, O. B., Tihtih, M., Sun, S., (2020) Natural titanium dioxide nanotubes, Építőanyag – JSBCM, vol. 72, no. 5, pp. 152–155, https://doi.org/10.14382/epitoanyag-jsbcm.2020.25

[16] Ibrahim, J.-E. F. M., Mergen, A., Parlak, U., Tihtih, M., Gömze, L. A., (2021) Synthesis and Characterization of iron-doped $GdMnO_3$ multiferroic ceramics, Építőanyag – JSBCM, vol. 73, no. 1, pp. 24–27, https://doi.org/10.14382/epitoanyag-jsbcm.2021.5

[17] Khirade, P. P., Shinde, A. B., Raut, A. V., Birajdar, S. D., Jadhav, K. M., (2016) Investigations on the synthesis, structural and microstructural characterizations of Ba1-xSrxZrO_3 nanoceramics, Ferroelectrics, vol. 504, no. 1, pp. 216–229, https://doi.org/10.1080/00150193.2016.1241633

[18] Viviani, M., Buscaglia, M. T., Nanni, P., Parodi, R., Gemme, G., Dacca, A. (1999) XPS investigation of surface properties of $Ba_{(1-x)}Sr_xTiO_3$ powders prepared by low temperature aqueous synthesis, J. Eur. Ceram. Soc., vol. 19, no. 6–7, pp. 1047–1051, Jun. 1999, https://doi.org/10.1016/S0955-2219(98)00371-9

[19] Hong, K. S. et al., (2015) Structural characteristics and chemical bonding states with temperature in barium titanate nanopowders prepared by using the solvothermal method, Curr. Appl. Phys., vol. 15, no. 11, pp. 1377–1383, https://doi.org/10.1016/j.cap.2015.06.028

[20] Yadav, A. K., Gautam, C. R., Mishra, A. (2014) Mechanical and dielectric behaviors of perovskite (Ba,Sr)TiO_3 borosilicate glass ceramics, J. Adv. Ceram., vol. 3, no. 2, pp. 137–146, https://doi.org/10.1007/s40145-014-0104-2

[21] Ibrahim, J. F. M., Mergen, A., Sahin, E. İ., Basheer, H. S., (2017) The effect of europium doping on the structural and magnetic properties of $GdMnO_3$ multiferroic ceramics, Adv. Ceram. Prog., vol.3, no.4, p.1

[22] Ibrahim, J. F. M., Mergen, A., Parlak, U., Kurovics, E. (2019) The Influence of Cr doping on the Structural and Magnetic Properties of HoMnO3 Multiferroic Ceramics, IOP Conf. Ser. Mater. Sci. Eng., vol. 613, no. 1, https://doi.org/10.1088/1757-899X/613/1/012009

[23] Rani, A., Kolte, J., Gopalan, P. (2018) Structural, electrical, magnetic and magnetoelectric properties of Co-doped $BaTiO_3$ multiferroic ceramics, Ceram. Int., vol. 44, no. 14, pp. 16703–16711, Oct. 2018, https://doi.org/10.1016/j.ceramint.2018.06.098

[24] Van Der Veer, E., Acuautla, M., Noheda, B. (2020) Ferroelectric PbZr 1-x Ti x O 3 by ethylene glycol-based chemical solution synthesis,

[25] Huang, S. T., Lee, W. W., Chang, J. L., Huang, W. S., Chou, S. Y., Chen, C. C. (2014) Hydrothermal synthesis of SrTiO3 nanocubes: Characterization, photocatalytic activities, and degradation pathway, J. Taiwan Inst. Chem. Eng., vol. 45, no. 4, pp. 1927–1936, Jul. 2014, https://doi.org/10.1016/j.jtice.2014.02.003

[26] Rosa Silva, E., Curi, M., Furtado, J. G., Ferraz, H. C., Secchi, A. R. (2019) The effect of calcination atmosphere on structural properties of Y-doped $SrTiO_3$ perovskite anode for SOFC prepared by solid-state reaction, Ceram. Int., vol. 45, no. 8, pp. 9761–9770, Jun. 2019, https://doi.org/10.1016/j.ceramint.2019.02.011

[27] Khirade, P. P., Birajdar, S. D., Raut, A. V., Jadhav, K. M. (2016) Effect of Fe – substitution on phase transformation, optical, electrical and dielectrical properties of $BaTiO_3$ nanoceramics synthesized by sol-gel auto combustion method, J. Electroceramics, vol. 37, no. 1–4, pp. 110–120, https://doi.org/10.1007/s10832-016-0044-z

[28] Choi, G., Choi, A. H., Evans, L. A., Akyol, S., Ben-Nissan, B. (2020) A review: Recent advances in sol-gel-derived hydroxyapatite nanocoatings for clinical applications, J. Am. Ceram. Soc., vol. 103, no. 10, pp. 5442–5453, Sep. 2020, https://doi.org/10.1111/jace.17118

[29] Tihtih, M., Limame, K., Ababou, Y., Sayouri, S., Ibrahim, J.-E. F. M. (2019) Sol-gel synthesis and structural characterization of Fe doped barium titanate nanoceramics, Építőanyag – JSBCM , vol. 71, no. 6, pp. 190–193, https://doi.org/10.14382/epitoanyag-jsbcm.2019.33

[30] Mohammadi, M. R., Fray, D. J. (2011) Sol-gel derived nanocrystalline and mesoporous barium strontium titanate prepared at room temperature, Particuology, vol. 9, no. 3, pp. 235–242, https://doi.org/10.1016/j.partic.2010.08.012

[31] Bujakiewicz-Koronska, R., Vasylechko, L., Markiewicz, E., Nalecz, D. M., Kalvane, A. (2017) X-ray and dielectric characterization of Co doped tetragonal $BaTiO_3$ ceramics, Phase Transitions, vol. 90, no. 1, pp. 78–85, Jan. 2017, https://doi.org/10.1080/01411594.2016.1252978

[32] Phan, T. L. et al., (2015) Local geometric and electronic structures and origin of magnetism in Co-doped BaTiO3 multiferroics, J. Appl. Phys., vol. 117, no. 17, p. 17D904, May 2015, https://doi.org/10.1063/1.4907182

[33] Nath, D., Singh, F., Das, R. (2020) X-ray diffraction analysis by Williamson-Hall, Halder-Wagner and size-strain plot methods of CdSe nanoparticles-a comparative study, Mater. Chem. Phys., vol. 239, p. 122021, Jan. 2020, https://doi.org/10.1016/j.matchemphys.2019.122021

[34] Hall, W. H. (1949) X-ray line broadening in metals, Proceedings of the Physical Society.Section A, vol. 62, no. 11. pp. 741–743, Nov. 01, 1949, https://doi.org/10.1088/0370-1298/62/11/110

[35] Woldu, T., Raneesh, B., Sreekanth, P., Ramana Reddy, M. V., Philip, R., Kalarikkal, N. (2015) Size dependent nonlinear optical absorption in $BaTiO_3$ nanoparticles, Chem. Phys. Lett., vol. 625, pp. 58–63, https://doi.org/10.1016/j.cplett.2015.02.020

[36] Chandel, S., Thakur, P., Tomar, M., Gupta, V., Thakur, A. (2017) Investigation of structural, optical, dielectric and magnetic studies of Mn substituted $BiFeO_3$ multiferroics, Ceram. Int., vol. 43, no. 16, pp. 13750–13758, Nov. 2017, https://doi.org/10.1016/j.ceramint.2017.07.088

[37] Priya, A. S., Banu, I. B. S., Geetha, D., Sankar, S. (2019) Investigations of the magnetic and dielectric behaviour of (Zr, Cu) co-doped $BiFeO_3$-$BaTiO_3$ composite, Mater. Res. Express, vol. 6, no. 10, p. 106116, Sep. 2019, https://doi.org/10.1088/2053-1591/ab3e86

[38] Krimech, F. Z., Sayouri, S. (2019) Structure and dielectric behavior of Cu-doped $BaTiO_3$ ceramics, in Materials Today: Proceedings, 2019, vol. 30, pp. 909–917, https://doi.org/10.1016/j.matpr.2020.04.349

[39] Soni, M., Saleem, M., Bajpai, N., Chouhan, S., Varshney, M. D., Mishra, A. (2019) Structural and optical properties on Na doped $BaTiO_3$, AIP Conf. Proc., vol. 2100, no. April, 2019, https://doi.org/10.1063/1.5098739

Ref.:
Tihtih, Mohammed – **Sevostianova**, Irina N. – **Kurovics**, Emese – **Sablina**, Tatiana Yu. – **Kulkov**, Sergei N. – **Gömze**, László A.: *Examination of the Influence of Cobalt Substitution on the Properties of Barium Titanate Ceramics*
Építőanyag – Journal of Silicate Based and Composite Materials, Vol. 73, No. 4 (2021), 160–165. p.
https://doi.org/10.14382/epitoanyag-jsbcm.2021.24

GUIDELINE FOR AUTHORS

The manuscript must contain the followings: title; author's name, workplace, e-mail address; abstract, keywords; main text; acknowledgement (optional)**; references; figures, photos with notes; tables with notes; short biography** (information on the scientific works of the authors).

The full manuscript should not be more than 6 pages including figures, photos and tables. Settings of the word document are: 3 cm margin up and down, 2,5 cm margin left and right. Paper size: A4. Letter size 10 pt, type: Times New Roman. Lines: simple, justified.

TITLE, AUTHOR

The title of the article should be short and objective.

Under the title the name of the author(s), workplace, e-mail address.

If the text originally was a presentation or poster at a conference, it should be marked.

ABSTRACT, KEYWORDS

The abstract is a short summary of the manuscript, about a half page size. The author should give keywords to the text, which are the most important elements of the article.

MAIN TEXT

Contains: materials and experimental procedure (or something similar), results and discussion (or something similar), conclusions.

REFERENCES

References are marked with numbers, e.g. [6], and a bibliography is made by the reference's order. References should be provided together with the DOI if available.

Examples:

Journals:

[6] Mohamed, K. R. – El-Rashidy, Z. M. – Salama, A. A.: In vitro properties of nano-hydroxyapatite/chitosan biocomposites. *Ceramics International.* 37(8), December 2011, pp. 3265–3271, http://doi.org/10.1016/j.ceramint.2011.05.121

Books:

[6] Mehta, P. K. – Monteiro, P. J. M.: Concrete. Microstructure, properties, and materials. *McGraw-Hill*, 2006, 659 p.

FIGURES, TABLES

All drawings, diagrams and photos are figures. The **text should contain references to all figures and tables**. This shows the place of the figure in the text. Please send all the figures in attached files, and not as a part of the text. **All figures and tables should have a title**.

Authors are asked to submit color figures by submission. Black and white figures are suggested to be avoided, however, acceptable.

The figures should be: tiff, jpg or eps files, 300 dpi at least, photos are 600 dpi at least.

BIOGRAPHY

Max. 500 character size professional biography of the author(s).

CHECKING

The editing board checks the articles and informs the authors about suggested modifications. Since the author is responsible for the content of the article, the author is not liable to accept them.

CONTACT

Please send the manuscript in electronic format to the following e-mail address: femgomze@uni-miskolc.hu and epitoanyag@szte.org.hu or by post: Scientific Society of the Silicate Industry, Budapest, Bécsi út 122–124., H-1034, HUNGARY

We kindly ask the authors to give their e-mail address and phone number on behalf of the quick conciliation.

Építőanyag – *Journal of Silicate Based and Composite Materials*, Quarterly peer-reviewed periodical of the Hungarian Scientific Society of the Silicate Industry, SZTE.
http://epitoanyag.org.hu